Intertidal Flats in Engineered Estuaries

On the Hydrodynamics, Morphodynamics, and Implications for Ecology and System Management

de Vet, P.L.M.

DOI
10.4233/uuid:2b392951-3781-4aed-b093-547c70cc581d

Publication date
2020

Intertidal Flats in Engineered Estuaries

P.L.M. de Vet

Intertidal Flats in Engineered Estuaries

On the Hydrodynamics, Morphodynamics, and Implications for Ecology and System Management

INTERTIDAL FLATS IN ENGINEERED ESTUARIES

ON THE HYDRODYNAMICS, MORPHODYNAMICS, AND IMPLICATIONS FOR ECOLOGY AND SYSTEM MANAGEMENT

Proefschrift

ter verkrijging van de graad van doctor
aan de Technische Universiteit Delft,
op gezag van de Rector Magnificus, Prof. dr. ir. T.H.J.J. van der Hagen,
voorzitter van het College voor Promoties,
in het openbaar te verdedigen op woensdag 15 april 2020 om 12:30 uur

door

Paul Lodewijk Maria DE VET

Ingenieur in de Civiele Techniek, Technische Universiteit Delft, Nederland,
Master of Science in Hydraulic Engineering and Water Resources Management,
National University of Singapore, Singapore,
geboren te Breda, Nederland.

Dit proefschrift is goedgekeurd door de promotoren.

Samenstelling promotiecommissie:

Rector Magnificus,	voorzitter
Prof. dr. ir. Z.B. Wang,	Technische Universiteit Delft, promotor
Dr. ir. B.C. van Prooijen,	Technische Universiteit Delft, promotor
Onafhankelijke leden:	
Dr. G. Coco,	The University of Auckland, Nieuw-Zeeland
Prof. dr. D. van der Wal,	Universiteit Twente
Prof. dr. ir. A.J.F. Hoitink,	Wageningen University & Research
Prof. dr. ir. A.J.H.M. Reniers,	Technische Universiteit Delft
Prof. dr. ir. S.G.J. Aarninkhof,	Technische Universiteit Delft, reservelid
Overige leden:	
Prof. dr. P.M.J. Herman,	Technische Universiteit Delft

Dr. T. Ysebaert heeft in belangrijke mate aan de totstandkoming van het proefschrift bijgedragen.

EMERGO project consortium partners: Deltares, Natuurmonumenten, Rijkswaterstaat, Royal Netherlands Institute for Sea Research, Svašek Hydraulics, Wageningen Marine Research, and World Wide Fund for Nature (WWF).

Keywords: Intertidal Flats, Estuaries, Human Interventions, Natural Processes, Morphodynamics, Hydrodynamics, Ecology, Numerical Modeling, Field Measurements

Printed by: Gildeprint

Front & Back: Sediment nourishment works on the Roggenplaat intertidal flat in the Eastern Scheldt. This dissertation contributed to the design of these nourishments. Aerial photo by Edwin Paree, 22 November 2019.

ISBN 978-94-6384-123-8

An electronic version of this dissertation is available at
`http://repository.tudelft.nl/`.

Luctor et Emergo

— I struggle and emerge

Motto of the Dutch Province of Zeeland

CONTENTS

SUMMARY

Intertidal flats — regions of estuaries that emerge every tide from the water — form unique ecosystems. Benthic communities living in the bed are a valuable food source for wading birds. Salt marshes present on these flats further enhance the biodiversity. Through the damping of waves, intertidal flats also contribute to the safety of the hinterland against flooding. In engineered estuaries, human interventions such as storm surge barriers, navigation channels, dams, and levees affect these ecologically valuable intertidal flats and may even threaten their existence. Therefore, these systems should be managed with care, requiring a thorough understanding of the mechanisms shaping intertidal flats.

This dissertation aims to identify and quantify the natural and anthropogenic processes driving hydrodynamics and morphodynamics of intertidal flats, and to reveal the implications for ecology and system management. The Eastern Scheldt and Western Scheldt estuaries (the Netherlands) were selected for this study. These were chosen because of the extensive datasets measured in both estuaries and the different types of human interventions affecting these systems. In the Eastern Scheldt, a storm surge barrier closes during storm conditions and reduces tidal flow velocities inside the estuary at normal conditions. Tidal velocities are also reduced by dams in the branches of this estuary. In the Western Scheldt, sediment is being relocated from too shallow parts of the navigation channel to other parts of the estuary, enabling navigation to economically important harbors.

With almost 60 years of bathymetric data, the morphology and morphological evolution of the intertidal shoals (intertidal flats surrounded by channels) of the Eastern Scheldt and Western Scheldt are analyzed. We quantified for every intertidal shoal its volume, area, average height, and integral steepness based on its full geometry. The intertidal shoals in the Eastern Scheldt are less steep than those in the Western Scheldt. While the intertidal shoals in the Western Scheldt generally steepened and increased in height, the intertidal shoals in the Eastern Scheldt lowered after the completion of the storm surge barrier. These differences in evolution are related to differences in tidal flow velocities, in part due to human interventions in these systems. We revealed that the lowering rates of the intertidal shoals in the Eastern Scheldt reduced within decades.

The relative importance of natural processes (tide, surge, wind, and waves) for the hydrodynamics and sediment transport on intertidal flats is unraveled. With a numerical model of the largest intertidal shoal of the Eastern Scheldt (Roggenplaat), the spatiotemporal variation of the relative importance of each process is systematically assessed. The water level differences between the surrounding channels steered the flow over the shoal. The flow in the main creeks of the intertidal shoal is tide-dominated. In contrast, the flow direction and magnitude on the intertidal shoal, especially in the highly elevated areas, are largely influenced by the wind. We derived that wind speeds of approximately 40 times the tidal velocity are sufficient to completely alter the flow. As

a result, the bulk of the sediment transport on the highly elevated regions of intertidal shoals occurs during storm events, also due to large waves during these events.

Spatiotemporal variations in the forcing processes have implications for intertidal flat morphodynamics and ecology. With decades of bed level measurements on intertidal flats, we showed that storm events may have long-term effects on the morphological evolution; persisting morphological impacts can compare to years of continuous evolution. Furthermore, the data indicated a clear spatial inhomogeneity in the magnitudes of the bed level changes. Additionally, for one month we measured the hydrodynamics and morphodynamics across an intertidal flat to unravel the hydrodynamic processes driving bed level changes on intertidal flats. These measurements captured a storm event and its post-storm recovery. We identified that it is not solely the magnitude of the hydrodynamic forcing processes that determines morphological impact, but also their relative timing and duration. Not only the bed level dynamics are spatially inhomogeneous, the impact of storm events on benthic communities also varies across intertidal flats. We conclude that spatial patterns in bed level dynamics result from inhomogeneous distributions of the forcing processes across intertidal flats and spatial variations in bed slope.

The detailed eco-morphological effects of sediment disposals in a channel on an adjacent intertidal flat are investigated. Decades of high-frequency monitoring data on the intertidal flat morphology, grain sizes, abundance of benthic macrofauna, and position of the salt marsh are analyzed. Additionally, changes in tidal velocities are modeled. A chain of cascading consequences that follows sediment disposals is identified. Sediment disposals in channels affect the channel bank migration due to the increased availability of sediment, which drives changes in the evolution of the intertidal flat hydrodynamics, morphology, and grain sizes. These changes impose consequential adaptations of benthic communities and changes in evolution of adjacent salt marshes. Changes to such intertidal flats may occur years after the start of sediment disposals as the morphological changes propagate over these areas. The response of the intertidal flat to the local sediment disposals illustrates that system-wide changes in hydrodynamics are not required to largely affect intertidal flats.

It is the aggregated system of natural forces and human interventions that drives the eco-morphological evolution of intertidal flats in estuaries. Intertidal flats respond to local as well as to system-wide changes in sediment availability and hydrodynamics due to human interventions. Even under major human interventions, the natural forces remain relevant. Due to many spatial and temporal scales involved in the eco-morphological response of intertidal flats to changing natural and anthropogenic forces, estuaries require adaptive management strategies.

SAMENVATTING

Intergetijdengebieden — vlaktes in estuaria die tijdens elk getij droogvallen — vormen unieke ecosystemen. Benthische gemeenschappen die in de bodem leven, zijn waardevolle voedingsbronnen voor foeragerende vogels. Schorren vullen de biodiversiteit in deze intergetijdengebieden verder aan. Bovendien dragen deze gebieden, door het breken van golven, bij aan het beschermen van het achterland tegen overstromingen. In door de mens beïnvloede estuaria doen menselijke ingrepen als stormvloedkeringen, scheepvaartgeulen, dammen en dijken deze ecologisch waardevolle gebieden veranderen of zelfs verdwijnen. Daarom moeten deze gebieden zorgvuldig beheerd worden. Dit vereist een diepgaand begrip van de mechanismen die deze gebieden vormgeven.

Dit proefschrift heeft tot doel de natuurlijke en de door de mens beïnvloede processen die de hydrodynamica en morfodynamica van intergetijdengebieden sturen, te identificeren en te kwantificeren. Verder is het doel de hieruit volgende implicaties voor de ecologie en het beheer van deze systemen te bepalen. De Oosterschelde en Westerschelde (Nederland) zijn voor deze studie geselecteerd omdat er in deze systemen veel is gemeten en omdat deze systemen aan verschillende menselijke ingrepen onderhevig zijn. In de Oosterschelde is een stormvloedkering aanwezig die tijdens stormcondities sluit en die tijdens normale condities de getijdestroming binnen het estuarium beperkt. De getijdestroming is daar ook beperkt doordat de aftakkingen van het estuarium zijn afgedamd. In de Westerschelde wordt met baggerschepen sediment verplaatst om de scheepvaartgeul naar de economisch waardevolle havens bevaarbaar te houden.

Met bijna 60 jaar aan bodemhoogtemetingen zijn de morfologie en morfologische ontwikkelingen van de intergetijdenplaten — intergetijdengebieden omringd door geulen — van de Oosterschelde en Westerschelde geanalyseerd. Voor elke intergetijdenplaat is het volume, de oppervlakte, gemiddelde hoogte en integrale steilheid gekwantificeerd op basis van de volledige geometrie. De intergetijdenplaten zijn in de Oosterschelde minder steil dan in de Westerschelde. Terwijl de intergetijdenplaten in de Westerschelde over het algemeen steiler en hoger zijn geworden, zijn de intergetijdenplaten in de Oosterschelde juist lager aan het worden door de aanwezigheid van de stormvloedkering. Deze verschillen in ontwikkeling zijn gerelateerd aan verschillen in de sterkte van de getijdestroming, die deels zijn veroorzaakt door de menselijke ingrepen. Wij hebben vastgesteld dat de snelheid waarmee de platen in de Oosterschelde na de bouw van de stormvloedkering daalden, binnen decennia was afgenomen.

Het belang van elk van de natuurlijke processen (getij, opzet, wind en golven) is voor de hydrodynamica en sedimenttransporten in intergetijdengebieden ontrafeld. Met een numeriek model dat de grootste intergetijdenplaat van de Oosterschelde beschrijft (de Roggenplaat), zijn de ruimtelijke en temporele variaties van de processen systematisch onderzocht. Het zijn de verschillen in waterstand tussen de omliggende geulen die de stroming over de plaat drijven. De stroming in de grootste kreken van de plaat wordt gedomineerd door het getij. Daarentegen worden de richting en de sterkte van de stro-

ming op de plaat, vooral op de hoge delen, sterk beïnvloed door de wind. Wij hebben bepaald dat een windsnelheid van ongeveer 40 maal de getijdesnelheid voldoende is om de stroming volledig te veranderen. Daardoor vindt het grootste deel van het sedimenttransport op de hoge delen van intergetijdenplaten tijdens stormen plaats, mede ook door de grote golven tijdens deze stormen.

Ruimtelijke en temporele variaties in de hydrodynamische processen hebben implicaties voor de morfodynamica en ecologie van intergetijdengebieden. Met decennia aan bodemhoogtemetingen in intergetijdengebieden hebben wij laten zien dat stormen langdurige effecten kunnen hebben op de morfologische ontwikkelingen; blijvende morfologische veranderingen door een individuele storm kunnen even groot zijn als jaren aan continue ontwikkeling. Verder zijn er duidelijke ruimtelijke variaties in de grootte van de bodemveranderingen geconstateerd. Aanvullend hebben wij ook voor een maand de hydrodynamica en morfodynamica in een intergetijdengebied gemeten om de hydrodynamische processen in kaart te brengen die de bodemveranderingen veroorzaken. Deze metingen beslaan de morfologische impact van een individuele storm evenals het herstel na deze storm. Wij hebben aangetoond dat het niet alleen de sterkte van de hydrodynamische processen is die de morfologische impact bepaalt, maar juist ook of de processen parallel plaatsvinden en hoe lang dit duurt. Niet alleen de bodemdynamiek is ruimtelijk variërend, ook de impact van stormen op benthische gemeenschappen varieert in intergetijdengebieden. Wij concluderen dat ruimtelijke patronen in bodemdynamiek het gevolg zijn van zowel variaties in de hydrodynamische processen in intergetijdengebieden als van ruimtelijke variaties van de bodemhelling.

De eco-morfologische effecten van sedimentstortingen in geulen op de aangrenzende intergetijdengebieden zijn in detail onderzocht. Decennia aan hoogfrequente metingen van de morfologie, korrelgrootte, aanwezigheid van benthische gemeenschappen en de positie van het schor zijn geanalyseerd. Daarnaast zijn de getijdesnelheden gemodelleerd. Een reeks van opeenvolgende consequenties van sedimentstortingen is geïdentificeerd. Sedimentstortingen in geulen beïnvloeden, middels een toename in de sedimentbeschikbaarheid, de geulwandmigratie die daardoor ook de ontwikkeling van de hydrodynamica, morfologie en korrelgrootte van intergetijdengebieden beïnvloedt. Deze veranderingen sturen vervolgens ook veranderingen in de benthische gemeenschappen en veranderingen in de ontwikkeling van de aangrenzende schorren aan. Veranderingen kunnen op deze intergetijdengebieden jaren na de start van de stortingen optreden, omdat de veranderingen over deze gebieden migreren. De respons van het onderzochte intergetijdengebied op de lokale sedimentstortingen toont aan dat systeembrede veranderingen in hydrodynamica niet noodzakelijk zijn om intergetijdengebieden substantieel te beïnvloeden.

Het is het samengestelde systeem van natuurlijke processen en menselijke ingrepen dat de eco-morfologische ontwikkeling van intergetijdengebieden in estuaria aanstuurt. Intergetijdengebieden reageren zowel op lokale als op systeembrede veranderingen in sedimentbeschikbaarheid en hydrodynamica als gevolg van menselijke ingrepen. Maar zelfs onder grote menselijke ingrepen blijven natuurlijke processen relevant. Door de vele ruimtelijke en temporele schalen die van toepassing zijn op de eco-morfologische respons van intergetijdengebieden op veranderende natuurlijke en door de mens beïnvloede processen, is het noodzakelijk estuaria adaptief te beheren.

Chapter 1

Introduction

Cover photo: on an intertidal flat in the Western Scheldt during the field campaign.

Figure 1.1: Photos of intertidal flats emerging from the water; taken from an airplane at low tide. Left: Western Scheldt estuary (the Netherlands) with its navigation channel in the background. Right: Eastern Scheldt estuary (the Netherlands) with its storm surge barrier in the background. Courtesy of Edwin Paree.

This dissertation focuses on **intertidal flats in engineered estuaries**. During every tide, the sea retreats and large regions of estuaries called **intertidal flats** emerge from the water (see for example the cover photo and the aerial photos in Figure 1.1). At first sight, these emerging intertidal flats may appear rather barren. However, nothing could be further from the truth; these intertidal flats provide the basis for rich ecosystems. As soon as the sea retreats, wading birds forage on the large variety of worms, clams, and shrimps that live in the bed (the so-called benthic communities; Figure 1.2). Despite the never ending cycles of forces that drive emergence and submergence of the intertidal flats, engineering works (e.g., storm surge barriers, navigation channels, dams, and levees) threaten the value or, possibly, the existence of these ecologically valuable areas in **engineered estuaries**.

Ecosystems of intertidal flats are not only formed by the benthic communities present in the bed and foraging wading birds, but also by the salt marshes (coastal wetlands that are frequently flooded) that may be present on these areas. Furthermore, through the damping of waves, intertidal flats contribute to flood safety of the hinterland. By (indirectly) affecting the morphology of intertidal flats, engineering works inherently threaten the services these areas provide (*Cozzoli et al.*, 2017; *Reed et al.*, 2018).

Figure 1.2: Left: photo of a locally excavated intertidal flat in the Western Scheldt, revealing traces of benthic communities living in the bed (courtesy of Edwin Paree). Right: underwater photo of benthic communities on the bed of an intertidal flat in the Eastern Scheldt (courtesy of Brenda Walles).

1

Estuaries, both engineered and natural, are shaped by various natural processes. The emergence and submergence of intertidal flats is a direct consequence of tides. Tides result from forces that the solar system place on the water body, and are transformed by the morphology of coastal systems (*Dronkers*, 1964). Apart from water level variations, tides enforce also consequential flows. The water level variations and flows are both influenced by meteorological events (*Le Hir et al.*, 2000). Waves strongly affect the resulting sediment transports, especially in shallow areas (*Green and Coco*, 2014). The width of these relatively flat areas is typically several orders-of-magnitude larger than the tidal range (*Dyer et al.*, 2000).

Engineering works can modify the availability of sediments, as well as the magnitudes and patterns of the natural processes, initiating changes in the evolution of intertidal flats. Many estuaries around the world contain engineering works. Examples include San Francisco Bay (United States), the Wadden Sea, the Eastern Scheldt, the Western Scheldt (the Netherlands), Venice Lagoon (Italy), and the Yangtze (China). Figure 1.3 indicates key elements that may be present in such engineered estuaries. Classically, an estuary is considered the interface between the *sea* and a *river*. Intertidal flats are either adjacent to the outer contours of the estuary (*fringing flat*) or surrounded by *channels* (*intertidal shoals*). *Salt marshes* are generally found at the highest elevations of intertidal flats. A key primary motive for engineering works is to protect the *hinterland* from flooding by means of *levees* surrounding the estuary, upstream *damming*, and/or a *storm surge barrier* that closes during storm events. Economic gain is another fundamental primary motive for engineering works. This may translate to the deepening of *navigation channels* to ensure the accessibility of inland *harbors* through dredging works. Sediments retrieved from these works can be disposed elsewhere in these systems.

In this dissertation, both natural and anthropogenic processes that shape the eco-morphology of intertidal flats are studied.

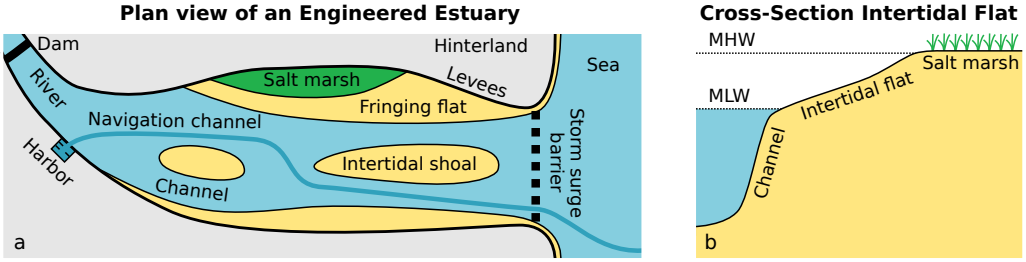

Figure 1.3: (a) Conceptual visualization of elements that may be present in engineered estuaries. (b) Example cross-section of an intertidal flat (not to scale), with the MLW (Mean Low Water) and MHW (Mean High Water) lines.

1.1. THE EASTERN SCHELDT AND WESTERN SCHELDT

In this dissertation, the Eastern Scheldt and Western Scheldt estuaries (the Netherlands) are considered (Figure 1.4). The names of these estuaries relate to the river Scheldt which originates in the north of France. In the past, this river bifurcated into eastern and western branches leading towards the Eastern Scheldt and Western Scheldt, respectively. In

1867, the Eastern Scheldt was disconnected from the river through the construction of a dam. Since then, both estuaries developed independently. By considering the different responses of intertidal flats to the different engineering works present in these estuaries, broad insights on the effects of engineering works on intertidal flats are gathered. Another reason for the selection of these specific systems is the availability of extensive datasets that have been measured in both estuaries over the last decades.

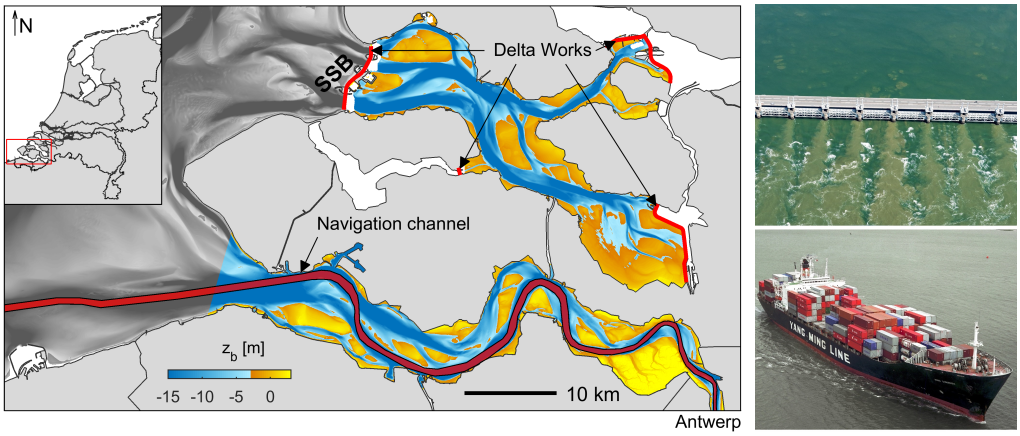

Figure 1.4: Left: Eastern Scheldt (the northern estuary) and Western Scheldt (the southern estuary), with bathymetry data (source: Rijkswaterstaat) with respect to NAP (Dutch Ordnance Level, close to mean sea level). The Western Scheldt navigation channel and the Eastern Scheldt Delta Works (the compartment dams and the storm surge barrier; SSB) are indicated. Top right: aerial photo of several SSB gates (courtesy of Edwin Paree). Bottom right: a container vessel in the Western Scheldt (courtesy of Rijkswaterstaat, beeldbank.rws.nl).

Eastern Scheldt The geometry of the Eastern Scheldt (Figure 1.4) is the result of centuries of land reclamations and inundations of the hinterland (*Eelkema*, 2013). A storm surge barrier closes the mouth of the Eastern Scheldt during high storm surges, but also affects the flow during normal conditions. The storm surge barrier is 8 km long and contains 62 gates of each 42 m long. The storm surge barrier was completed in 1986 as part of the "Delta Works" project (in response to the 1953 North Sea flood), in which also all former connections to neighboring estuaries were closed with compartment dams. Despite these major engineering works, the ecological value of the estuary is broadly recognized (e.g., it is designated as a European Natura 2000 area).

Western Scheldt In contrast, the Western Scheldt has no barriers within its system, but contains levees surrounding the estuary. This allows navigation to adjacent harbors, including the economically important harbor of Antwerp, Belgium. To provide access to larger commercial vessels, the depth of the navigation channels had been increased via dredging several times and has been maintained continuously. These activities add up to around 10 million m^3 of sediment retrieval and relocation within this estuary each year. Dredged sediments are disposed on edges of intertidal flats, in non-navigation channels, and in deep parts of navigation channels of the estuary.

1

1.2. STATEMENT OF AIM AND RESEARCH QUESTIONS

Anthropogenic pressures affect the ecological values of intertidal flats so significantly that governments are actively seeking for solutions to preserve these values. However, due to the complexity of forcing processes and spatiotemporal scales involved, system managers need continuous updates on guidelines in managing these systems adequately. The key processes shaping intertidal flats in engineered estuaries must be understood before one can (1) improve guidelines that minimize the negative consequences of engineering works and (2) optimize the design of mitigation measures. This dissertation acts on this knowledge gap.

The morphology of intertidal flats is the result of the combined natural and anthropogenic forces that act on various timescales. Storm events also affect intertidal flats in highly engineered estuaries. Engineering works do not necessarily shape intertidal flats directly, but rather adjust the natural forcing processes (or sediment availability). Hence, understanding the natural processes is key toward understanding the impact of human interventions. Also, the relevance of climate change for these systems (e.g., through sea level rise and increasing wind speeds; *Young and Ribal*, 2019), depends on the extent to which engineering works steer the evolution of the intertidal flats. For all these reasons, the natural and anthropogenic processes are considered integrally in this dissertation.

Aim of the dissertation

To identify and quantify the natural and anthropogenic processes driving hydrodynamics and morphodynamics of intertidal flats, and to reveal the implications on ecology and system management.

This aim is pursued with the following questions that form the core of this dissertation:

(i) How do intertidal flats evolve under influence of human interventions such as sediment relocations and a storm surge barrier?

(ii) How do tidal and meteorological forces affect the flow and sediment transport on intertidal flats?

(iii) What drives the spatiotemporal variations in bed level dynamics across intertidal flats?

(iv) How do sediment disposals in channels affect the eco-morphology of adjacent intertidal flats?

The first question is introduced to draw a general picture on how, on a system scale, different types of human interventions change the evolution of intertidal flats. The second question deals with clarification of the relative importance of natural forcing processes on hydrodynamics and sediment transport on these flats. The third question is introduced to reveal the spatiotemporal patterns in bed level dynamics and the underlying mechanisms of such changes. The fourth question addresses a knowledge gap regarding the unknown mechanism that drives eco-morphological evolution of an intertidal flat following sediment disposals in an estuarine channel.

1.3. STRUCTURE OF THE DISSERTATION

The four research questions are addressed in Chapters 2–5, respectively, with analyses on both the Eastern Scheldt and Western Scheldt. Various methods were combined to answer the variety of research questions: decades of morphologic data were analyzed, physical processes were measured in the field, and hydrodynamics and sediment transport were modeled numerically. The focus is both on human interventions (Chapters 2 and 5) and on natural processes (Chapters 3 and 4). Each chapter was set up as a journal paper. The structure of the papers was maintained for consistency.

In **Chapter 2**, the historical evolution of the intertidal shoals in the Eastern Scheldt and Western Scheldt is derived from almost six decades of bathymetric data. The morphologies of the intertidal shoals are compared (based on their area, volume, average height, and steepness), and their evolution is analyzed and related to the human interventions in these systems.

In **Chapter 3**, the importance of combined tidal and meteorological forces for the flow and sediment transport on intertidal shoals is revealed. The contribution of each process is analyzed using a numerical model of the Roggenplaat, the largest intertidal shoal of the Eastern Scheldt. Also, the importance of the geometry of the surrounding channels and the local morphology for the flow patterns is discussed.

In **Chapter 4**, the focus extends to variations in bed level dynamics across intertidal flats. The bed level dynamics is quantified with decades of time series measured in both estuaries. The processes driving the spatiotemporal variations in bed level dynamics are revealed with one month of continuous field measurements on the hydrodynamics and morphodynamics, including one storm event.

In **Chapter 5**, the spatiotemporal eco-morphologic response of an individual intertidal flat to sediment disposals in its adjacent channel is investigated. This provides a higher level of detail compared to Chapter 2. With decades of measurements at a monthly to an annual frequency, the impact of the sediment disposals on the morphology of the intertidal flat, including its grain sizes, flow velocities, salt marsh, and benthic communities, are considered.

In **Chapter 6**, the implications of this dissertation's results (both the anthropogenic and natural aspects) on system management strategies are discussed. The focus is placed on implications for estuaries in which navigation channels are dredged, for estuaries with storm surge barriers, and for the design of nourishments on intertidal flats.

Finally, in **Chapter 7** the general conclusions are presented. These are followed with recommendations for further research.

Chapter 2

The Differences in Morphological Development Between the Intertidal Flats of the Eastern and Western Scheldt

This chapter has been published as:
Geomorphology (*De Vet et al.*, 2017),
co-authors: Van Prooijen and Wang.

Cover photo: satellite imagery of the Eastern Scheldt and Western Scheldt, taken by the Sentinel-2B satellite (25 February 2018). Courtesy of ESA (European Space Agency).

Engineering works affect the morphology of estuaries. In this chapter, the morphology and evolution of the intertidal flats of two estuaries with different engineering works are compared: the Eastern Scheldt and Western Scheldt. Within the Eastern Scheldt, the consequences of a storm surge barrier and compartment dams are assessed, in the Western Scheldt the consequences of sediment relocation works for the deepening and maintenance of its navigation channel are investigated. The focus is on the major intertidal shoals of both estuaries, which are studied using decades of bathymetric data.

ABSTRACT

Human interventions have a large impact on estuarine morphology. The intertidal flats in the Eastern Scheldt and Western Scheldt estuaries (the Netherlands) have faced substantial morphological changes over the past decades. These changes are thought to be caused by human interventions, such as the construction of the storm surge barrier in the mouth of the Eastern Scheldt, and the deepening of the navigation channels of the Western Scheldt. This chapter analyzes several datasets and numerical simulations of hydrodynamics, providing an overview of the various morphological characteristics of the intertidal flats in the two estuaries over time and space. Apart from the volume, area and average height of these areas, also the integral steepness of each flat is quantified based on its full geometry. The analyses focus on the intertidal flats surrounded by water, which allows for a robust comparison between the different flats. The intertidal flats in the Western Scheldt appear to be substantially steeper compared to those in the Eastern Scheldt. The data indicates that a larger average height of a flat is related to a larger steepness. Despite variations in the evolution of the different flats, distinct characteristics of both estuaries are observed. Opposing trends are identified over time: the flats in the Western Scheldt have mainly increased in height, whereas the flats in the Eastern Scheldt have lowered after the completion of the storm surge barrier. These opposing developments are associated with differences in tidal flow velocities in the estuaries, which are the result of human interventions.

2.1. INTRODUCTION

Morphological changes of intertidal areas threaten the ecological value of estuaries all around the world (*Smaal and Nienhuis*, 1992; *Wilson et al.*, 2005; *Murray et al.*, 2014). The Eastern Scheldt (ES) and the Western Scheldt (WS) are two neighboring estuaries located in the southwest of the Netherlands with a substantial amount of intertidal areas (see Figure 2.1). Both estuaries face various human interventions, which influence the morphological changes of these systems (*Wang et al.*, 2015). In recent decades, the intertidal flats in the ES were lowering (*Louters et al.*, 1998), whereas those in the WS have mainly been increasing in elevation (*Cleveringa*, 2013). Further, previous studies suggest that the intertidal flats in the WS have been steepening (e.g., *Bolle et al.*, 2010; *Kuijper and Lescinski*, 2013), which could induce an impoverishment of the natural habitats (*De Jong and De Jonge*, 1995; *Fujii and Raffaelli*, 2008). However, these suggestions are based on individual cross-sections or changes of individual bulk quantities (i.e., height, area or volume of flats), which do not necessarily imply a general steepening of the bed slopes. Knowledge is still limited on how individual intertidal flats are developing within these estuaries and on what causes the differences in morphological development between these flats.

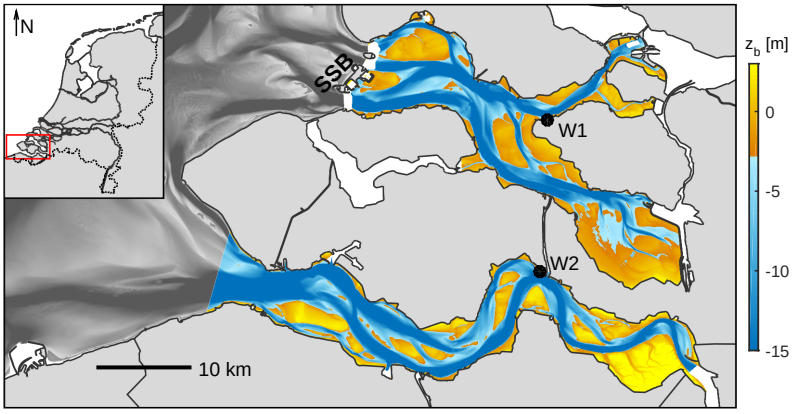

Figure 2.1: Overview of the Eastern Scheldt (North) and Western Scheldt (South). The Eastern Scheldt is partially closed by the storm surge barrier (SSB). Areas with no bathymetric data are marked white. The bathymetric data (source: Rijkswaterstaat) is with respect to NAP (Dutch Ordnance Level). The dots indicate the wind measurement stations Stavenisse (W1) and Hansweert (W2).

The WS estuary is the Dutch part of the River Scheldt which is connected to the North Sea. From the mouth of the estuary to the Dutch/Belgian border, the tidal range increases from 3.5 m to 5 m. The average river discharge of around 100 m^3/s is very limited compared to the tidal discharges, causing the estuary to be well mixed (*Cancino and Neves*, 1999; *De Vriend et al.*, 2011). The WS provides access to various harbors, of which the port of Antwerp (Belgium) is the largest. To keep the ports accessible for the cargo vessels of increasing size, the navigation channels were deepened to 14.5 m in the 1970s and deepened further to 16 m around 1997 (*De Vriend et al.*, 2011). More recently, the channels where deepened by another 1.2 m in 2010. Most of the annually dredged sedi-

ment is dumped at assigned areas within the estuary. Large parts of the intertidal areas had already been reclaimed before these dredging activities took place (*Van den Berg et al.*, 1996). The intertidal areas surrounded by water in the WS are characterized by a typical grain size of 50–150 μm (D_{50}), and contain typically less than 10% mud (*Van Eck*, 1999). However, there are regions with higher mud fractions on several flats.

In contrast, the ES has no river inflow as it is only in connection to the North Sea. In the past, the ES was also linked to neighboring estuaries including the WS. During the past centuries, land reclamation projects have been taken place in the ES (*Eelkema et al.*, 2009). After the North Sea flood of 1953, the Dutch government initiated the Delta Project to protect the southwest of the Netherlands against flooding. In 1986, the storm surge barrier (SSB in Figure 2.1) was completed, closing the estuary under severe storm conditions and constricting the discharge during regular conditions. In the same project, various other dams were constructed, closing off the remaining openings of the estuary. All these interventions induced substantial changes to the tidal flow velocities and reduced the tidal range by more than half a meter, which currently ranges between 2.5 m and 3.5 m (*Louters et al.*, 1998; *Eelkema et al.*, 2009). The intertidal areas near the mouth of the ES are characterized by a typical median grain size of around 200 μm (D_{50}), whereas farther from the mouth grain sizes in the order of 150 μm are more typical (*Kohsiek et al.*, 1987).

The impact of the interventions in the ES and WS on the morphological processes of the intertidal areas in these systems can be related to changes in the physical processes. *Eisma* (1998) and *Le Hir et al.* (2000) indicate that the tide, the waves, the wind-induced circulation, the density-driven circulation and the drainage are important processes for sediment transport on intertidal areas. *Friedrichs* (2011) presents a qualitative understanding, supported by idealized numerical models and field observations, of the shape and morphological response of intertidal areas related to changes in the forcing. Friedrichs indicates that a variation in the relative importance of the tide to the waves induces changes in the geometry of these flats. This framework is in line with the findings of *Louters et al.* (1998) and *Wang et al.* (2015), who argued that the reduction of the tidal flow in the ES caused a relative increase of the erosive effects of waves. According to *Green and Coco* (2014), there is sufficient evidence to conclude that waves erode and tidal currents cause accretion of intertidal areas on the long term.

Previous studies applied various methods to analyze datasets of intertidal areas. For example, *Dyer et al.* (2000) applied a cluster analysis to produce a classification scheme of mudflat types, considering several mudflats in European estuaries with various hydrodynamic, geometric, biological and sediment characterizing variables. *Bearman et al.* (2010) focused on the shape of intertidal areas, by analyzing eigenfunctions of cross-shore profiles in San Francisco Bay. With this approach, a correlation was revealed between the degree of convexity or concavity of profiles and the rate of deposition, tidal range, fetch length, grain size and tidal flat width. *Santinelli and de Ronde* (2012) analyzed cross-sections measured on the intertidal areas in the ES, identifying an average erosion trend of 0.9 cm per year. In addition, other studies applied a more descriptive approach to identify local morphological characteristics of individual intertidal areas in more detail (e.g., *Cleveringa*, 2013).

This study focusses on identifying and understanding the state and temporal devel-

opment of the morphology of individual intertidal flats in the ES and WS. The analyses are limited to the major intertidal areas which are surrounded by water at MLW (see Figure 2.2), as it is not straightforward to robustly define the boundaries of intertidal flats adjacent to the land. Still the methodology of this study could be applied to those intertidal flats with a land boundary, but the lateral boundaries require case-dependent definitions which make these areas less applicable for comparison studies. Appropriate bulk properties are derived from full-domain digital elevation models. For each intertidal flat, the area, volume and average height are determined. Changes in these parameters are relevant indicators for the ecological development of intertidal flats, as a clear relation exists between the vertical distribution of species and the immersion period of a flat (*Wolff*, 1973). Further, the methodology of *Strahler* (1952) is applied to robustly describe the steepness of intertidal flats, without the use of arbitrary cross-sections. By analyzing the hydrodynamic forcing, a possible explanation for identified morphological differences between flats is given.

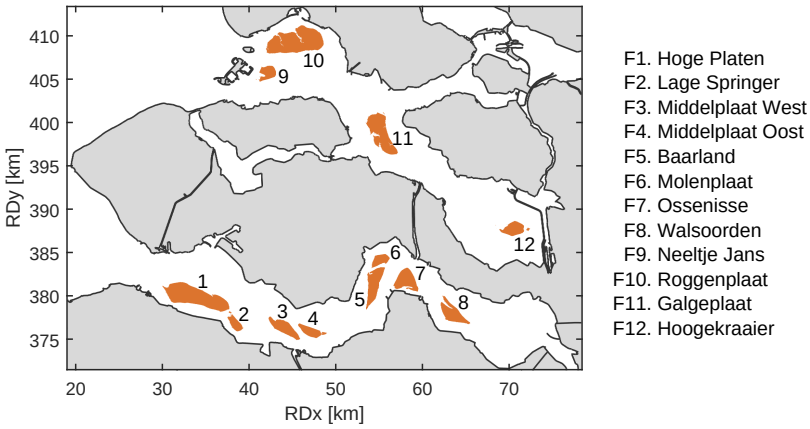

Figure 2.2: The studied intertidal areas in the WS (flats F1–F8) and in the ES (flats F9–F12). The individual tidal flats are sorted with increasing distance from the mouth.

2.2. FIELD AND MODEL DATA

2.2.1. DATASETS

In recent decades, data on the morphology of tidal flats have been gathered in both estuaries. Various digital elevation models provide a spatial coverage of the bathymetry of the intertidal areas. The so-called *Vaklodingen* dataset covers both estuaries with a grid resolution of 20 m (*Marijs and Paree*, 2004; *Wiegmann et al.*, 2005). This dataset combines single beam measurements at 100/200 m transects with GPS Real-Time Kinematic (RTK) measurements on top of the tidal flats (with more primitive levelling techniques before GPS-RTK existed). Since 2001, the dry parts of the estuaries have also been measured with the Light Detection and Ranging (LiDAR) technique. This dataset is included in the Vaklodingen dataset, but it is also available separately on a finer grid with a resolution of 2 m or 5 m. Parts of the data with documented measurement mistakes (*Marijs*

and Paree, 2004) are excluded from this research. In this study, the high resolution LiDAR data are preferred. The Vaklodingen dataset is analyzed for the long-term analyses, which also includes measurements before 2001.

Wiegmann et al. (2005) estimated the vertical accuracy of the Vaklodingen dataset at 50 cm (2σ), independent of whether the data is measured by single beam or with RTK, as the interpolation process dominates this error. The LiDAR data is considered as slightly more accurate, approximately 30 cm (2σ). However, as this study considers cumulative quantities, the net inaccuracies reduce substantially. For a large number of grid cells, the cumulative interpolation error averages out. Systematic errors could still be present if a large amount of cells are considered, these are especially substantial in the old data by less accurate measurement techniques and could be in the order of 10 cm (*Marijs and Paree*, 2004).

Additionally, various cross-sections have been measured by Rijkswaterstaat (part of the Dutch Ministry of Infrastructure and the Environment) in great detail for over 25 years. These cross-sections are especially useful for analyzing local morphological changes. In this study, some of the cross-sections are presented to indicate the diversity in geometry and morphological response of the system and to analyze morphological changes at shorter time scales than the temporal resolution of the Vaklodingen dataset. According to *Wiegmann et al.* (2005), the accuracy of those measurements can be estimated at 6 cm (2σ).

Rijkswaterstaat provides long-term measurements of the water levels, waves and wind at various stations in the ES and WS. By the presence of the storm surge barrier in the ES, the majority of the waves is generated inside this estuary (*Louters et al.*, 1998). The mouth of the WS is exposed to waves from the North Sea, but farther inside the estuary, the waves are expected to be mainly generated locally. The wave climate at individual locations is not considered as it depends highly on local geometry. Instead, the wind climate, driving the wave generation within the estuaries, is presented for two centrally located measuring stations in Figure 2.3.

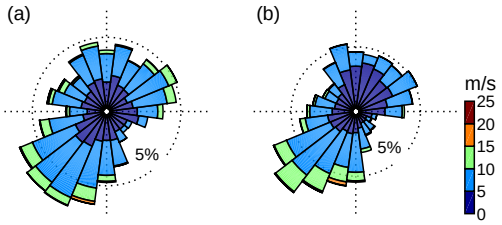

Figure 2.3: Wind climate of 2013 at (a) Stavenisse (ES) and (b) Hansweert (WS), based on measurements by Rijkswaterstaat (HMCZ). The locations of the measurement stations are indicated in Figure 2.1.

2.2.2. NUMERICAL MODEL RESULTS

Existing numerical model schematizations with Delft3D (*Lesser et al.*, 2004) provide spatial distribution information on the hydrodynamics. The ScalOost model describes the full ES and ranges up to 30 km offshore, taking the damping effect of the storm surge barrier into account (*Pezij*, 2015). In the WS, the NeVla model is shown to provide reliable

predictions of the hydrodynamics (*Van der Werf et al.*, 2015a).

The spatial distribution of the tidal range (MHW–MLW) can be estimated based on the modeled hydrodynamics (see Figure 2.4a). The modeled tidal range deviates not more than 0.10 m from the water level measurements for the full year of 2014. A robust estimate for the tidal range for each individual tidal flat can therefore be derived. Another relevant hydrodynamic indicator is the average magnitude of the flow velocities in the estuaries (see Figure 2.4b). Clearly, the tidal range is not a proper indicator for the local flow velocities, as the tidal flow velocities might be very small in channels with a relatively large tidal range (e.g., around Hoogekraaier (F12)). Therefore, both indicators should be considered individually, if the hydrodynamic forcing on intertidal flats is concerned.

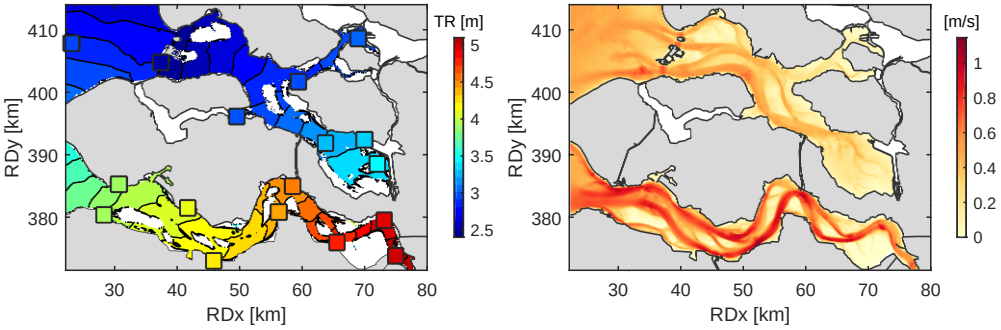

Figure 2.4: A spatial overview of (a) the tidal range and (b) the average magnitude of the depth-average flow velocities, computed with a one-month model run (August 2014) of the ScalOost model (ES) and the NeVla model (WS). The black contour lines in (a) illustrate 0.1 m intervals of the tidal range and the colored squares present the tidal range calculated from the full 2014 time series of the water level stations of Rijkswaterstaat.

2.3. METHODOLOGY

Hypsometric curves provide valuable insights into morphodynamic systems (*Strahler*, 1952; *Boon and Byrne*, 1981). In various previous studies, hypsometric curves are considered for whole basins or sections of these (e.g., *Dieckmann et al.*, 1987; *Kirby*, 2000; *Stanev et al.*, 2003; *Wang et al.*, 2002; *Kuijper and Lescinski*, 2013). However, this study focusses on the characteristics of individual flats. Therefore, the hypsometric curves of individual flats are studied, which are constructed by the following procedure (illustrated in Figure 2.5):

(a) Polygons are drawn around the MLW line of the targeted tidal flats. The polygons are not necessarily the same for all considered years, because tidal flat planform changes as the morphology evolves;

(b) The grid cells within the polygon and of which the bed level is between MLW and MHW, are considered as the intertidal region of the flat, all other grid cells are discarded;

(c) The hypsometric function $A(z) = A(Z > z) - A(Z > \text{MHW})$ is obtained by multi-

plying the surface area per grid cell with the number of grid cells of which the bed level is larger than z, but smaller than MHW.

Because of the large spatial inhomogeneity of the tidal range (see Figure 2.4a), a local estimate for the tidal range is made for each tidal flat, instead of a single one for each estuary. Regions with vegetation are considered part of the tidal flats as long as these are between MLW and MHW.

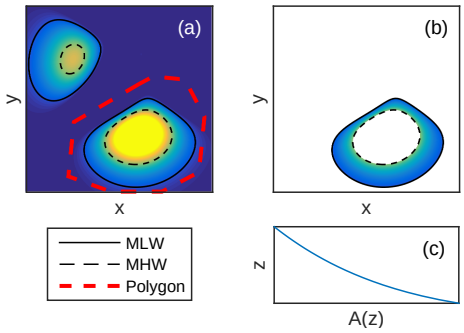

Figure 2.5: The three steps to derive the hypsometric curve of an individual tidal flat (example with synthetic data).

In addition to the hypsometric curve, the volume distribution of a flat $V(z) = V(Z > z) - V(Z > \text{MHW})$ can be derived by including the bed level per grid cell in step (c). Based on these functions, the average height of an intertidal area with respect to MLW follows as:

$$h = \frac{V(Z > \text{MLW}) - V(Z > \text{MHW})}{A(Z > \text{MLW}) - A(Z > \text{MHW})}. \tag{2.1}$$

The determination of the bed slope of a tidal flat is arbitrary, if based on cross-sections. First, a cross-section is not necessarily perpendicular to all depth contours. Second, a limited amount of cross-sections are not necessarily representative of the full inhomogeneous geometry of a flat. In this study, the integral method of *Strahler* (1952) is considered (originally developed for drainage basins), such that the full morphology of the flats is accounted for.

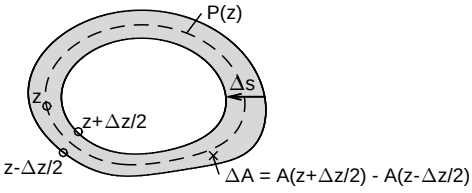

Figure 2.6: Illustration derivation bed slopes.

Strahler (1952) showed that the bed slopes of a digital elevation model are related to the derivative of the hypsometric curve and the length of the contour lines. Consider the decrease of the surface area ΔA between the contour lines, when the elevation level

increases from $z-\Delta z/2$ to $z+\Delta z/2$ (see Figure 2.6). In this study, a small value of 1 cm is used for Δz. This surface area decrease divided over $P(z)$, the length of the contour lines at z, results into the average horizontal shift of the contour line ($\Delta\bar{s}$):

$$\Delta\bar{s} = -\frac{\Delta A}{P(z)}. \tag{2.2}$$

With this average horizontal shift of the contour line, the integral bed slope at a certain bed level elevation can be evaluated as follows:

$$\frac{dz}{d\bar{s}} = \lim_{\Delta\bar{s}\to 0}\frac{\Delta z}{\Delta\bar{s}} = \lim_{\Delta A\to 0} -P(z)\frac{\Delta z}{\Delta A} = \lim_{\Delta A\to 0} -P(z)\frac{1}{\frac{\Delta A}{\Delta z}} = -P(z)\frac{1}{\frac{dA}{dz}}. \tag{2.3}$$

The derivative $\frac{dA}{dz}$ in this formulation is readily evaluated from the hypsometric function $A(z)$. The hypsometric function is slightly smoothed, with a moving average over a depth of 20 cm, to get to a proper derivative without local non-physical numerical steps. These are present as discrete bathymetric data is considered. The determination of the perimeter $P(z)$ is sensitive to the resolution of the bathymetric data and to noise in these data. Therefore, the digital elevation models are interpolated to the same 2 m × 2 m grid and smoothed with a Gaussian convolution filter (σ = 5 cells = 10 m, resulting average RMSD of 0.06 m). The derived perimeter represents the main geometry, instead of the noise (see Figure 2.7). This essential smoothing process affects the magnitude of the perimeter, and with that also the magnitude of the calculated bed slopes. Nevertheless, a comparison between the bed slopes of different tidal flats is robust, as precisely the same settings are used for all flats in all studied years. As the top of the flats are described by a small amount of data points, the upper 5% of the intertidal area are excluded from the analysis. Otherwise, inaccuracies in the small amount of data points dominate these results.

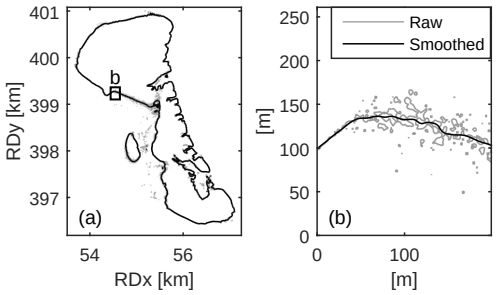

Figure 2.7: The MLW+0.5 m contour lines for the Galgeplaat (F11). Both the contour lines as calculated with the raw bathymetry data and as calculated with the smoothed data are presented.

2.4. RESULTS

2.4.1. PRESENT MORPHOLOGICAL STATE OF THE INTERTIDAL FLATS

To compare the intertidal areas between both systems, aggregated morphological changes of the intertidal flats during recent years are presented in Figure 2.8. This figure shows

the average height, total area and total volume of all studied flats for each estuary. The total area of the studied flats in the ES is 25% smaller compared to those in the WS. However, the larger tidal range in the WS causes the intertidal volume of the ES flats to be 75% smaller than the intertidal volume of the WS flats. This difference in intertidal volume is also due to the substantially lower flats in the ES. Figure 2.8 indicates the flats in the ES to be on average more than 0.75 m lower compared to the WS flats, with respect to NAP (Dutch Ordnance Level).

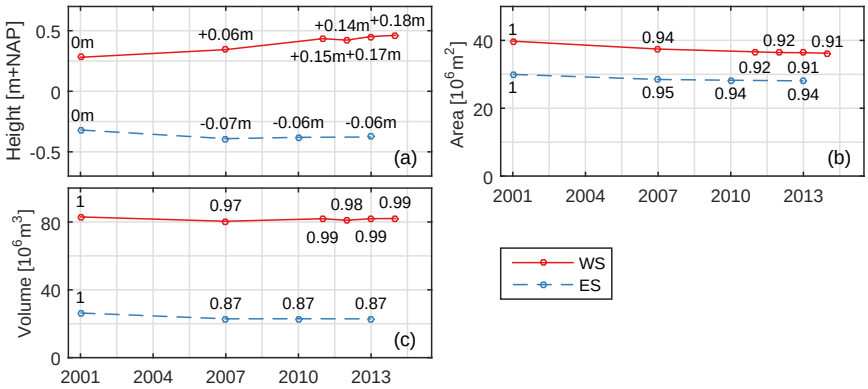

Figure 2.8: Recent changes of (a) the intertidal height, (b) the area and (c) the volume of the studied tidal flats in each estuary, based on the LiDAR data. The aggregated intertidal height is a weighted average, with respect to the area of each flat. The numbers in (a) indicate the absolute changes whereas the numbers in (b) and (c) show the changes relative to the initial (2001) values.

Figure 2.8 also shows the recent changes over time of the intertidal tidal flats in both estuaries. Although the tidal flats in the WS have mainly increased in elevation, the intertidal volume of these flats has remained more or less constant as the intertidal area was reduced at the same time (i.e., a general steepening of the hypsometry of the intertidal flats). Over these years, the ES has faced substantial intertidal sand losses, indicated also by the decrease of the average height and area of its intertidal flats. Although previous studies did not define the tidal flats with respect to the local tidal range, the lowering of the flats in the ES, and the heightening of the flats in the WS, are in line with the findings of *Louters et al.* (1998) and *Cleveringa* (2013). The data indicates that the heightening of the flats in the WS appeared to be fairly linear, whereas the full change in the bulk parameters for the ES appeared during the first half of the considered period. Nevertheless, it is hardly possible to draw conclusions on the morphological evolution with such a limited amount of data points.

The geometry and evolution of the individual intertidal flats are of interest, to reveal the similarities and differences between the flats. For this purpose, Figure 2.9 presents the hypsometric curves for each flat studied. These curves indicate the total area of each intertidal flat and how this area is distributed over the elevation of these flats. A large diversity in the geometry is evident. Some of the hypsometric curves appear to be fully concave-up, some are fully convex-up and others are a combination of both. However, the shape of these curves does not provide direct insight into the shape of the bed pro-

files, as the shape of the hypsometric curves should be corrected for the perimeter variation over depth first (Equation 2.3). Apart from Ossenisse (F7) and Walsoorden (F8), the height of the flats with respect to NAP reduces with the distance from the mouth of the estuaries.

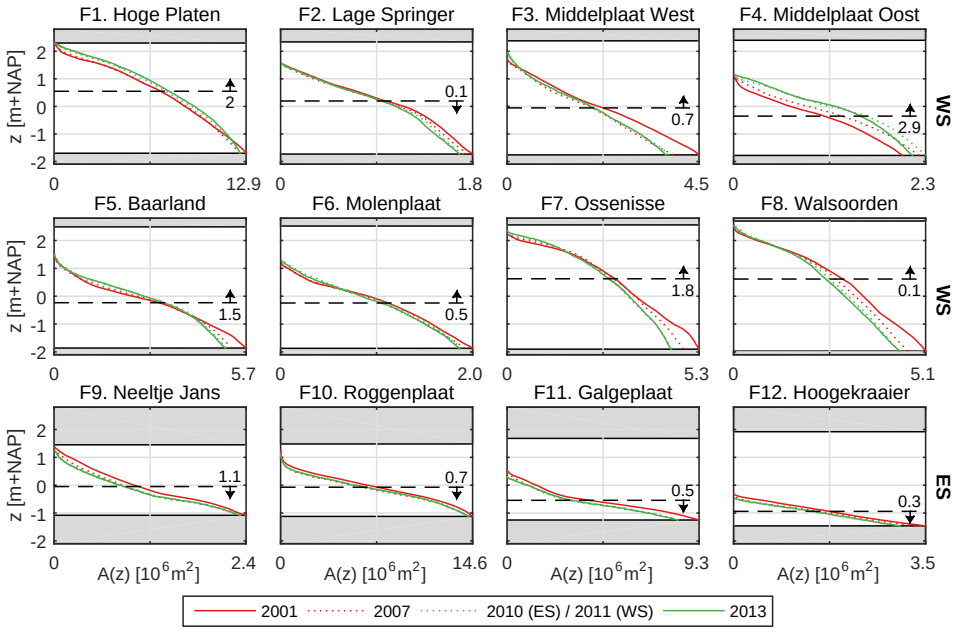

Figure 2.9: Comparison of the hypsometric curves between MLW and MHW for the eight tidal flats in the WS and the four flats in the ES (ordered with increasing distance from the mouth) based on the LiDAR data. The gray areas indicate the elevations outside of the mean tidal range. The horizontal dashed lines illustrate the average height of each intertidal flat in 2001. The arrow indicates whether the average height increased or decreased from 2001 to 2013, the number next this arrow expresses the average change in average height of the flat per year in centimeters. The 2012 and 2014 data of the WS are not considered in this figure, to enhance readability.

Apart from the relatively small Lage Springer (F2), all the flats in the WS have been rising over these years. This is in contrast to the trend in the ES, where the flats have been lowering consistently. The almost uniform decrease of the hypsometric curves in the ES indicates that the flats in the ES have been lowering over the full vertical range of the flats. In the WS, a comparable uniform, but opposing, vertical shift of the hypsometric curve was present for Hoge Platen (F1) and Middelplaat Oost (F4). For other flats in the WS, a reduction of the area at MLW in combination with a heightening of the higher parts of the flats, indicates a steepening of the hypsometric curves. The evolution of Lage Springer (F2) and Walsoorden (F8) illustrates that an almost constant average height does not necessarily imply a flat to be in equilibrium, as the decrease in area was still substantial for both flats. This illustrates the importance to analyze the various bulk properties simultaneously.

Although the shape of the hypsometric curves provides insight in the geometry of the flats, these curves should be combined with their perimeters to result in an actual

representation of the bed slopes, as discussed in Section 2.3. The integral bed slopes for the 2013 LiDAR data are provided in Figure 2.10 over the full tidal range, for each estuary. Generally, milder bed slopes are found at higher elevations. Apart from some fluctuations at the lower elevations, the integral bed slopes appear to be approximately linearly decreasing with the bed level elevation (i.e., bed profiles are on average convex-up). A clear distinction is visible between the flats in the ES and those in the WS: the flats in the ES are substantially flatter compared to the WS flats. The difference in steepness between the flats in the two estuaries is more than 50% around NAP+0 m (roughly MWL). At the same time, there are differences between the intertidal areas of each estuary. The flattest of all these intertidal areas is Hoogekraaier (F12), which is also the lowest one (Figure 2.9). Consistently, the steepest of the flats, Ossenisse (F7) and Walsoorden (F8), are also the highest ones. These two steepest flats were the only flats opposing the relation between the height of the flats and the distances from the mouth of each estuary.

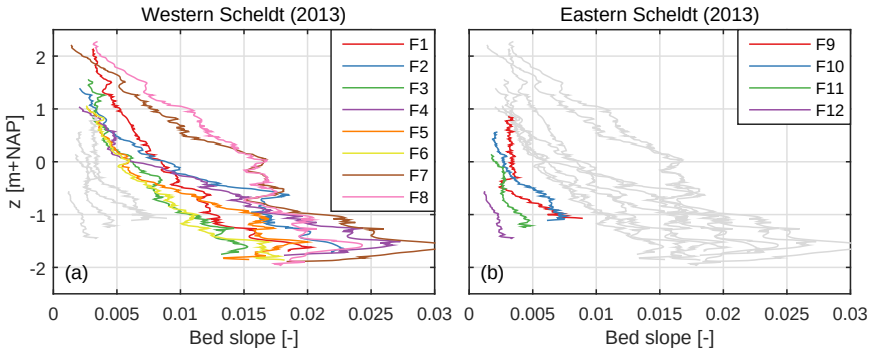

Figure 2.10: The integral bed slopes for (a) the WS and (b) the ES, based on the 2013 LiDAR dataset. In each figure, the flats of the other estuary are plotted in light gray. Details of the derivation are provided in Section 2.3.

2.4.2. LONG-TERM MORPHOLOGICAL CHANGES

As the LiDAR data have been measured only since 2001, the lower resolution Vaklodingen dataset is studied to assess the long-term tendency of the flats. The tidal range is considered constant over time in the long-term analyses, by using the spatial distribution of Figure 2.4a. With this approach, the focus of this study is on the pure morphological changes, and not on the influence of changes in tidal range on the bulk parameters. Figure 2.11 provides the evolution of the average height, area and volume for the WS flats over a measurement period of 59 years (1955–2013), and for the ES flats over a measurement period of 45 years (1968–2013). As Walsoorden (F8) was merged with the mainland in the past, this flat is considered only after 1989. The substantial changes of the bulk parameters of the WS flats, measured on average once every 1.8 years, indicate that the long-term changes exceed the inaccuracies of the data (which is in the order of 10 cm, see Section 2.2.1). In contrast, the ES data should be analyzed with more restraint as the maximum changes in bulk parameters are closer to the order of magnitude of the measurement errors. As well as these were measured on a substantially larger average interval of 5.5 years, providing a maximum of eight points over time per flat.

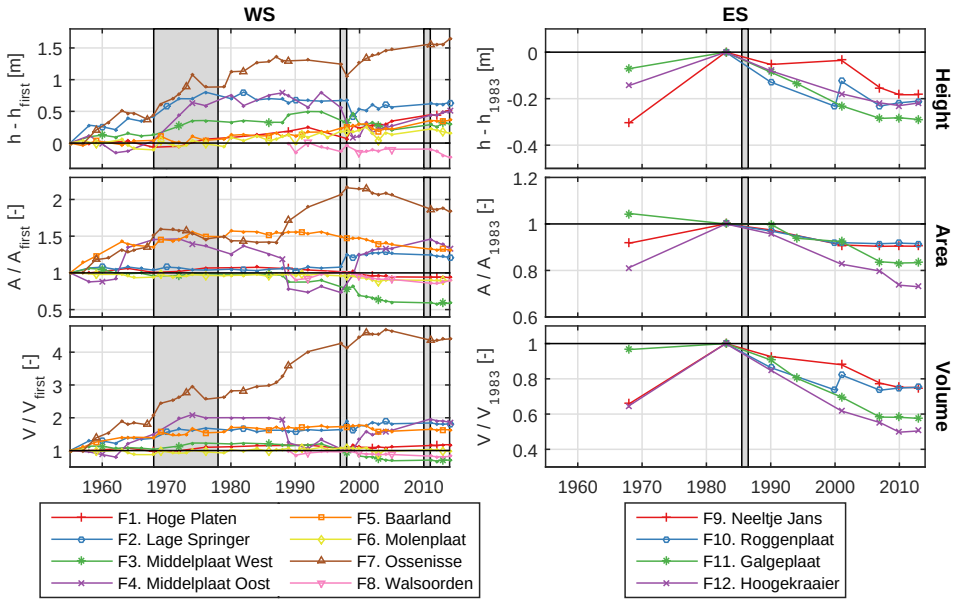

Figure 2.11: Long-term changes of the average height, area and volume of all studied flats of each estuary as derived from the Vaklodingen dataset. For the WS, the data are presented relative to the first measurement year: 1989 for Walsoorden (F8) and around 1955 for all other flats. The data in the ES is presented relative to the last measurement year before the completion of the storm surge barrier (1983). The vertical gray boxes on the background indicate the deepening projects in the WS and the completion of the storm surge barrier of the ES.

These long-term data indicate that the flats in the WS, especially the large Hoge Platen (F1) and Ossenisse (F7), have increased in height fairly monotonically after 2001 (also in accordance with Figure 2.8). However, this continuous tendency does not hold for all other flats in the estuary. For example, Molenplaat (F6) and Walsoorden (F8) lowered over four succeeding years after the third deepening project (2010). If the full measurement period is considered, the average height, area and volume fluctuated over time for almost all flats. For Ossenisse (F7), one of the most dynamic flats, these bulk quantities faced a substantial net increase over time, despite the fluctuations. Over this period, the intertidal volume of this flat has increased up to 430% of its original value. In contrast, the area and volume of Middelplaat Oost (F4) fluctuated around an almost constant value. Figure 2.11 indicates that these fluctuations could be related to the deepening projects of the WS, as these coincide with some of the major changes in the trends, especially around the second deepening project. Nevertheless, this is not the case for all the flats and there were also other activities ongoing over these 59 years (e.g., dredging and dumping projects). Especially around the flats with sudden changes in area and volume (Middelplaat Oost (F4) and Ossenisse (F7)) there were frequently dredging and dumping activities. Despite the non-uniform long-term evolution of the WS flats, the aggregated average intertidal height, weighted with respect to the area of each flat, increased from NAP-0.12 m around 1955 to NAP+0.45 m in 2014. This implies an average

increase in height of almost 1 cm per year. The mean absolute deviation of the average heightening rate between the flats equals to 0.5 cm per year.

A clear change in the trend of the evolution of the ES flats are indicated by the results. Before the completion of the storm surge barrier, all flats for which data is available increased in height. Although this is supported by just two measurement points for each flat, the observed changes are substantial: an heightening up to 0.3 m for Neeltje Jans (F9). After the barrier was completed, all flats in the ES faced net erosion. For Galgeplaat (F11) and Hoogekraaier (F12), the bulk parameters changed quite continuously, whereas this is not the case for Neeltje Jans (F9) and Roggenplaat (F10). The latter could be caused by inaccuracies of the historical data, as the morphological changes are in the order of the measurement error. If all ES flats are aggregated, the data indicates a net lowering from NAP-0.17 m in 1983 to NAP-0.38 in 2013, which equals to an average lowering rate of 0.7 cm per year. This lowering coincided with a net decrease in the volume of the flats (25–50%) which was substantially larger than the net decrease of area of the flats (9–27%). As also indicated by Figure 2.8, the changes in the bulk parameters over the recent years (2007–2013) was small compared to the changes in the past.

Three of the studied flats contain a substantial amount of frequently measured cross-sections: Neeltje Jans (F9), Roggenplaat (F10) and Galgeplaat (F11). By the relatively limited amount of Vaklodingen data in the Eastern Scheldt, 7–8 measured years per flat, these are a valuable addition for insights on the temporal changes. The evolution of the average height of the cross-sections of each flat are presented in Figure 2.12. The mismatch in the average height between the Vaklodingen data and the average height of the cross-sections is because the elevation of the cross-sections is not necessarily representative of the full intertidal area. For example, the Neeltje Jans (F9) cross-sections are located on the low parts of the flat. Nevertheless, the cross-sectional data indicates that the period of negligible changes of the average height between 2007 and 2013, as observed with the Vaklodingen dataset (Figure 2.11), was probably not a measurement artefact. Especially for a large proportion of the cross-sections at the Roggenplaat (F10) (profiles 3–6), a change in trend is visible around 2007. Before 2007, an almost linear lowering of the average height appeared for these profiles, whereas their average height was fairly constant afterwards. The constant average heights of the profiles do not imply that the Roggenplaat (F10) did not erode locally, e.g., horizontally propagating bed forms were still present. However, they do indicate that the net differences between erosion and accretion reduced over time.

The evolution of the bulk parameters (i.e., average height, volume and area) of the flats do not provide direct insight on the evolution of their hypsometry. To this extent, Figure 2.13 presents the evolution of the area of each height class over time (i.e., discretized hypsometric curves). In line with the observations related to Figure 2.9, a diverse behavior of the flats is present. Hoogekraaier (F12) is a good example of a flat of which the hypsometry lowered almost uniformly after the completion of the storm surge barrier. In contrast, Molenplaat (F6) faced a slight reduction of the total intertidal area since 1955, whereas the highest heightclasses showed a contrary increase in area. Based on this figure, the sudden changes of Middelplaat Oost (F4) could better be understood. The reduction of the intertidal area just before 1990 did not change the average height of the flat as all height classes faced a more or less similar decrease, whereas the average

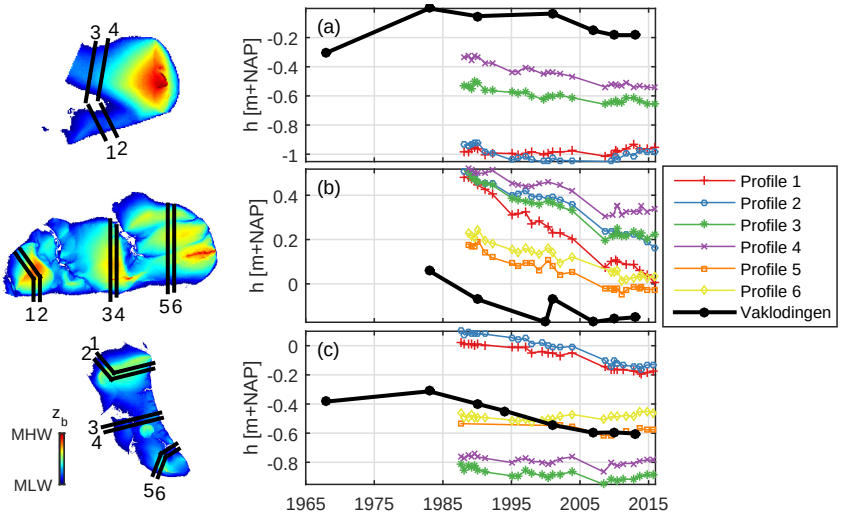

Figure 2.12: Comparison of the height evolution between the Vaklodingen dataset and the cross-section data for (a) Neeltje Jans (F9), (b) Roggenplaat (F10) and (c) Galgeplaat (F11). Measurement campaigns that covered only a small part of the cross-sections are not considered, and only the parts of cross-sections that were measured in all considered years are taken into account. The positions of the cross-section profiles are indicated on the accompanying maps, which are not on scale (see Figure 2.2).

height decreased just before 2000 by an increase of the low elevations and a decrease of the high elevations of the flat. The latter is evidence for the non-uniformity of the morphological changes of an individual flat at different elevations.

The long-term evolution of the integral bed slopes is presented in Figure 2.14. Clearly, the steepness of the flats did not evolve monotonous over time. Within a decade, the integral bed slope could halve or double. Especially for the morphologically active Middelplaat Oost (F4) and Ossenisse (F7), the vertical profiles of the integral bed slopes have been highly variable over time. Certainly, those two flats steepened over the past decade. The other intertidal flats in the WS did not show such a strong increase in steepness over this period, or even a slight flattening (e.g., Molenplaat (F6)). The bed slopes did not change necessarily uniformly over depth. For example, the lower part of Ossenisse (F7) steepened over the past decade, whereas the higher regions of the flat remained more or less unchanged. Based on the vertical diversity in the changes of the bed slopes and on the fluctuations in the bed slopes over the past 59 years, the intertidal flats in the WS could not be classified as purely steepening flats. After the construction of the storm surge barrier, especially the lower regions of the ES flats flattened slightly. Nevertheless, the flats in ES were already substantially milder than those in the WS before the construction of the storm surge barrier.

The vertical shift of a certain integral bed slope corresponded, at least roughly, with the change of the average height of these flats. This indicates that the time scales of these indicators are related to each other. Further, Figure 2.10 suggests that also the absolute value of the steepness might be related to the absolute value of the height of a flat, as the steepest flats corresponded to the highest ones, and vice versa. To test this relation,

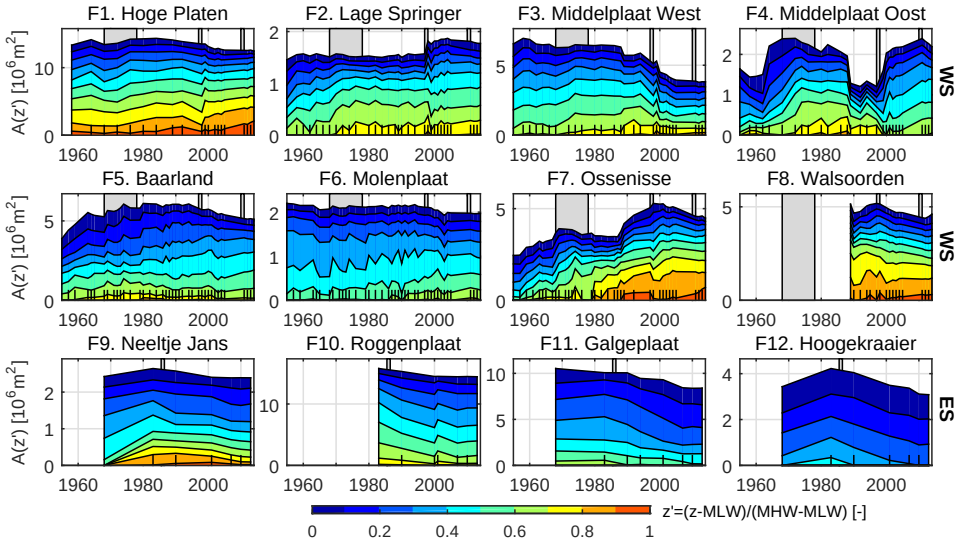

Figure 2.13: Evolution of each height class per flat over time as calculated with the Vaklodingen dataset. The height classes are relative to the tidal range (MHW: z' = 1, MLW: z' = 0). The vertical gray boxes on the background indicate the deepening projects in the WS and the completion of the storm surge barrier of the ES.

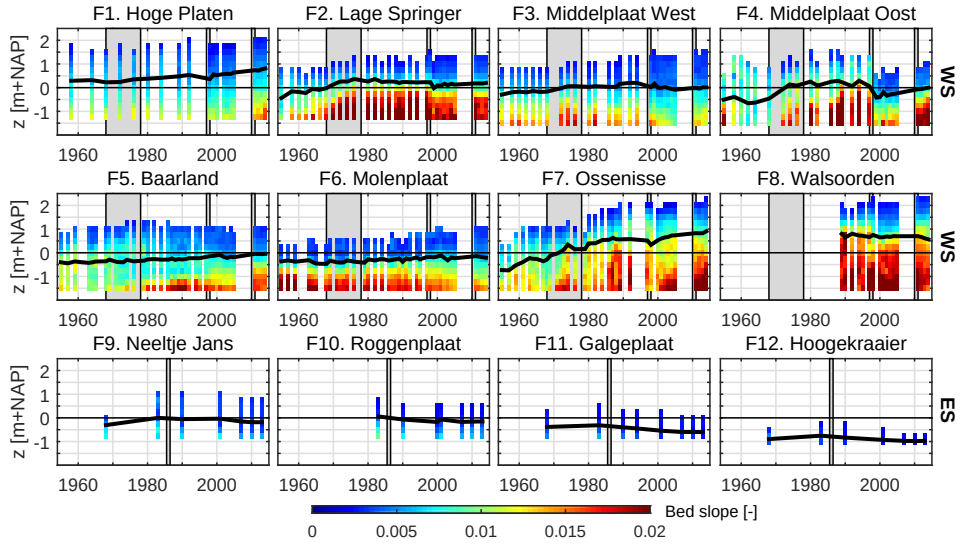

Figure 2.14: Integral bed slope of the tidal flats over time, as calculated with the Vaklodingen dataset. The black line indicates the average height of the intertidal area. Bed slopes could be steeper than 0.02 (e.g., Figure 2.10), but are limited in this figure to this value to distinguish also some of the vertical variation of the relatively mild ES flats. The vertical gray boxes on the background indicate the deepening projects in the WS and the completion of the storm surge barrier of the ES.

Figure 2.15 compares the height of the intertidal areas above MLW with the bed slopes at MWL. These variables are found to be significantly correlated. This relation is not necessarily linear, as a better fit could be achieved by allowing more degrees of freedom. Further, this relation holds for a great variety of reference levels. However, at the high and low elevations, this relation is not significant, which might be explained by a small amount of intertidal flats covering these elevation levels.

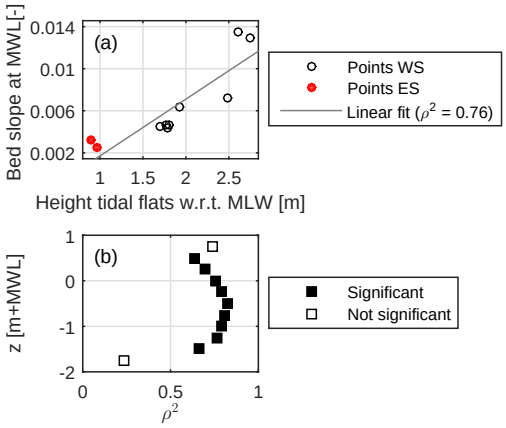

Figure 2.15: The relation between the integral bed slope and the height of the intertidal areas for the 2013 LiDAR data: (a) at MWL; (b) at various other reference levels. The amount of flats with a bed slope calculated at a certain reference level varies as the tidal range differs per flat. Only reference levels with at least 5 data points are taken into account. A relation is considered as significant if the null hypothesis of no correlation can be rejected with a probability of 99% or more (t-test).

2.5. DISCUSSION

2.5.1. LIMITATIONS OF THE INDICATORS FOR THE MORPHOLOGY

Various indicators can be used to express the geometrical state of an intertidal flat: the volume, area, average height and integral steepness of these areas. The local variability is lost with these indicators, as they aggregate the full geometry of an intertidal flat. However, the profile of the flats can be substantially different at zones exposed to waves compared to sheltered ones (*Friedrichs*, 2011). For example, Figure 2.16 indicates some of the spatial inhomogeneity around Galgeplaat (F11). At the northern cross-section (a), a locally concave-up profile has been formed, being evidence for an increased importance of waves (in line with *Friedrichs*, 2011). Such a concave-up profile formation was not visible at the southern cross-section (c), where the wind fetch is much shorter. Still, valuable insights have been achieved into the general morphological trends of the intertidal flats in the ES and WS, by analyzing trends in these aggregating indicators. In particular since a robust inter-comparison is possible with these indicators, which could not be derived from a limited amount of cross-sections at arbitrary locations. As the different indicators could show completely different tendencies (e.g., Figure 2.11), they should be considered simultaneously to properly account for the morphological changes.

Defining a robust estimate for "the" height of an intertidal area is not trivial. Sim-

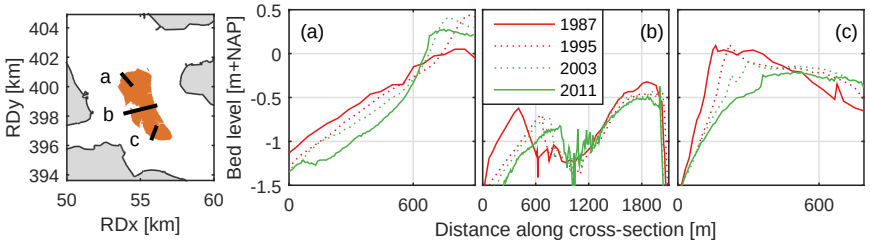

Figure 2.16: RTK-dGPS cross-section data at Galgeplaat (F11) shown over a uniform eight year interval. The distances along the cross-sections are with respect to the most western point of each cross-section.

ply considering the highest bed level elevation of a flat is undesirable, as it is doubtful how representative that single value is for the full intertidal area. Furthermore, the measurement method and resolution could affect this value substantially. Instead, this study considered the average height of a tidal flat, by dividing the total sediment volume between MLW and MHW by the area of the intertidal region, as expressed with Equation 2.1. However, an intertidal area does not necessarily shift uniformly in the vertical plane (Figures 2.9 and 2.13). By pure erosion around MLW, the area of the low region of a flat will reduce, causing the average height to increase (e.g., Middelplaat West (F3) in Figure 2.9). Based on these considerations, the average height of the intertidal flat should be considered as an indicator for the vertical distribution of the sediment volume, not as a direct representation of the top of the flat.

The tidal range is kept constant over time in the analyses, to allow a direct comparison of the morphology between the different years. This has no implications for the evolution of the bed slope over time, as these are calculated with respect to a fixed reference frame (NAP). However, the area and volume estimates depend directly on the considered tidal range. As the tidal range in the WS was smaller in the past (*Van den Berg et al.*, 1996), the area and volume of the intertidal flats are slightly overestimated for these past years. These quantities are underestimated in the ES for the years before the completion of the storm surge barrier, as this barrier reduced the tidal range substantially.

2.5.2. RELATION BETWEEN HEIGHT AND STEEPNESS OF INTERTIDAL AREAS

The relation between the height of the intertidal areas and their steepness, as suggested by Figure 2.15, should not be considered as a universal law. For instance, a flattening of the lower zone of Molenplaat (F6) did not coincide with an average lowering of this flat. Still, this relation appeared to be a good indicator for many flats. Figure 2.17a illustrates this relation to satisfy the geometrical extremes: a flat with an extremely high average intertidal height (almost MHW) will be almost infinitely steep as hardly any bed level elevations are between MLW and MHW, whereas an extremely low intertidal flat (i.e., average height just above MLW) would be extremely mild. Furthermore, a homogeneous lowering of an idealized convex-up (e.g., parabolic) tidal flat, with its top below the MHW level, would induce a flattening of the bed at all elevations (see Figure 2.17b). Such a vertical translation in the bed slope profile is not that unrealistic for real world flats (e.g.,

Figure 2.14). At certain elevations, the bed slope might flatten less (or even steepen), if the shape of the flat changes. Nevertheless, the bed slope has to decrease at least at some elevations to satisfy the geometrical constraint of a horizontal top of the intertidal area. Therefore, the lowering of a flat should coincide with at least some flattening of an intertidal area, and the heightening with at least some steepening.

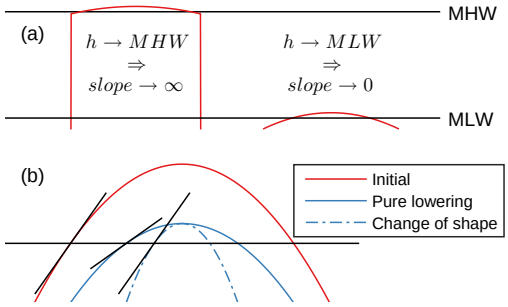

Figure 2.17: Cross-sections of idealized tidal flats to illustrate: (a) the relation of the extremes of the average height of a flat with the extremes of the bed slopes and (b) the reduced bed slope caused by the lowering of tidal flats.

With the presence of channels nearby intertidal areas, a horizontal expansion of an accretive tidal flat could be counteracted by the transport capacity of those channels. For an intertidal area which is located closely to a channel, such as Ossenisse (F7), the flat could only increase in volume by a steepening, a migration of the side of the channel or a combination of both. If such a migration is not possible, only a steepening allows those horizontally constraint tidal flats to increase in volume (i.e., heighten).

2.5.3. DIFFERENCES IN MORPHOLOGICAL DEVELOPMENT BETWEEN THE EASTERN SCHELDT AND WESTERN SCHELDT

The differences in morphological evolution between the intertidal flats of both systems are probably related to the differences in hydrodynamic forcing. This hypothesis is strengthened by the fact that the intertidal areas in the ES were in a dynamic equilibrium or even slightly heightening before the construction of the storm surge barrier (*Mulder and Louters*, 1994; *Louters et al.*, 1998). After the construction of this barrier, the intertidal areas of the ES have been eroding strongly (Figure 2.11). This change in trend is most likely related to changes in hydrodynamics imposed by the barrier.

Figure 2.4b presents a spatial overview of the depth-averaged flow velocities in both estuaries. The flow velocities in the main channels of the WS are significantly larger than those in the ES. There are various reasons for the differences in flow velocities. First, the flow velocities in the ES are reduced by the presence of the storm surge barrier and compartment dams (*Louters et al.*, 1998; *Eelkema et al.*, 2009). The tide propagates far upstream in the River Scheldt, whereas the tidal propagation in the ES is limited by the closure of its branches (i.e., limited tidal prism). Second, the substantially larger tidal range in the WS (see Figure 2.4a) implies a relatively larger ebb/flood volume.

Comparing the wave forcing between both estuaries is challenging, as the wave characteristics depend highly on the considered wave climate. We expect the waves in both

systems to be mainly generated locally, as the geometry of the WS and the presence of the storm surge barrier in the ES do not allow sea waves to propagate deeply into the estuaries. Within the estuaries, there is a variability of the wave energy by a natural inhomogeneity in local fetch. This inhomogeneity causes also a variation in the wave climate at different sides of a tidal flat, which could therefore evolve differently (e.g., Figure 2.16). However, both estuaries contain flats with a relatively large fetch and flats with a relatively short fetch, as the ES and WS have a similar geometry. Furthermore, the wind climate in both estuaries is comparable (see Figure 2.3). Therefore, the wave forcing on itself is not considered as the explanatory variable for the differences observed in the evolution of the flats between the two estuaries.

Based on these considerations, the tidal flow with respect to the wave forcing is relatively large in the WS and relatively small in the ES. A relatively large tidal forcing is in line with increased deposition on the tidal flats, whereas increased wave forcing coincides with increased erosion (*Friedrichs*, 2011; *Green and Coco*, 2014). Therefore, this theoretical insight supports the suggestion that the differences in morphological response between both estuaries are closely related to the differences in flow velocities.

For a more detailed understanding of the changes of the intertidal flats in both estuaries, more research on the local characteristics of individual flats is required. Besides the considered processes, also the net import/export of sediment for an estuary (*De Vriend et al.*, 2011; *Yang et al.*, 2006), the seasonal variability of mud content (*Pethick*, 1996) and the differences in sediment characteristics play a role in these changes. These have not been included in this study as a robust inter-comparison between individual flats becomes less trivial.

2.5.4. FUTURE FATE OF THE INTERTIDAL AREAS

The data analyzed in this chapter provided various insights on the historical evolution of the considered intertidal areas. Although the future changes of the tidal flats are not necessarily a simple extrapolation of the historical evolution, valuable considerations can be drawn by combining the insights from the historical evolution with expected future conditions (e.g., sea level rise).

With ongoing human interference, both systems are expected to evolve toward a new equilibrium (*De Vriend et al.*, 2011; *Wang et al.*, 2015). This is thought to be a dynamic equilibrium as changes in the hydrodynamic forcing are ongoing. In this study, the tidal datums are considered to be constant over time. However, in reality these tidal datums are affected by sea level rise (*Mawdsley et al.*, 2015) and dredging activities (*Kuijper and Lescinski*, 2013). *Mawdsley et al.* (2015) indicate that the MLW and MHW datums do not change necessarily with the same rate and direction as the mean sea level. With the uncertainty of future sea level rise rates and the complexity of the spatial inhomogeneity of the changes of the tidal datums, the temporal changes of the datums are not considered in this study.

No simple linear relations could describe the evolution of the intertidal flats in the WS on the time scale of half a century (see Figure 2.11). Still, the flats in the WS increased in height on average almost 1 cm per year over this period, which is substantially larger than the faced sea level rise rate. As the fairly high Hoge Platen (F1) has still been rising substantially over past years (see Figure 2.9), there is no indication that the heightening

of the flats in the WS will be limited in the near future. In fact, marsh vegetation could establish on the high intertidal elevations (*Kirby*, 2000), which will increase the resistance against erosion (*Eerdt*, 1985). Hoge Platen (F1) is an example of a flat in the WS on which vegetation is expanding rapidly over recent years. If the heightening coincides with a steepening of the flats, the natural habitats are expected to impoverish even further (*De Jong and De Jonge*, 1995).

Although the long-term data in the ES is scarce, there is strong evidence for a consistent lowering of the flats (in line with *Louters et al.*, 1998). Figure 2.11 indicates that the erosion of the intertidal areas started directly after the completion of the storm surge barrier, with an average rate of approximately 0.7 cm per year. An important difference with the continuous dredging activities in the WS is the almost instantaneous introduction of the human interventions to the ES. Consequently, the lowering rate of the flats in the ES might eventually decrease when the intertidal areas approach an equilibrium height (also argued by *Louters et al.*, 1998). The most recent data indicates a slight change in trend of the average height evolution after 2007 in both the Vaklodingen data as in many of the more frequently measured cross-sections. However, future measurements should reveal whether a long-term equilibrium of the bulk quantities is approached, and if those flats are able to cope with sea level rise.

2.6. SUMMARY AND CONCLUSIONS

This chapter has analyzed the present state and long-term development of the intertidal areas in the ES and WS based on robustly defined bulk parameters. The flats in the WS are identified as substantially higher and steeper compared to those in the ES. None of the studied intertidal flats is found to be in a static equilibrium. The differences in the morphology of the flats between both estuaries increased over the past decades, by rising flats in the WS and lowering flats in the ES. Over the past 59 years, the flats in the WS did not change monotonously: the area, volume and average height of those flats fluctuated substantially. Still, the average height of the WS flats increased with 1 cm per year on average over this period. In the ES, a change in trend is observed. The considered flats lowered with an average rate of 0.7 cm per year after the completion of the storm surge barrier, despite the recently reduced erosion rates.

A larger steepness of intertidal flats has been related to a larger average height. This relation appeared not only from the present state of the intertidal flats, but was also observed in the change of the bed slopes of individual flats over time. Although there is evidence for steepening flats in the WS and flattening flats in the ES, not all flats changed with this tendency, and the changes in steepness were not necessarily uniform over depth.

The differences in tidal flow velocities between the ES and WS, for a substantial part caused by human interventions, are thought to explain an important part of the opposed morphological developments of the intertidal areas between both estuaries. It is expected that the observed morphological changes in the WS will continue. However, the recently reduced erosion rates of the flats in the ES could indicate the approach of an equilibrium.

Chapter 3

The Importance of Combined Tidal and Meteorological Forces for the Flow and Sediment Transport on Intertidal Shoals

This chapter has been published as:
Journal of Geophysical Research: Earth Surface (*De Vet et al.*, 2018),
co-authors: Van Prooijen, Schrijvershof, Van der Werf, Ysebaert, Schrijver, and Wang.

Cover photo: the moon, one of the driving forces of the tidal flow. Photo was taken during the full lunar eclipse of 21 January 2019.

Natural processes substantially shape, also in engineered estuaries, the morphodynamics of intertidal flats. This chapter aims to unravel the relative importance of tidal and meteorological processes for hydrodynamics and sediment transport on an intertidal flat. The effects of the processes are revealed through numerical model simulations of the Roggenplaat intertidal shoal. This is the largest intertidal shoal of the Eastern Scheldt, of which the morphological evolution was studied in Chapter 2. A special focus is placed on the spatiotemporal variations in the forcing processes and a quantification of the effect of wind on the flow.

Abstract

Estuarine intertidal areas are shaped by combined astronomical and meteorological forces. This chapter reveals the relative importance of tide, surge, wind, and waves for the flow and sediment transport on large intertidal shoals. Results of an intensive field campaign have been used to validate a numerical model of the Roggenplaat intertidal shoal in the Eastern Scheldt Estuary, the Netherlands, in order to identify and quantify the importance of each of the processes over time and space. We show that its main tidal creeks are not the cause for the dominant direction of the net flow on the shoal. The tidal flow over the shoal is steered by the water level differences between the surrounding channels. Also, during wind events, the tidal flow (enhanced by surge) is dominant in the creeks. In contrast, wind speeds of order 40 times the typical tidal flow velocity are sufficient to completely alter the flow direction and magnitude on an intertidal shoal. This has significant consequences for the sediment transport patterns. Apart from the wind-driven flow dominance during these events, the wind also increases the bed shear stress by waves. For the largest intertidal part of the Roggenplaat, only ~1–10% of the yearly transport results from the 50% least windy tides, even if the shoal is artificially lowered half the tidal range. This dominance of energetic meteorological conditions in the transports matches with field observations, in which the migration of the creeks and high parts of the shoal are in line with the predominant wind direction.

3.1. INTRODUCTION

Estuarine intertidal shoals are shaped by a combination of different hydrodynamic forces that vary significantly over time and space. Tidal forcing is generally considered as the most important process for intertidal areas, as it imposes variations in water level and velocity (*Le Hir et al.*, 2000). Wind induces a setup or setdown of the water level, a local shear at the surface, and surface waves. All these effects modify the flow and sediment transport rates and are especially effective for (very) shallow water conditions (*Talke and Stacey*, 2008; *Green and Coco*, 2014; *Shi et al.*, 2017). Furthermore, bathymetric variations on the intertidal flat and the geometry of the surrounding channels also influence the hydrodynamics. So far, it has been studied insufficiently to what extent each of these mechanisms is dominant for the hydrodynamics and sediment transport of intertidal shoals surrounded by channels.

Intertidal areas can be attached to the shore (fringing flats). For example, the Chongming intertidal flats in the Yangtze Estuary, China (*Yang et al.*, 2001; *Zhu et al.*, 2017), the flats in San Francisco Bay, United States (*Talke and Stacey*, 2008; *Van der Wegen et al.*, 2017), and Baie de Marennes-Oléron, France (*Bassoullet et al.*, 2000; *Le Hir et al.*, 2000). The attachment to the shore has significant consequences for the tidal flow. Especially cross-shore flows are limited by the closed boundary. Those limitations of the flow do not exist for intertidal shoals surrounded by channels, as the water could theoretically flow in any direction. Intertidal shoals are found in estuaries worldwide like the Eastern Scheldt and Western Scheldt, the Netherlands (Chapter 2; *Van den Berg*, 1984; *Van den Berg et al.*, 1996; *De Vet et al.*, 2017), Yangtze Estuary, China (*Gao et al.*, 2010; *Wei et al.*, 2016), Wadden Sea, the Netherlands (*Elias et al.*, 2012), and Columbia River Estuary, United States (*Sherwood et al.*, 1990). Intertidal shoals surrounded by channels have not been measured as often as fringing flats, possibly because intertidal shoals surrounded by channels are more difficult to access.

There is a growing need for deeper understanding of the hydrodynamics and sediment transport on intertidal shoals, as these areas provide a high ecological value (*Smaal and Nienhuis*, 1992) and support important ecosystem services (*Barbier et al.*, 2011). To understand the shoals surrounded by channels, complex models, covering the full geometry of the intertidal shoal and its surroundings, need to be applied (*Lettmann et al.*, 2009; *Luan et al.*, 2017). Despite the geometrical differences with fringing flats, the insights on intertidal shoals also benefit the understanding of intertidal areas in general.

However, the processes relevant for intertidal shoals surrounded by channels are not always well resolved. Even in recent modeling studies on the morphodynamics of estuarine shoals, wind and waves are not always included (e.g., *Dam et al.*, 2016; *Van de Lageweg and Feldman*, 2018). The inclusion of these processes adds complexity and demands large computational power if the full wind climate and nonidealized geometry are considered (e.g., 118 computational cores in the study of *Becherer et al.*, 2018). Also, (very) high resolution data (in the order of 10 m) are needed to capture the small-scale bathymetry features like local elevation differences and tidal creeks. Such tidal creeks are an essential part of the (de)watering system of intertidal areas and are ecologically valuable (*Mallin and Lewitus*, 2004). *Eisma* (1998) provided a classification of tidal creeks. In many cases, tidal creeks are connected to marsh channels, but a presence of a marsh is not a requirement for the existence of a tidal creek. Although tidal creeks are

no full cross-connecting channels, they have similarities. Just as cross-connecting channels (*Swinkels et al.*, 2009), tidal creeks can be affected by flows induced by water level gradients between the surrounding channels (*Van den Berg*, 1986).

This study identifies and assesses the relative importance of the tide, surge, wind, and waves for hydrodynamics and sediment transport on intertidal shoals surrounded by channels. Furthermore, we identify to what extent the flow patterns on such a shoal are driven by its local elevation differences, its tidal creeks and its surrounding channels. The Roggenplaat, a shoal in the Eastern Scheldt in the Netherlands, is considered as a case. We combine an extensive field campaign, containing 16 Acoustic Doppler Current Profilers (ADCPs), with a numerical model. Instead of modeling the long-term evolution with a prerequisite low resolution, we use a high-resolution (grid size 30 m) model schematization to unravel the hydrodynamic and sediment transport processes from a single tide to a full year. We use elevation data with a high horizontal resolution (< 10 m) such that also the major creeks are well resolved. The different contributions of the processes are unraveled by systematically switching on and off specific processes in the simulations. First, the focus is on the implications on the hydrodynamics. Second, the implications on the sediment transport rates are considered. Finally, the results are extended toward general indicators for intertidal shoals.

3.2. METHODOLOGY

3.2.1. DESCRIPTION OF ROGGENPLAAT INTERTIDAL SHOAL

The Roggenplaat, located in the southwest of the Netherlands in the Eastern Scheldt basin (Figure 3.1a), is an example of a major intertidal shoal surrounded by channels. With an intertidal surface area of 14.6 million m^2, it is the largest intertidal shoal of the Eastern Scheldt. The Roggenplaat is a valuable case to analyze the importance of the different processes, as an extensive data set on morphology and hydrodynamics exists. Two channels surround the shoal; the northern channel is substantially longer and deeper than the southern one (Figure 3.1f). The Eastern Scheldt is characterized by a typical tidal range of 2.5 m near the mouth, which amplifies up to 3.5 m in the southeast branch of the basin (Chapter 2; *De Vet et al.*, 2017). As the branches of the estuary are closed, there is no river inflow. Around the Roggenplaat, MLW (Mean Low Water) equals MSL-1.2 m (MSL = Mean Sea Level) and MHW (Mean High Water) equals MSL+1.3 m. The surge within this area is 50% of the time between -0.11 m and +0.14 m, but can extend for severe storms to -1 or +1.5 m (2015 data). Typically, the timescale of such an intense surge is 1 day. The shoal is sandy with a median sediment grain size of 210 ± 2.5 μm (n=150), with less than 5% silt (<63 μm) at most locations. Oyster patches (*Crassostrea gigas*) cover 3% (45 ha) of the Roggenplaat. Around these patches more silty sediments are found. After the completion of the storm surge barrier (SSB in Figure 3.1) and the closure of the branches of the estuary in 1986, the previously accreting Roggenplaat faced severe erosion due to reduced tidal flow within the estuary (Chapter 2; *Louters et al.*, 1998; *De Vet et al.*, 2017). This is a possible threat to the nature value of this Natura 2000 estuary (*Ostermann*, 1998).

Figure 3.2 indicates the changes in the geometry of the Roggenplaat complex over past centuries. Around 1827, the complex consisted of various individual intertidal shoals.

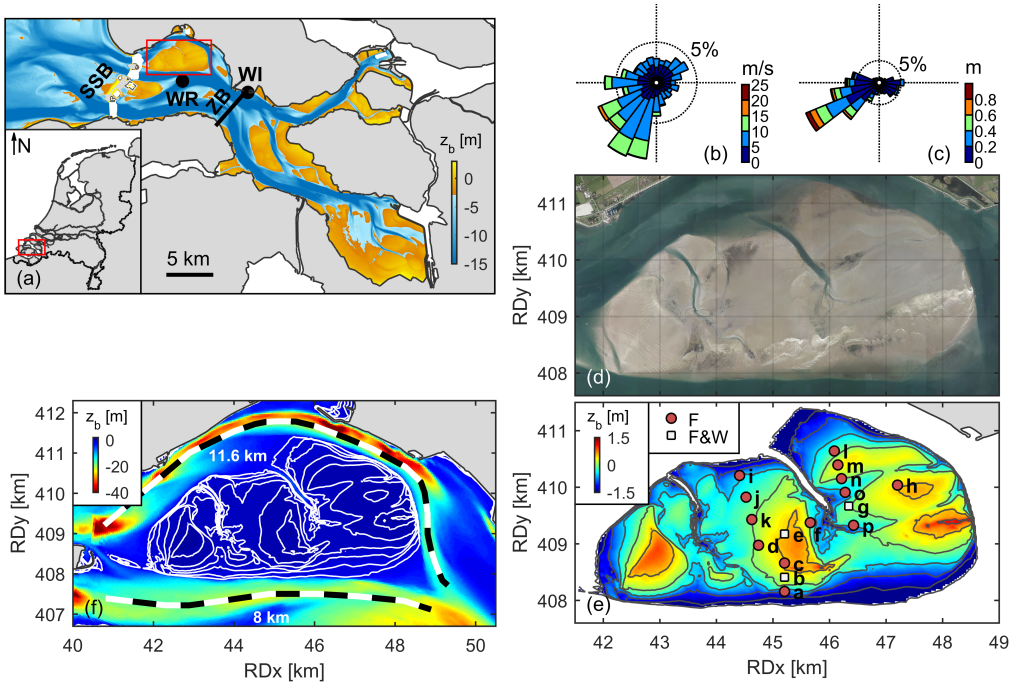

Figure 3.1: An overview of the Eastern Scheldt is provided in (a) with an indication of the storm surge barrier (SSB), Zeeland Bridge (ZB), wave rider (WR), wind station (WI), and Roggenplaat (red box). The wind rose for 2015 as measured at WI is visualized in (b), and the wave rose for March–December 2015 as measured at WR in (c). An aerial picture of 2014 (courtesy of Cyclomedia) of the Roggenplaat is shown in (d). In (e) the 2013 bathymetric data of the Roggenplaat are visualized with respect to MSL, based on single beam and LiDAR data (source: Rijkswaterstaat). Contour lines are indicated every 0.5 m over the vertical. The locations of the 16 measurement stations (*a*–*p*) are marked of which all stations included an ADCP measuring flow (F) and some stations also included a wave logger (F+W). In (f) the bathymetric data are visualized again, but now with a color scale focusing on the bathymetry of the surrounding channels. The mentioned distances in (f) indicate the length of the channels along the dashed lines.

These smaller intertidal shoals merged into a smaller number of larger intertidal shoals. A similar merging also occurred for the intertidal areas in the Western Scheldt Estuary (*Cleveringa and Taal*, 2015). With the merging, the complex of flats evolved into two major intertidal areas divided by a major tidal channel: the Roggenplaat and Neeltje Jans. The southern edge of the Roggenplaat faced a 5–10 m/year northward retreat, which is still observed in recent years. The two major tidal creeks of the Roggenplaat, both orientated toward the NW, are former channels which were the division between the different areas of the Roggenplaat complex (*Van den Berg*, 1984). Figure 3.2 indicates that the tidal creeks moved in NE direction while decreasing in length. Despite the dynamic historical evolution of the Roggenplaat and the decreased depth and discharge in its creeks (*Nio et al.*, 1980), the creeks still exist and their orientation remained directed toward the NW.

The more recent evolution of the elevation of the Roggenplaat is shown in Figure 3.3. A clear lowering of the high ridges of the Roggenplaat is visible, in contrast to the ac-

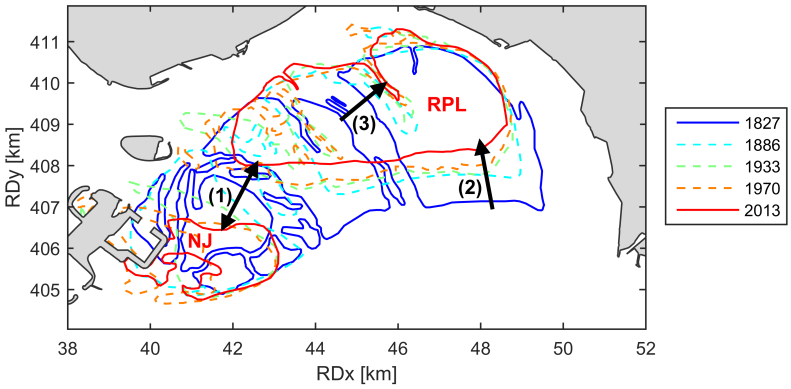

Figure 3.2: Evolution of the MLW contour lines of the Roggenplaat complex from 1827 to 2013. Both Roggenplaat (RPL) and Neeltje Jans (NJ) intertidal areas are shown as they were part of the same complex in the past. Contour lines are digitalized based on historical maps (*Haring*, 1947; *Van den Berg*, 1986) and for 2013 based on single beam and LiDAR measurements (*Marijs and Paree*, 2004; *Wiegmann et al.*, 2005). Not all years with data availability are shown to ensure readability. The arrows mark (1) the division between the Roggenplaat and Neeltje Jans, (2) the retreat of the southern edge of the Roggenplaat, and (3) the propagation of the eastern creek.

cretion before the construction of the barrier (*Louters et al.*, 1998). While lowering, they propagated in N/NE direction, indicated by erosion on the stoss side and accretion at the lee side (in addition to a net sand loss). The high ridges in the south are partly covered with dead cockle shells (white patches in the aerial picture of Figure 3.1d), which faced a similar N/NE propagation pattern over recent years. Currently, the eastern creek is the largest tidal creek of the shoal, with a width exceeding 100 m and an average depth of around 5 m.

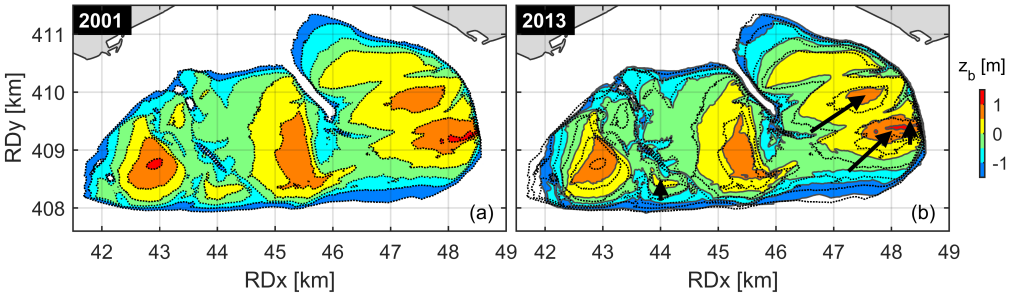

Figure 3.3: Bathymetry of the Roggenplaat in (a) 2001 and (b) 2013, based on single beam and LiDAR data with respect to MSL. The dashed contour lines of the bathymetry of 2001 are also shown in (b) to allow for a comparison between both years. The arrows in (b) indicate the main retreat direction at these locations.

3.2.2. NUMERICAL MODEL SET-UP

A numerical model schematization is set up with the package Delft3D (*Lesser et al.*, 2004). The differences in the hydrodynamics between three-dimensional simulations and depth-

averaged simulations were small for this case: the different physical processes considered in this study have orders of magnitude larger effects on the residual flow than the errors introduced by the depth-averaged approach. Therefore, the depth-averaged approach is followed in line with prior studies of intertidal areas (e.g., *Le Hir et al.*, 2000; *Gong et al.*, 2012). The model domain extends from the Storm Surge Barrier (SSB) to the Zeeland Bridge (ZB), both indicated in Figure 3.1a. In Figure 3.4 the computational grid is shown. Discharges are prescribed on the boundary segments at the SSB, whereas weakly reflective Riemann invariants (combination of water levels and velocities) are prescribed on the boundary at the ZB. The model is forced on these boundaries with time series of 2015 derived from a nesting procedure in a model covering the full Eastern Scheldt and its outer delta, which is coupled to an even larger model covering a large part of the North Sea (the DCSMv6-ZUNOv4-Kf model schematization; *Zijl et al.*, 2013, 2015). The year 2015 was a representative year for the local wind climate. Some simulations intentionally did not include surge; the surge in those cases was removed from the boundary conditions by considering only astronomical components with harmonic analysis.

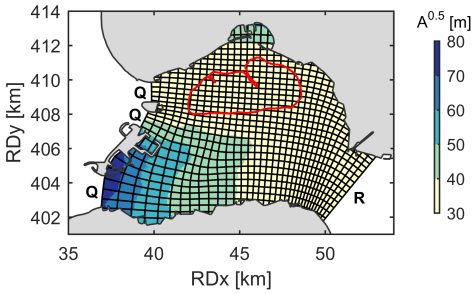

Figure 3.4: Visualization of the computational grid. One percent of the grid lines are shown to ensure readability. The colors indicate the grid resolution, represented by the square-root of the grid cell surface. The boundary containing Riemann segments is marked with R; the boundaries containing discharge segments are marked with Q. The contours of the Roggenplaat are shown as a reference in red.

The intertidal area of the Roggenplaat is captured with a model grid size of ≈30 m (Figure 3.4). A simulation with a finer grid size of ≈10 m gave very similar results in hydrodynamics (up to a few cm/s differences in the area of interest), which indicates that the ≈30 m resolution is sufficient for this study (and favorable because of approximately 27 times smaller computational times). The bathymetry on the shoal is based on LiDAR (LIght Detection And Ranging) data of 2013, and multi beam data of 2015 was used in the two major tidal creeks. For the rest of the domain, the Vaklodingen data set of 2013 were used, which is a combination of single beam measurements and LiDAR data (*Marijs and Paree*, 2004; *Wiegmann et al.*, 2005). A uniform Manning roughness of 0.022 s/m$^{1/3}$ was applied over the full domain, which resulted in flow velocities most in line with the observations. For simulations that include sediment transport, the *Van Rijn* (2007a,b) transport model was used with a median sediment grain size of 210 μm (based on field observations).

To assess the importance of waves, a stationary SWAN wave model (2017 version: 41.10; *Booij et al.*, 1999) was coupled to the Delft3D flow model at an interval of 30 min-

utes. The wave forces, based on the wave energy dissipation rate, are included in the momentum equations of the flow model. Also the bed shear stresses in the flow model are enhanced by the waves. Two modifications to the default settings were made to achieve decent results in shallow regions. First, instead of using a constant gamma value (maximum wave height to depth ratio), the β-kd model (*Salmon et al.*, 2015; *Salmon and Holthuijsen*, 2015) was used, which improved depth-induced wave breaking by taking the bottom slope and the normalized wave number into account. This implies a gamma value smaller than 0.73 (minimal 0.54 in this formulation) for mild sloping beds, in line with observations on intertidal areas (e.g., *Le Hir et al.*, 2000). Second, the Madsen roughness model (*Madsen et al.*, 1989) with a 5 cm roughness length scale was applied uniformly over the domain.

3.2.3. Comparison Between Model Predictions and Field Measurements

Over one month (February/March 2015), 16 ADCPs were simultaneously employed in upward looking mode to provide flow velocity measurements on the intertidal shoal. The instruments were placed in four transects as indicated in Figure 3.1e. Every 10 minutes, flow velocities were measured and averaged over periods of 400 seconds with 10 cm bin sizes and blanking. In this study, the ADCP measurements were used to validate the model. No detailed analysis of the time series is provided here.

The model is compared to the flow velocity measurements in Figure 3.5. The model results are relatively well in line with the measurements; the absolute bias in the magnitude of the velocities is at most 3.5 cm/s, and the absolute bias in direction is less than 14°. The root-mean-squared deviations range between 3.5–7 cm/s and 6–39°. Some local deviations are unavoidable, as real-world spatial irregularities in bed roughness (e.g., due to oyster reef patches that cover part of the shoal) are too complex to take into account and outside the scope of this chapter. A variation in various model parameters (e.g., bed roughness and background horizontal eddy viscosity) did not result in better results. Given the relatively small model domain, the quality of the boundary conditions and the high-resolution bathymetric data proved fundamental to describe the flow over the shoal accurately.

Even though extensive field measurements are available for the validation of the model, the validation of individual processes is only possible up to a limited extent. The correlation between the wind and the wind-driven waves (*Le Hir et al.*, 2000) causes the wind-driven flow to occur simultaneously with the wave-driven flow. Therefore, only the combined result of the wind- and wave-driven flow is validated with the measurement data.

Since March 2015, a wave rider measured wave characteristics south of the Roggenplaat. Furthermore, for three months (February–April 2015) three wave loggers were deployed on the intertidal shoal (5 Hz, OSSI pressure sensors). The locations of the instruments are indicated in Figure 3.1e. Figure 3.6 shows a comparison between the modeled and measured wave heights. Especially the higher wave heights are relatively well in line between the model and the measurements. The quality of the model is considered good enough for the desired analyses of this study (bias ranges between -1.5 cm and 5.1 cm and root-mean-squared deviations between 3.8 cm and 7.0 cm). Also the peak periods

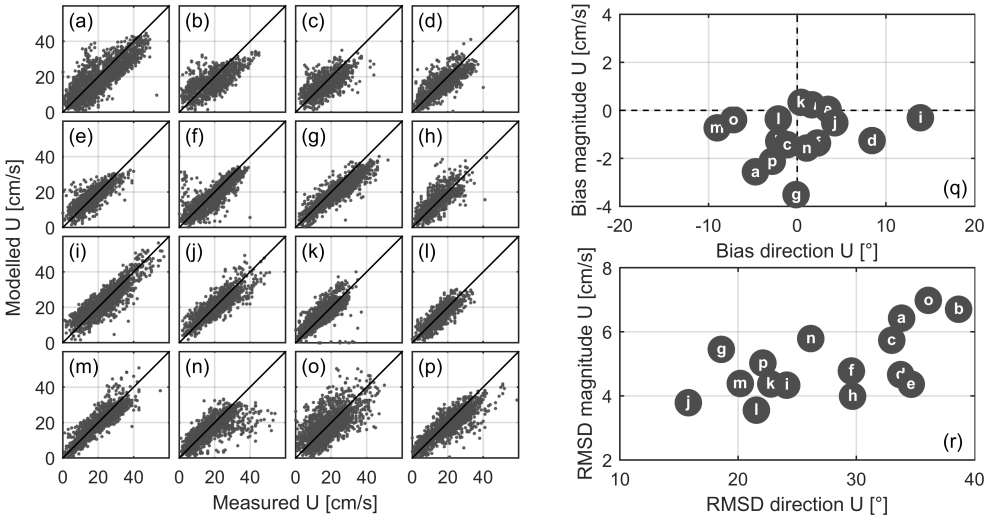

Figure 3.5: Modeled flow velocity magnitudes compared to measured flow velocity magnitudes for stations *a–p* (subfigure letters correspond to station names in Figure 3.1e). In (q) the biases (modeled minus observed) for the magnitude and direction of each station are shown. In (r) the root-mean-square deviations (RMSD) between the model results and measurements are presented. All processes (including wind and waves) were enabled in this simulation.

of the waves are modeled in agreement with the wave logger measurements (bias of -0.2 s to -0.5 s and root-mean-squared-deviation of 0.2 s to 0.4 s). Deviations between the model and measurements are not necessarily the result of model inaccuracies. The translation of pressure fluctuations measured near the bottom to wave heights will also induce inaccuracies (*Bishop and Donelan*, 1987).

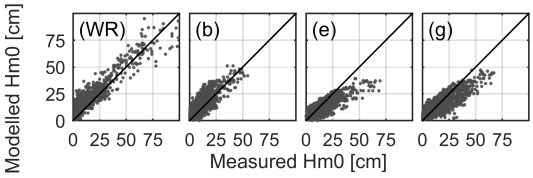

Instrument	WR	b	e	g
Bias	5.1 cm	3.7 cm	-1.5 cm	0.5 cm
RMSD	7.0 cm	5.3 cm	3.8 cm	4.7 cm

Figure 3.6: Modeled significant wave heights (Hm0) compared to measured significant wave heights for the wave rider (WR) and the available pressure boxes at stations *b*, *e*, and *g* (see Figure 3.1e for locations) for a two-month simulation (March and April 2015). The table provides the bias and the root-mean-square-deviations (RMSD).

3.3. RESULTS

We assess the importance of the different processes focusing on the intertidal zone of the shoal and on the major tidal creek. First, we analyze the main driver of the flow on the shoal, for a tide without substantial wind. Then, the focus is on a tide with strong wind speeds, to assess the consequences of a wind event. To analyze the fluctuations in the

importance of the processes over a year, scenarios were set up of full-year simulations in which the different processes are included one by one. Finally, sediment transport simulations were run to assess the consequences of the different processes on the transport rates.

3.3.1. THE DRIVER OF THE NET FLOW ON THE SHOAL WITHOUT WIND

To analyze the general pattern of the flow on the shoal, Figure 3.7b shows the discharges through a W-E and a N-S cross-section (indicated in Figure 3.7a). This is based on a model simulation of a single tide on 5 March 2015, which is a representative tide for calm wind conditions, as the wind did not exceed 4 m/s during the considered tidal cycle. The simulation with the actual bathymetry shows that the flow with rising water levels is mainly directed to the SE, whereas already before HW the flow turns toward the NW. The discharge during the first half of the tidal cycle is substantially smaller compared to the second half, during which high velocities lasted longer. Figure 3.7c shows that this net NW discharge of water over the shoal is well visualized by a simulation of drogues, released during rising water levels just before MWL (Mean Water Level). The drogues released in the tidal creek are initially steered in SE direction onto the shoal but then driven to the NW where they leave the shoal toward the northern channel. The drogues released at the southern edge of the intertidal shoal are driven onto the intertidal area during the inundation phase, and then also face a net NW movement with the strong flow speeds occurring after HW.

The bathymetry of the intertidal shoal is characterized by two NW orientated tidal creeks which are surrounded by relatively low regions compared to the rest of the intertidal area (Figure 3.1e). To test whether the net NW flow is a consequence of these NW orientated lower regions on the intertidal shoal, the simulation is repeated for a fully flattened and smoothed bathymetry of the intertidal area; the rest of the system is left unchanged. Figure 3.7d shows the tracks of the drogues for both the actual bathymetry, and the flattened and smoothed one (height of MSL+0.0 m, equal to the average height of the actual bathymetry). Differences in the pathways of the drogues between both simulations are visible (with the smoothed bathymetry the drogues are less dispersive), but the net NW movement of all drogues is still clearly there. This is also expressed well by the discharges through the cross-sections for the smoothed bathymetry in Figure 3.7b. Differences are also visible here, mainly around or below MWL where the smoothed bathymetry fully submerges and especially in the N-S transect where the tidal creek is part of. But also the net NW movement is still strongly visible in this flattened and smoothed bathymetry. Therefore, the local bathymetry definitely affects the detailed flow patterns, but it is certainly not the main cause for the net NW flow on the intertidal shoal. Contrariwise, the tidal creeks may result from the main flow.

Without substantial meteorological influences, the flow on the shoal is driven by water level gradients and bed friction. A regular tidal analysis (e.g., *Pawlowicz et al.*, 2002) is not possible for intertidal areas because of discontinuous time series every tide. Instead, Figure 3.8a shows the spatial distribution of the average high water levels over the model domain. Apart from providing insights in the gradients on the shoal, such an analysis is suitable for this study as the timing of the NW flow coincides with HW (see Figure 3.7). Although water level gradients can also follow by spatial differences in the timing of the

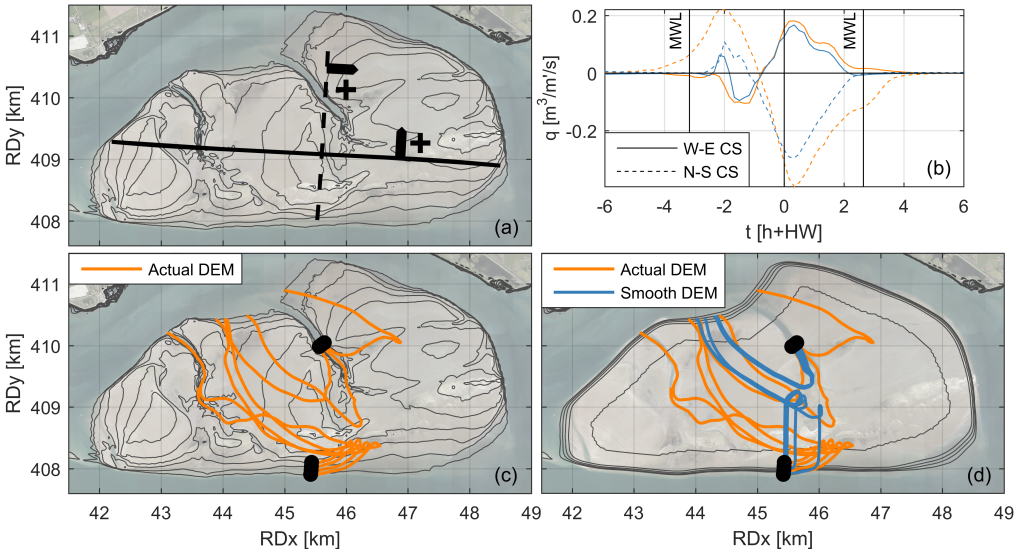

Figure 3.7: Model results for a typical tidal cycle with mild wind conditions (5 March 2015; wind speeds smaller than 4 m/s). (a) The cross-sections considered in this study, with their positive flow directions. The instantaneous discharges per unit width through these cross-sections are shown in (b) for both the actual DEM (Digital Elevation Map) as for a smoothed DEM of the shoal (colors match legend of (d)), with the time axis relative to the high water level timing. (c) The tracks of the drogues released at the black dots during rising tide just before MWL for the actual DEM. (d) The same tracks, but additionally, the tracks are shown for the simulation with the smoothed DEM. Black lines indicate elevation contour lines (0.5 m distance).

tides, Figure 3.8b indicates that these differences in timing are limited (order of minutes) compared to the tidal period. Hence, the spatial distribution of the high water levels is a good indicator for the water level gradients around high water. Although not everywhere with exactly the same direction, Figure 3.8a shows that the water level gradients on the shoal are directed to the NW/NWW on the largest part of the area (mainly in the center and east part of the shoal). This is in line with the net flow direction over the shoal (e.g., Figure 3.7). The isolines of the high water levels indicate that the northwestern gradient is caused by differences in high water levels along the surrounding channels. The differences in water level gradients in both surrounding channels originate from differences in the geometry of both channels. The northern curved channel is substantially longer (11.5 km) and deeper compared to the shorter (8 km) and almost straight southern channel (Figure 3.1f). Differences in tidal propagation are hence a necessary consequence, also because both channels are connected to each other and, therefor, have a similar water level east and west of the shoal.

3.3.2. THE IMPACT OF A SINGLE WIND EVENT ON THE FLOW

To analyze whether the previous observations are also representative for days with more severe wind speeds, a tide that coincided with a strong wind is considered (1 March, wind speeds on average 11 m/s from SW). Figure 3.9 shows the tracks of the drogues modeled both for a simulation with the actual wind climate and for a simulation without any wind

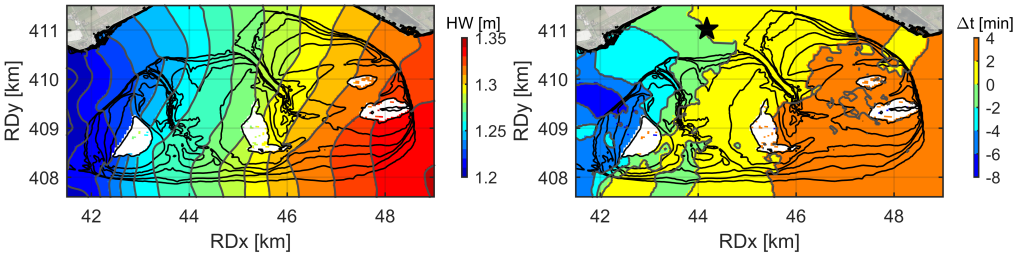

Figure 3.8: (a) High water level with respect to MSL for each computational cell averaged over the high waters of the first half of March 2015. Cells with a bed level higher than the lowest high water level were not considered (white in the figure). (b) The difference in timing of the mean high water level with respect to a reference point (indicated with the star). Black lines indicate elevation contour lines (0.5 m distance).

forcing. Although the tidal range of this specific tide is different compared to the previously considered tide, the tracks for the case without wind forcing are very similar to the results of 5 March which was characterized by limited wind speeds (compare Figure 3.9 to Figure 3.7c). However, when the simulation with the actual wind climate of 1 March is considered, the drogue tracks are substantially different. With the inclusion of such a wind event, the main flow on the shoal is well in line with the governing wind direction (NE directed) and hence not in the NW direction as observed in cases without wind.

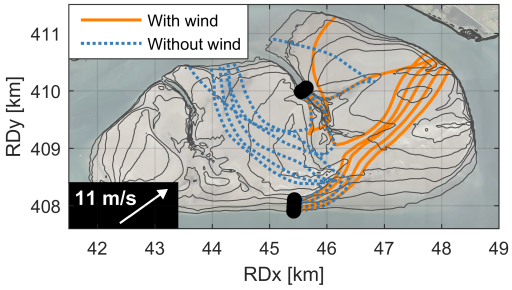

Figure 3.9: Model results for a tidal cycle with a relatively strong wind (1 March 2015; average wind speed of 11 m/s from SW). Both the drogue tracks for a simulation with and a simulation without the wind forcing are shown. Black lines indicate elevation contour lines (0.5 m distance).

Figure 3.10 shows the flow velocity through the eastern tidal creek for this tide of 1 March. Similar to Figure 3.9, both a simulation with and without the presence of the wind is considered, to assess the effect of such a wind event on the depth-averaged flow in a tidal creek. Apart from a very short period around high water slack, the flow in the creek is less affected by the wind compared to the flow on the shoal (Figure 3.9). Still, the wind causes deviations in flow velocities up to 10 cm/s during the considered tide. However, the peak velocities in the creek are almost unaffected by the presence of the wind (<3 cm/s and <2° deviation), as these peaks occur around MWL. Around MWL, the intertidal area is not fully inundated, hindering a full flow over the shoal (see Figure 3.1e). Also, the direction of the flow in the creek, aligned with the channel axis during substantial flow velocities, is only slightly affected by the wind.

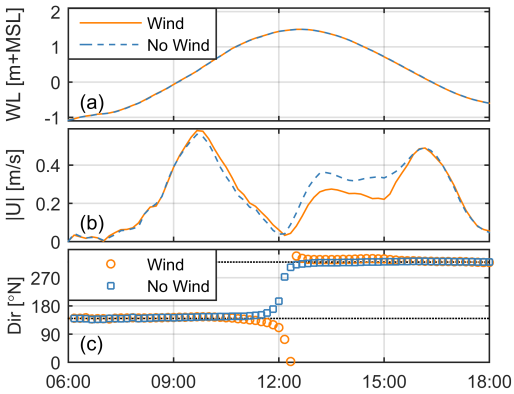

Figure 3.10: Time series of water level elevation (a), depth-averaged flow velocity magnitude (b), and flow direction (c), modeled in the center of the eastern tidal creek (same location as the released drifters in Figure 3.9). Similar as in Figure 3.9, the tide of 1 March is considered in a simulation with wind (average wind speed of 11 m/s from SW) and without wind. In (c) the orientation of the channel axis is marked with the black dashed lines.

3.3.3. FLUCTUATIONS OVER A YEAR

Previous sections have shown that the tides result in a net flow in NW direction, but that wind can change this pattern. To determine whether this modification is a result of the surge, wind-induced shear stress, or wave-induced flow a set of simulations is carried out to unravel these contributions. A full year (2015) is simulated, with each simulation different processes enabled: (T) tide only; (T+S) tide and surge; (T+S+Wi) tide, surge, and wind-induced shear stress; and (T+S+Wi+Wa) tide, surge, wind-induced shear stress and wave forces. Comparing the different simulations, the added contribution of each process can be assessed. To visualize the result, the net discharge through the cross-sections W-E and N-S (see Figure 3.7a) was determined per tidal cycle and plotted as a function of the high water level of that tide in Figure 3.11.

First, only astronomical tidal signals were imposed on the boundaries of the model domain. In this case, a possible surge was filtered out by means of a tidal analysis (*Pawlowicz et al.*, 2002) and wind and waves were not imposed. Figure 3.11 shows always a positive flux for the W-E cross-section and a negative flux for the N-S cross-section. This indicates a net discharge always directed to the northwest if the model is only enforced by tides. Furthermore, an almost linear relationship is found between the high water level of each tide and the net discharge over the shoal during that tide (r^2 of 0.73 for the W-E cross-section and 0.95 for the N-S cross-section). The results are very similar if the actual surge is imposed: a larger range of high water levels coincides with a larger range of net discharges. Still, the almost linear relationship holds (r^2 of 0.87 for the W-E cross-section and 0.97 for the N-S cross-section) and all considered tides have a net discharge toward the NW.

The results are substantially more scattered with the inclusion of the wind forcing (waves still omitted). For the simulation with tides and surge, the standard deviation of the net discharge was 264 $m^3/m'/tide$ for the W-E cross-section and 800 $m^3/m'/tide$

for the N-S cross-section. With wind forcing, these increase to 936 $m^3/m'/tide$ and 1596 $m^3/m'/tide$, respectively. The wind is capable of fully altering the direction of the main flow, as also concluded from Figure 3.9. The almost linear relationship no longer holds. The deviation from the simulation with only tides and surge increases substantially for higher high water levels and for the highest high water levels there are even more tides with a net discharge to the east than to the west. This is due to the correlation between wind speeds and water levels (through the wind-induced surge). Finally, the scatter increases slightly more if also waves are included in the model simulation due to wave-induced flow. The standard deviation of the net discharge equals now to 1216 $m^3/m'/tide$ for the W-E cross-section and to 2051 $m^3/m'/tide$ for the N-S cross-section. Such a net wave-induced flow is similarly observed for shallow reefs (*Symonds et al.*, 1995). Because waves are mainly locally generated in this area, the direction of the wave-induced flow is generally in line with the direction of the wind-induced flow.

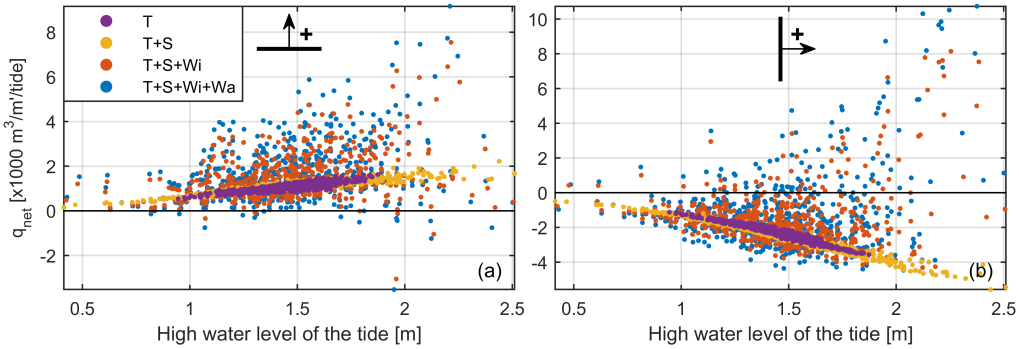

Figure 3.11: Net flow discharges per tide through the (a) W-E and (b) N-S cross-sections as defined in Figure 3.7a. Every dot represents the net discharge through the cross-section versus the high water level (with respect to MSL) for each single tide. Four different simulations are considered with different processes enabled: (T) tide only; (T+S) tide and surge; (T+S+Wi) tide, surge, and wind; and (T+S+Wi+Wa) tide, surge, wind, and waves. Results are based on simulations of the full year 2015.

The discharges of each individual tide are now related to the average wind speed of each tide for the simulation including all processes in Figure 3.12, to better understand the scatter found in Figure 3.11. The scatter does increase not only with higher high water levels (as observed in Figure 3.11), but also strongly with increasing wind speeds. Together with the magnitude of the wind speed, the wind direction is another strong indicative parameter for the discharge over the area (Figure 3.12).

Especially for large wind speeds, the flow over the shoal is driven by the wind. The net discharge is directed to the NW for all considered tides with a wind speed smaller than 7 m/s, whereas the net discharge is directed to the NE for all considered tides with a wind speed larger than 13 m/s. The limited variation in net flow direction during high wind speeds (e.g., no net western flow for high wind speeds) is a consequence of the local wind climate. SW is namely the only direction where these strong winds originated from in 2015 (see Figure 3.1b). Still, there were some tides with moderate winds from the NW for which the net northward flow was substantially reduced or even a net SE directed flow was the result.

In conclusion, the wind results in surge, wind-induced flow, and wave-induced flow. Although there is a relation between the high water level and the discharge over the shoal, it is especially the wind-driven flow that is responsible for the fluctuations in the net flow over the considered year.

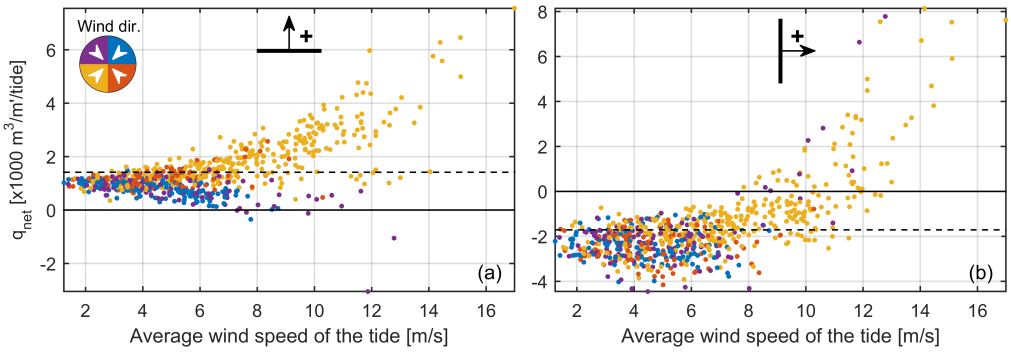

Figure 3.12: Net flow discharges per tide through the (a) W-E and (b) N-S cross-sections as defined in Figure 3.7a. Every dot represents the net discharge through the cross-section versus the average wind speed for each single tide. The colors indicate the direction of the wind for each tide. Results are based on a simulation of full 2015 including all processes (tide, surge, wind, and waves). The dashed line represents the yearly-averaged tidal discharge.

3.3.4. IMPLICATIONS OF THE DIFFERENT PROCESSES ON THE SEDIMENT TRANSPORT RATES

So far, we focused on the importance of local bathymetry and the different forcing mechanisms on the residual flow over the shoal. Now, the focus is on the impact of each of these processes on the sediment transport rates. We consider an individual tide, to rule out the complexity induced by wind speeds and directions changing all year long. Again, the tide of 1 March is considered which was characterized by relatively strong wind speeds (on average 11 m/s from the southwest; see Figure 3.9).

In Figure 3.13, the net sediment transport rates on the shoal are shown (with the *Van Rijn* (2007a,b) transport model), for simulations with the inclusion of all processes and also with the exclusion of waves, wind, or surge. The main transport is in NE direction for the simulation with all processes (Figure 3.13a). This is in line with the prevailing wind direction. For the higher regions of the shoal, a consequential NE propagation of the bed profile can be deduced by the increasing transport rates at the stoss side and decreasing transport rates on the lee side of those high elevated regions (especially visible around RDx = 47 km and RDy = 410.5 km). The bed level changes are namely the direct result of the divergence in the sediment transport fluxes. There is a substantial spatial variability in hydrodynamic forcing and hence in sediment transport present over the intertidal shoal. At the edges of the shoal, the largest transport rates are observed as a consequence of the relatively high flow velocities and the substantial wave breaking processes. In the creek, the net transport rates are substantially smaller during this wind event.

If waves are disabled (Figure 3.13b), the net transport rates on the intertidal shoal are several orders of magnitude smaller (also orders of magnitude smaller compared to the

rates in the creek). This implies that waves are crucial for the sediment transport on this intertidal area. In contrast to the wind, waves induce apart from a flow (as visualized in Figure 3.11) also additional stirring of the sediment by velocity fluctuations near the bed. However, this does not imply that the other processes are irrelevant. In fact, the sediment transport rates on the shoal are highly reduced if the wind is disabled while waves are still imposed (Figure 3.13c). The wind itself is hence an important amplifier of the sediment transport rates by affecting the flow on the shoal. When similarly only the surge is not considered (Figure 3.13d), the transport rates are also slightly reduced but substantially less compared to the case without wind.

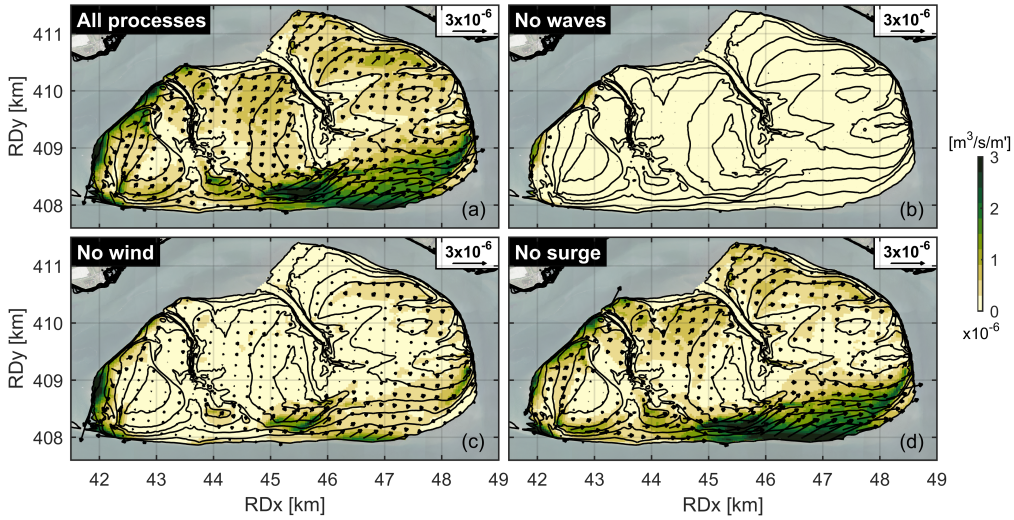

Figure 3.13: Mean total transport rates (bed load + suspended load) in the intertidal zone of the shoal for (a) including all processes, (b) excluding only waves, (c) excluding only wind, and (d) excluding only the surge for a tidal cycle with a relatively strong wind (1 March 2015; average wind speed of 11 m/s from SW). Only the transport rates on the shoal (for bed elevations higher than 2 m below MWL, i.e., roughly above MLW) and within the tidal creeks (all depths) are visualized to improve clarity. For the same reason, only 1/36th of the modeled arrows are shown.

The major tidal creeks on the intertidal area are characterized by lower bed levels (around MWL-5 m) and consequently larger depths than on top of the shoal. Therefore, the relative importance of the tide, wind, and wave processes for the sediment transport rates is not necessarily the same for these creeks as for the shoal. Figure 3.10 already showed that flow velocities in the eastern creek are hardly affected by wind events. To test the importance of the different processes for the sediment transport rates in the eastern tidal creek, the sediment transport rates through a cross-section are analyzed in Figure 3.14.

If only the tidal forcing is imposed (Figure 3.14b), the net sediment transport direction in the creek is mainly directed to the north for relatively small high water levels and mainly directed to the south for relatively large high water levels. More importantly, the net transport rates are highly different if the surge is also included now. For similar high water levels, the net transport rates can be an order of magnitude larger. Although

higher high water levels result in a larger variation in the net transports, the high water level does not provide a direct relation with the magnitude of the net sediment transport rates itself. The spread changes slightly when also the wind or both the wind and the waves are included. But this is of minor importance compared to the impact of the surge on the sediment transport rates.

The hydrodynamics and sediment transport in the center of the cross-section are analyzed in more detail for a single tide in Figures 3.14c– 3.14f. The focus is now on the tide of 30 September, as it is a good example of a tide with much higher net sediment transport rates if all processes are considered compared to the tide-only simulation, more than a factor of 7 difference (see Figure 3.14b). This tidal cycle is characterized by a wind speed of 6 m/s from ENE direction. First, Figure 3.14c indicates a setdown in the estuary of 0.35 m for this specific tidal cycle. Nevertheless, the peak flood velocity is larger with the inclusion of the surge/setdown (Figure 3.14d) which imposed significantly larger magnitudes of flood sediment transport rates (Figure 3.14f). These larger peak velocities are the direct consequence of the faster rising rate of the water level around MWL when the surge is included (Figure 3.14c), the surge affects hence the asymmetry of the tidal wave. Because the surge imposes a setdown, the timing of the flow velocity and sediment transport peaks is altered, but Figure 3.14e indicates that the direction of the flow is still in line with the channel axis. Only around slack water, some deviations in direction are visible, but these are with the low velocities irrelevant for the sediment transport. The inclusion of wind, even together with the waves, does not imply any consequences for the sediment transport rates in these deep parts of the creek, in line with the already minor impact of a stronger wind event in Figure 3.10 on the hydrodynamics in the creek.

Figures 3.15c and 3.15d quantify the relative importance of the wind and waves on the cumulative transport magnitude at various locations for a simulation of a full year. In line with Figure 3.14, the wind and waves hardly affect the transport in the creek. Contrarily, the transport rates on the largest part of the intertidal shoal are strongly dominated by the wind and waves as the tides with the 50% lowest wind speeds (<5.5 m/s) only explain ~1–10% of the yearly transport (see also Figure 3.15b). These tides determine only 3% of the transport at point *a* (exposed edge of the shoal). At point *i* (sheltered edge of the shoal) wind and waves are slightly less important as these tides determine still 14% of the transport. The largest relative dominance by the wind and waves is found for the highest elevations at the center of the shoal, for example, at point *h* less than 2% of the sediment is transported by the tides with the 50% lowest wind speeds.

To test how sensitive the dominance of the meteorological processes is to the height of the shoal, we lowered the shoal 1 m. This is roughly half the tidal amplitude (i.e., cells around MWL became roughly MLW), and only cells that were above MWL-2 m are lowered. Figures 3.15e and 3.15f show the cumulative sediment transport for this lowered shoal. After the lowering, the meteorological forcing is still essential for the shoal. The creek is still tide-dominated. The transport processes at point *a*, which is highly exposed to wave attack, are slightly less dependent on the extreme meteorological conditions. The water depth is larger, and waves are therefore less effective. Point *i* is more influenced by extreme wind conditions. The shoal is longer submerged, and wind can therefore play a role over a longer period. The simulations with the real bathymetry and the lowered shoal show that the exact bed level is not essential for the dominance of the

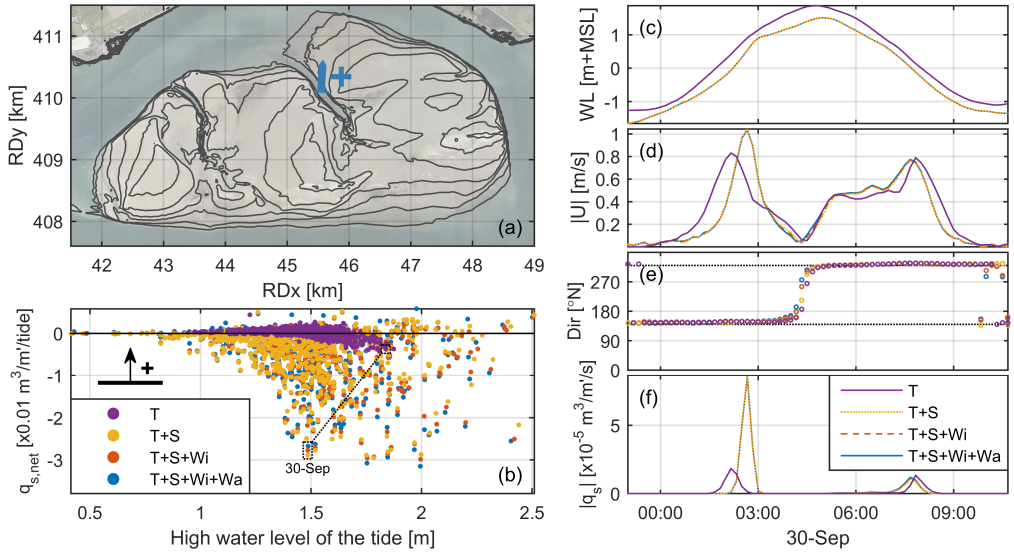

Figure 3.14: The net total (bed load + suspended load) sediment discharge for each tide as a single dot versus the high water level for each single tide in (b), for a W-E cross-section in the eastern tidal creek as indicated in (a). Similar to Figure 3.11, four different simulations of the full year 2015 are considered with different processes enabled: (T) tide only; (T+S) tide and surge; (T+S+Wi) tide, surge, and wind; and (T+S+Wi+Wa) tide, surge, wind, and waves. For each simulation, the water level (c), depth-averaged flow velocity magnitude (d), velocity direction (e), and total sediment transport magnitudes (f) are visualized for the deepest point of the cross-section for the tide of 30 September as marked also in (b). In (e) the orientation of the channel axis is indicated with the black dashed lines.

wind. Wind dominance on tidal shoals can therefore be expected for a variety of shoals and is not only important on the Roggenplaat.

In conclusion, the combination of waves and wind determines the sediment transport rates in the intertidal zone of the shoal. Contrarily, the rising and falling rate of the water level determines the transport rates in the deep creek. There is hence a major spatial variability in the importance of the different processes.

3.4. DISCUSSION

Hydrodynamic processes on an intertidal shoal appeared to be a complex outcome of tidal and meteorological (i.e., surge, wind, and waves) forcing mechanisms that strongly vary over time and space. Therefore, to understand sediment transport on such an intertidal shoal, the importance of each of these processes has to be considered both in space and time.

3.4.1. TEMPORAL VARIATIONS

The relative importance of the different hydrodynamic forcing mechanisms varies on different timescales. First, the flow on an intertidal shoal is diverse in magnitude and direction over an individual tidal cycle, still with a clear dominant net direction (e.g.,

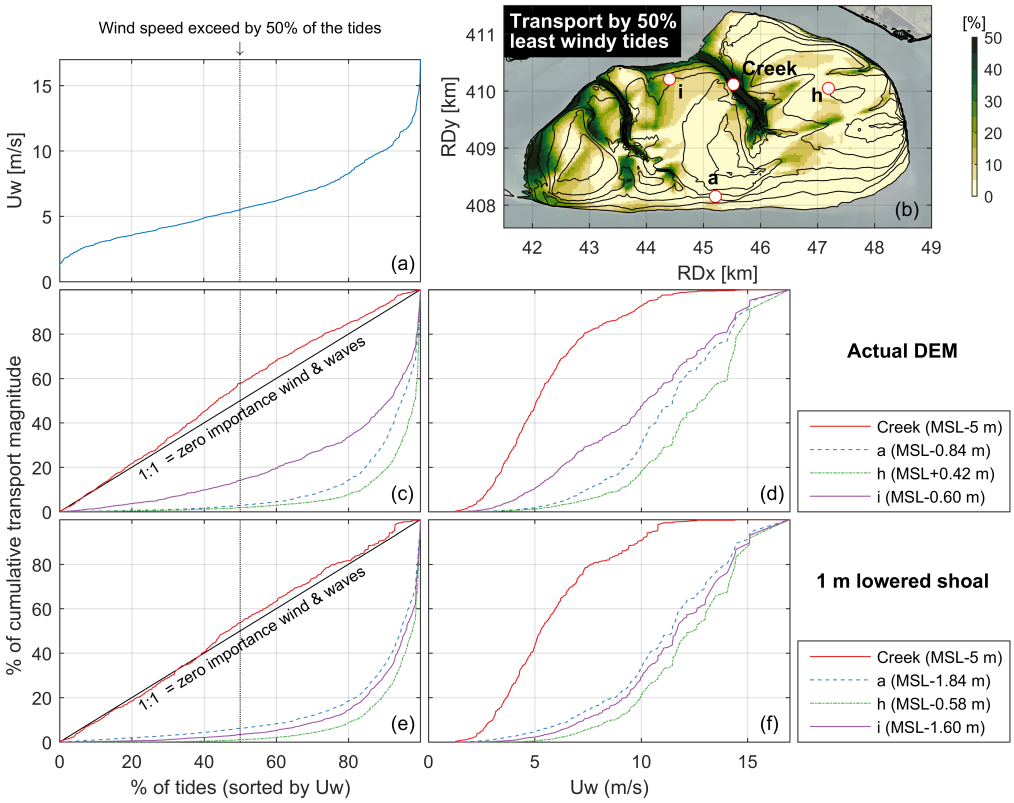

Figure 3.15: Quantification of the role of meteorological processes on the sediment transport rates on the shoal, based on a full year simulation including all processes. (a) The distribution of wind speed. The percentage of the cumulative sediment transport magnitude, in which the tides are sorted by the wind speed, is presented for the actual bathymetry in (c) as a function of the percentage of the tides and in (d) as a function of the wind speed. The same is presented in (e) and (f) after lowering the shoal with 1 m (only original cells above MWL-2 m). Panel (b) visualizes for the actual bathymetry the percentage of the cumulative transport magnitude that is generated by the 50% least windy tides, matching the vertical dotted line in (c) and (e). Furthermore, (b) also visualizes the location of the observation points of the other graphs, in line with Figure 3.1e.

Figure 3.7). Second, spring-neap variations cause variations in the magnitude of the flow over the shoal while leaving the orientation of the net flow unchanged (Figure 3.11). Other time fluctuations are related to meteorology. Meteorological events have a direct impact on the water level setup within the estuary, the wind-driven flow, and the wave-driven flow. A water level setup has a similar consequence as a higher astronomical high water level (Figure 3.11): an amplification of the magnitude of the flow without a substantial change in directions. In contrast, the locally generated wind- and wave-driven flow can alter both the magnitude and the direction of the flow on the shoal.

These, partly independent, temporal fluctuations shall have consequences for the long-term evolution of intertidal shoals. As sediment transport on the relatively sandy Roggenplaat takes place especially during energetic meteorological events (Figure 3.15),

as also observed on other intertidal areas (e.g., *Green et al.*, 1997; *Van der Werf et al.*, 2015b), those events are likely fundamental for the morphological evolution of such a shoal. In strong contrast to astronomical fluctuations, these meteorological events are not deterministic. Still, the wind climate (Figure 3.1b) provides important insights in the long-term fate of an intertidal shoal. Meteorological events capable of altering the flow (Figure 3.9) are not rare for the Roggenplaat area: 12.5% of the time wind speeds exceeded 10 m/s in 2015. Furthermore, these events have a clear dominant direction, well in line with the historical net propagation of the creeks and the bed features on the shoal. Still, the impact of individual meteorological events depends on the timing of these with respect to other time fluctuations (e.g., timing within an individual tidal cycle and within the spring-neap cycle). The existence of those different time fluctuations provides direct challenges for long-term modeling studies, in which simplification of the forcing mechanisms (e.g., meteorological climate) is required to save computational times.

3.4.2. SPATIAL VARIATIONS

The relevance of the different processes varies strongly on the shoal. It is shown that especially the tide and the surge dominate the flow velocities and sediment transport in the tidal creeks. The orientation of the tidal creeks is well aligned with the net flow over the shoal imposed by the tide and the surge. Similar to cross-connecting channels (*Swinkels et al.*, 2009), differences in the tidal wave propagation, dependent of the geometry of the surrounding channels (e.g., Figure 3.1f), are found to drive the flow direction. The shape of the tidal wave is crucial for the velocity in the creeks, specifically the fastest rising and falling rates. Wind and waves are only of minor importance in the creeks because of the relatively large water depths (to exclude depth-induced breaking of waves, i.e., ~2 times the maximum significant wave height in the creeks) and large flow velocities (characteristic peak flow in the considered creeks is ~1 m/s which dominates over the wind driven flow), in contrast to what was found on the shoal. Still, storms might affect the creeks when sediments transported on the shoal get trapped in the creeks. In this case the creeks will migrate in line with the main sediment transport direction on the shoal, as a consequence of gradients in sediment transport. On the shoal, the tide and surge are also relevant for the hydrodynamics during calm weather conditions. However, the wind and waves during energetic meteorological events are clearly the dominant processes for the sediment transport in the intertidal zone of the shoal. Under calm weather conditions, the flow velocities on the shoal are too small to induce substantial sediment transport rates, as waves are crucial for stirring the sediment.

Apart from a distinction between the creeks and the intertidal zone of the shoal, also over the shoal itself differences in the importance of the processes are present. As the net flow is a consequence of the geometry of the surrounding channels, it depends on the location on the shoal on how strong this gradient is and in which direction this is precisely pointed. Specifically for the Roggenplaat, Figure 3.8a indicates that this gradient is especially predominantly NW orientated on the center and east side of the shoal. On the west part, the gradients are more orientated to the west, as the water levels in the surrounding channels are more aligned around there. Also, the contribution of waves is not homogeneous over space for intertidal areas (also stressed by *Green and Coco*, 2014). A large fraction of the wave dissipation occurs at the edges of the intertidal area, im-

posing relatively large transport rates locally there, which coincides for the Roggenplaat with the region which faced the main erosion over the past (Figures 3.2 and 3.13d). The high-resolution output of the model allows for a spatial decomposition of the shoal in various zones. Figure 3.15b visualizes the percentage of the cumulative transport magnitude that is generated by the 50% least windy tides for each cell. In combination with Figure 3.13, and in line with the analyses of the points in Section 3.3.4, various zones are identified: (1) tidal creeks, which are strongly tide-dominated; (2) high ridges on the shoal with transport mainly during meteorological events; (3) exposed side (southern edge), which is wave-dominated; (4) sheltered tide-dominated side (W/NW of the shoal), which is sheltered and only tide-dominated; and (5) sheltered wind-dominated side (E/NE of the shoal), which is not exposed to waves and mainly influenced by wind-driven flow.

3.4.3. GENERAL INDICATORS

This study unraveled the relative importance of the processes for the Roggenplaat in detail. The insights are applicable beyond this specific case. For example, this holds for the crucial combined role of wind and waves on intertidal shoals. Morphodynamic studies which do not consider these processes at all (e.g., *Dam et al.*, 2016; *Van de Lageweg and Feldman*, 2018), hence have a limited predictive capacity on the intertidal shoals. This especially holds for the higher parts of the shoals. Furthermore, the insights on the driving mechanisms for the flow and sediment transport result in general indicators for other shoals. These are especially valuable if data are limited.

We suggest that by considering several basic indicators, the large-scale hydrodynamics and sediment transport on an intertidal shoal can be understood qualitatively without the need of thorough model simulations. First, geometrical features visible on satellite imagery indicate the orientation of the main flow on a shoal during mild wind conditions. The orientation of major tidal creeks is a good indicator for the main flow direction as meteorological events are of less importance for the orientation of these creeks. Also, the difference in length between the surrounding channels and their shape are, through the resulting water level gradients, indicators of the main flow. Second, a local wind rose can indicate a dominant transport direction for the high elevations of a shoal, as the transport rates on these high areas are highly affected by wind events and the related waves. Strong indications follow especially if a clear dominant wind direction is present.

To determine whether wind is important on tidal shoals, we make a first-order estimate. We consider the one-dimensional depth-averaged momentum equation and start for a wind-only situation (no tides). For shallow water, weak flow gradients, and limited temporal gradients, we can neglect the time variation of the velocity and the advective part of the momentum equations and reach a balance between three terms:

$$\rho_w g d \frac{\partial h}{\partial x} - \tau_{wind} + \rho_w c_f u|u| = 0 \tag{3.1}$$

where ρ_w is the density of water, g the gravitational acceleration, d the water depth, $\frac{\partial h}{\partial x}$ the water level gradient, τ_{wind} the wind shear stress, c_f the dimensionless friction coefficient, and u the flow velocity. If we simplify this equation further by neglecting the pressure gradient term, we get a balance between the wind shear stress and the

bed shear stress. Such a simplification is possible if the wind cannot result in an extra buildup of a pressure gradient. This is approximately the case for a shoal surrounded by channels, in which the return flow in its surrounding channels does not accommodate the pressure gradient buildup. Similarly, such pressure gradient cannot build up along an alongshore uniform fringing flat. Approximating the simplified balance between the wind shear stress and the resisting friction force with typical values (wind drag coefficient C_D ranges between 0.001 and 0.002 for wind speeds 10 m from the surface U_{10} of 5–20 m/s, an air density ρ_a of 1.23 kg/m^3, and c_f of 0.003) leads to the following:

$$0 = \tau_{wind} - \rho_w c_f u|u| = \rho_a c_D U_{10}|U_{10}| - \rho_w c_f u|u| \tag{3.2}$$

$$U_{10} = \sqrt{\frac{\rho_w c_f}{\rho_a c_D}}\, u \tag{3.3}$$

$$U_{10} \approx \sqrt{\frac{1000 \cdot 0.003}{1.23 \cdot 0.0015}}\, u \approx 40\, u \tag{3.4}$$

This factor of 40 is a first-order estimate of the wind-only velocity and should be considered with care. It is not intended as a predictor of the precise wind-driven flow velocity, as the resulting velocity is not simply the sum of the tide-only velocity and the wind-only velocity (see Equation 3.1). However, if the wind-only velocity is in the same order as (or especially if even larger than) the tide-only velocity, then the wind-only velocity definitely makes a significant contribution to the resulting velocity. Therefore, it is a simple indicator to determine for a shoal (or fringing flat in alongshore direction), based on the wind speed and the governing tidal velocity, whether wind is an important process to be considered. The results of the Roggenplaat showed that the factor of 40 is in the right order of magnitude. For this shoal with typical tidal velocities of 0.25 m/s (e.g., Figure 3.5), wind speeds in the order of 10 m/s and higher were sufficient to modify the net flow patterns substantially (Figures 3.9 and 3.12).

Every intertidal area is unique; still its uniqueness is the result of the same processes. The relative importance of the wind and waves on the sediment transport rates for other shoals depends on local characteristics (also sediment grain size), just as it also varies spatially over a single tidal shoal (e.g., Figure 3.15). In general, the larger the impact of wind and waves on the sediment transport rates, the further the curve in Figure 3.15c will be positioned to the bottom right corner, while tide-dominated areas will result in straighter lines in this graph. The latter holds for tidal creeks or edges of the shoal which are sheltered from waves but subject to a strong forcing from the channel. Shoals that inundate every tide allow the wind to alter the direction of the flow in any direction. In case a land boundary is present (i.e., for fringing flats), the degrees of freedom for the net flow direction are reduced. For such fringing flats, an alongshore pressure gradient in the channel or an alongshore directed wind stress will still affect the flow, similarly as shown in this study for an intertidal shoal. On intertidal shoals surrounded by channels with limited tidal flow velocities, smaller than several decimeters per second as on the Roggenplaat, only minor winds are required to affect the flows (e.g., *Christiansen et al.*, 2006). But even for intertidal areas with large tidal flow velocities, there are phases in each tidal cycle during which strong winds will control the flow, e.g., during slack wa-

ter. Therefore, we emphasize that the wind should generally be included in (modeling) studies on intertidal areas.

3.5. CONCLUSIONS

In the absence of wind, the net flow on an intertidal shoal surrounded by channels is primarily driven by water level gradients between its surrounding channels. These water level gradients depend on the geometry of these channels. The local bathymetry of the shoal and its tidal creeks influences the local details of the flow patterns. The tidal creeks are mainly important for the inundation and dewatering of the shoal when the water level is rapidly changing and the water depth on the shoal is limited. Higher high water levels, for example, due to spring-neap variations and storm surges, amplify the discharge over a shoal. Nevertheless, the rising and falling rates of the water level dominate the variability of the flow and transport in the creeks, not the height of the high water level. Wind and waves do not substantially affect the flow and transport in such creeks.

Wind is a crucial driver for the hydrodynamics and sediment transport on the intertidal shoals surrounded by channels. First, the wind-generated waves are key for the sediment transport in such environments. Second, strong wind and waves impose a net flow well in line with the governing wind direction. This is especially the case if the wind speed exceeds about 40 times the typical tidal velocity (based on a momentum balance), which occurs at least frequently around slack water. These two aspects indicating the crucial role of the wind explain that the bed profile on the shoal propagated in the main wind direction in the observations. There are regions slightly less affected by wind and waves, for example, the relatively sheltered edge of the shoal with relatively high tidal flow velocities and especially the deep tidal creeks. But the sediment transport on the intertidal shoal is clearly dominated by wind and waves, even in the less exposed areas of the shoal. In the investigated case, only ~1–10% of the transport was induced by the 50% least windy tides on the largest part of the shoal. Even an artificial 1 m lowering of the shoal (roughly half the mean tidal range) did not weaken the dominance of the meteorological processes on the shoal, highlighting the generic importance of the results. This emphasizes that the combination of waves and wind should always be considered in analyses and simulations of intertidal shoals.

Chapter 4

How Storms Impose Variations in Bed Level Dynamics Across Intertidal Flats

This chapter has been submitted to:
Scientific Reports (*De Vet et al.*),
co-authors: Van Prooijen, Colosimo, Steiner, Ysebaert, Herman, and Wang.

Cover photo: measurement frame on the Zuidgors intertidal flat.

While the previous chapter focused on the spatiotemporal variations in hydrodynamics and sediment transport, this chapter focusses on the resulting bed level dynamics across intertidal flats. With field measurements on hydro-morphodynamics, the impact and recovery of an individual storm is studied. Decades of time series on bed levels of various intertidal flats are used to reveal whether certain parts of intertidal flats are more dynamic (i.e., face structurally larger storm-impacts).

ABSTRACT

Hydrodynamic forces on intertidal flats vary over a range of temporal and spatial scales. These spatiotemporal inhomogeneities have implications for intertidal flat morphodynamics and ecology. We determine whether storm events are capable of altering the long-term morphological evolution of intertidal flats, and unravel the contributions of tidal flow, wind-driven flow, waves, and water depth on inhomogeneities in bed level dynamics across these areas. We complement decades of bed level measurements with an extensive one-month field campaign. Across an intertidal flat, the hydrodynamics and morphodynamics of a storm event were captured, including the post-storm recovery. It is shown that individual events can persistently alter the morphological evolution of intertidal flats; magnitudes of bed level changes can even compare to years of continuous evolution. The morphological impacts of events are largely controlled by the relative timing of the forcing processes, and not solely by their magnitudes. We revealed that spatiotemporal variations in bed level dynamics of intertidal flats can be explained by a combination of: (1) the inhomogeneous distributions of the hydrodynamic forcing processes (including the under-explored role of the wind); and (2) the linear proportionality between bed level dynamics and the local bed slope.

4.1. INTRODUCTION

With accelerated sea level rise and anthropogenic interventions, increasing interest is given to the long-term morphological evolution of estuarine intertidal flats (Chapter 2; *Benninghoff and Winter*, 2019; *Dam et al.*, 2016; *Elmilady et al.*, 2018; *Hu et al.*, 2015; *Mariotti and Fagherazzi*, 2010; *De Vet et al.*, 2017; *De Vriend et al.*, 2011; *Wang et al.*, 2015). These areas provide essential ecological values and ecosystem services (*Barbier et al.*, 2011; *Smaal and Nienhuis*, 1992). Even under the questionable existence of morphological equilibria (*Friedrichs*, 2011; *Maan et al.*, 2015; *Zhou et al.*, 2017), intertidal flats are continuously evolving under changing natural and anthropogenic forces (Chapter 2; *Benninghoff and Winter*, 2019; *Dam et al.*, 2016; *Elmilady et al.*, 2018; *De Vet et al.*, 2017; *De Vriend et al.*, 2011; *Wang et al.*, 2015). To understand long-term morphodynamics of intertidal flats, we must unravel the role of fluctuations in the forcing processes on the short-term. Seasonal changes are relatively well described (*Yang et al.*, 2008), but the role of storm events on the morphological evolutions and bed level dynamics are not yet well understood. This knowledge is also required to assess whether the exclusion of (variations in) wind-driven flow (*Elmilady et al.*, 2018; *Hu et al.*, 2015; *Mariotti and Fagherazzi*, 2010) and wind-driven waves (*Dam et al.*, 2016) results in realistic long-term model predictions. As bed level dynamics affect benthic macrofauna (*Bouma et al.*, 2001; *Ysebaert and Herman*, 2002) and salt marshes (*Bouma et al.*, 2016), this has also ecological implications.

Previous studies emphasized the role of storm events on the sediment transport and morphology of intertidal flats (Chapter 3; *Fan et al.*, 2006; *Friedrichs*, 2011; *Janssen-Stelder*, 2000; *Talke and Stacey*, 2008; *De Vet et al.*, 2018; *Yang et al.*, 2003). The spatial distribution in hydrodynamic energy is used to explain the erosion and accretion patterns following an individual event (*Postma*, 1967; *Yang et al.*, 2003). However, the spatial distribution of hydrodynamic energy is site-dependent (*Fan et al.*, 2006; *Yang et al.*, 2003). It varies even within an event as a result of the various time scales over which the underlying hydrodynamic forces fluctuate (*Fan et al.*, 2006; *Green and Coco*, 2014; *Le Hir et al.*, 2000; *Shi et al.*, 2014; *Talke and Stacey*, 2008; *Zhu et al.*, 2017). Therefore, the underlying variations in the hydrodynamic forcing need to be assessed. Only this knowledge can reveal if certain parts of intertidal flats are generally more vulnerable to events (i.e., are more dynamic) than other parts.

This study aims at unraveling the effects of short-term events (on the scale of days) on the long-term morphodynamics (on the scale of years—decades) of intertidal flats. We combine various datasets on intertidal flats in the Eastern Scheldt and Western Scheldt, the Netherlands (Figure 4.1). These intertidal flats are gradually evolving (e.g., Figures 4.1b–4.1c) in response to human interventions (Chapter 2; *De Vet et al.*, 2017; *De Vriend et al.*, 2011; *Wang et al.*, 2015). With decades of high resolution morphological measurements (average interval of 40 days), we identify the role of storm events on these evolutions and quantify the spatial inhomogeneities in bed level dynamics. Complementary measurements on the hydro-morphodynamics in the field provide insights on the forcing processes of the bed level dynamics. For one month we measured the hydro-morphodynamics over a cross-section on the Zuidgors intertidal flat (Western Scheldt; Figure 4.1), capturing the bed level impact and recovery of a storm event (with 10-minute averaged wind speeds of at most 22 m/s and above 15 m/s for 9 hours). Furthermore, ecological impli-

cations were assessed by investigating the abundance of the benthic macrofauna before and after storm events. Based on the data, we introduce new concepts to explain the spatiotemporal patterns in bed level dynamics.

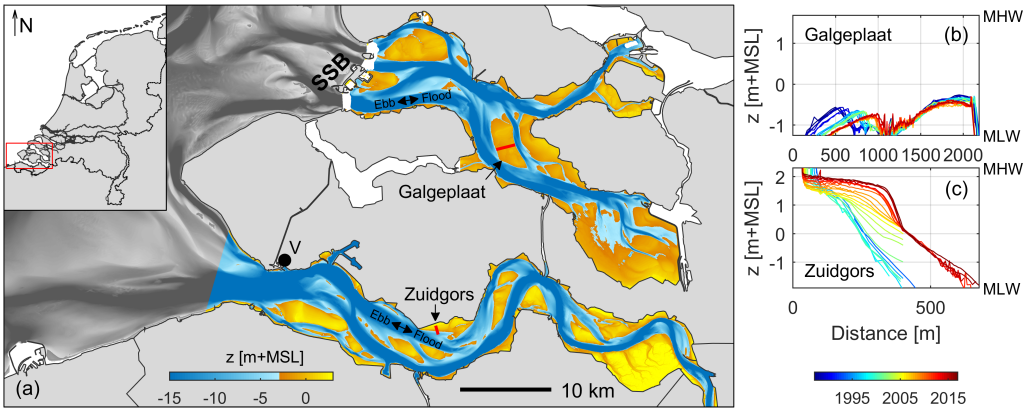

Figure 4.1: (a) Overview of the Eastern Scheldt (top estuary) with its storm surge barrier (SSB) and the Western Scheldt (bottom estuary), including their bathymetry. Both estuaries connect to the North Sea. The Zuidgors and Galgeplaat intertidal flats are indicated. The location of Vlissingen meteorological station (V) is indicated with the black marker. (b)–(c) The evolution of the red transects across the two intertidal flats over the past decades, vertically bounded between mean low water (MLW) and mean high water (MHW).

4.2. Results

4.2.1. Bed Level Dynamics on Decadal Time Scales

Figure 4.2 presents the bed level evolution at fixed locations on the Zuidgors and Galgeplaat intertidal flats (Figure 4.1a), measured on average 7 and 14 times a year, respectively. The measurement points (Z1–Z3; G1–G4) were 40 m to 175 m apart (Figures 4.2a–4.2b). Some short-term deviations along the long-term bed level trends only affected specific locations, while other impacts affected (almost) all measurement points (see Figures 4.2c–4.2d). Even then, the impact was non-uniform (e.g., the first highlighted event in Figure 4.2c). The intertidal flats recovered from various events in Figures 4.2c–4.2d within the next measurements, while other events affected the long-term evolution persistently.

Both identified setbacks (i.e., bed level changes against the long-term evolution) at Zuidgors (Figure 4.2c) had a vertical impact similar to approximately four months of evolution (impact of ~15 cm, evolution of ~50 cm/year). The largest bed level change that persisted at Galgeplaat occurred in 1990 simultaneously at stations G1–G3 (Figure 4.2d). The bed level changes resulted from a major storm event (26 February – 2 March), characterized by 10-minute averaged wind speeds in this area of at most 27 m/s and above 15 m/s for 73 hours. This system has a storm surge barrier in its mouth (Figure 4.1), that closed for four tides within this event, two more than any other storm in record. Figure 4.2e shows the evolution of G1 including a linear fit based on the data measured during the two years before the storm, and a linear fit based on the data measured af-

ter the storm. The bed level evolution rate did not significantly change: -1.90 cm/year before the storm and -1.94 cm/year after the storm, implying no sign of recovery. The 17 cm of erosion during that event was equivalent to nine years of erosion at the average rate.

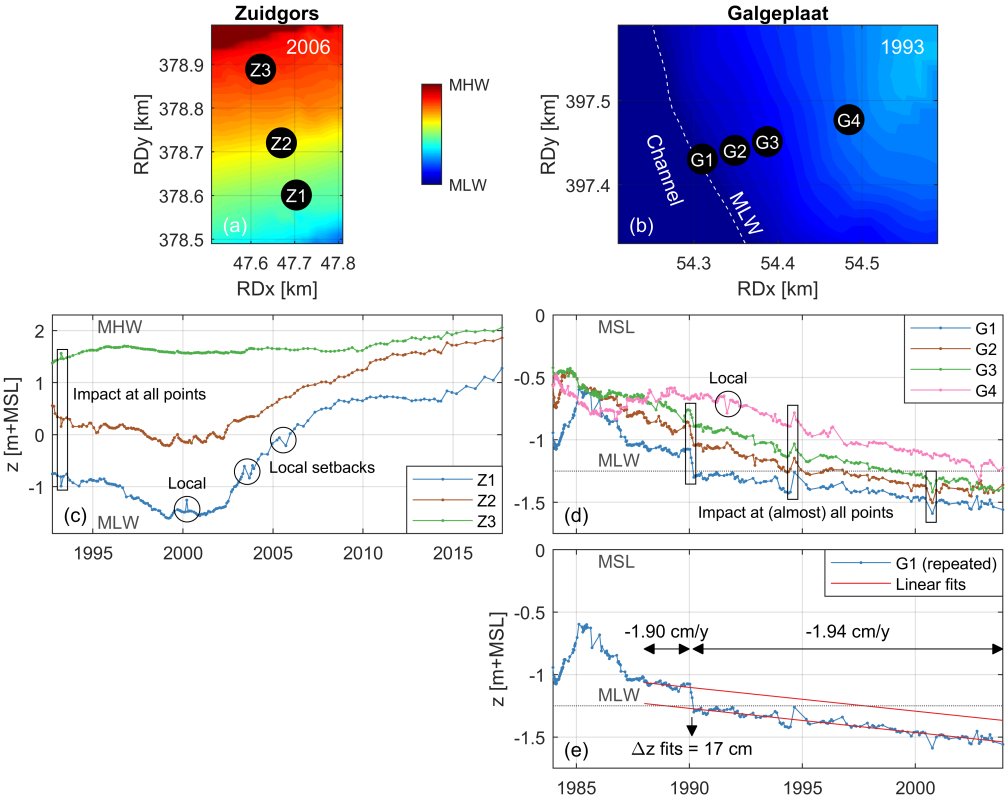

Figure 4.2: Bed level evolution of the point-elevation measurements. (a)–(b) Location of the sampling points Z1–Z3 on the Zuidgors intertidal flat and G1–G4 on the Galgeplaat intertidal flat. See Figure 4.1 for the position of these transects. The elevation maps, measured halfway the period of the time series, are shown as a reference. (c)–(d) Time series of the bed level evolution at Zuidgors and Galgeplaat, respectively. The black rectangular and circular annotations indicate examples of sudden changes in evolution. (e) The time series at Galgeplaat location G1 is repeated. Here, also a linear fit based on the data between 1988 and 1990 and a linear fit based on the data after February 1990 are shown (before and after the 1990 storm).

The bed level evolution at the highest location of Zuidgors Z3 (Figure 4.2c) had a more gradual character than at the other two locations (Z1 and Z2). While these two lower sampling locations increased in elevation, the bed level dynamics reduced in time (i.e., their evolution became more gradual). This suggests there may be a relation between the bed level dynamics and the bed elevation.

With Figure 4.3, the existence of such a relation is tested for intertidal flats in the Eastern Scheldt and Western Scheldt. Only locations with sufficient data are considered (Figure 4.3i): seven intertidal flats in the Western Scheldt and only the Galgeplaat

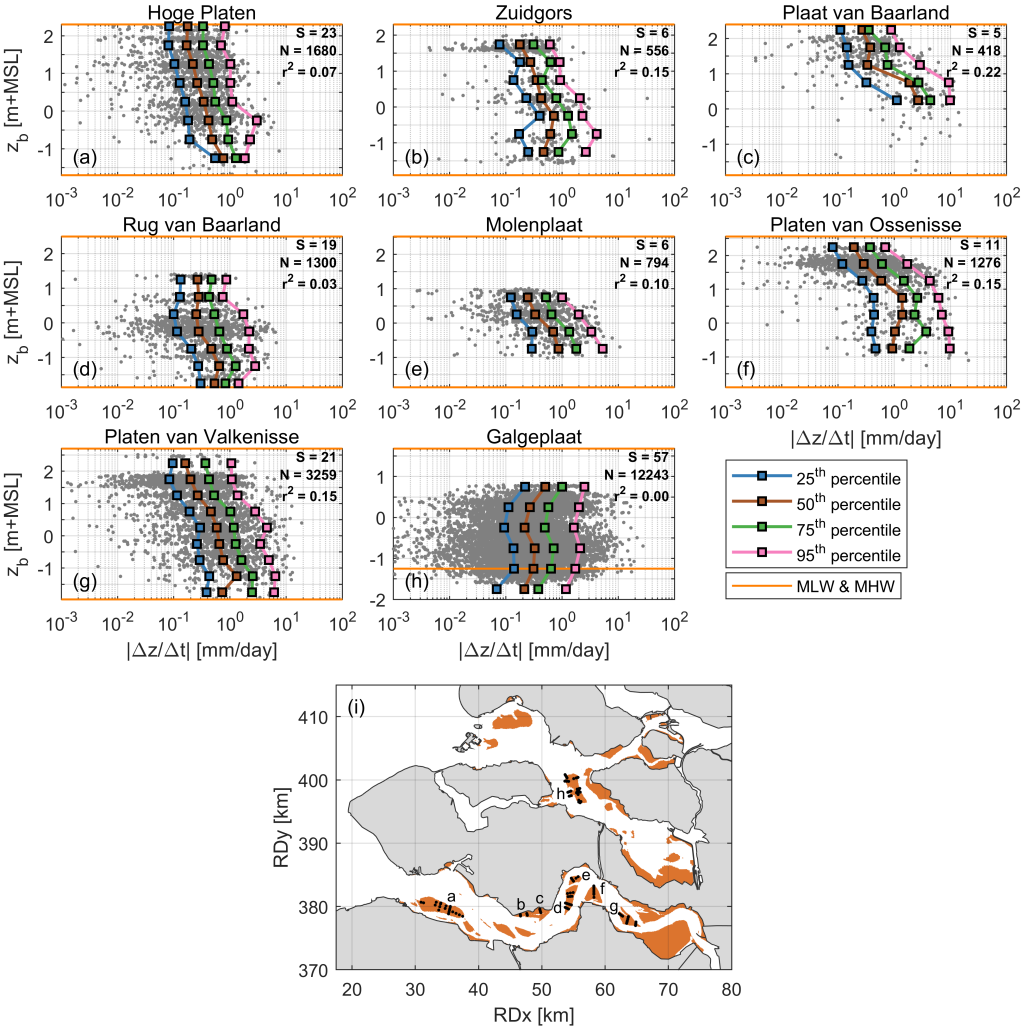

Figure 4.3: (a)–(h) Averaged bed level of two successive measurements versus the bed level rate of change between those measurements (considered as the bed level dynamics). The data is grouped per intertidal flat, see (i) for the location of intertidal flats a–h with the measurement locations indicated as black markers. The number of measurement locations for each flat (S), the total number of samples (N) and the coefficient of determination (r^2) are shown in the top right corner for each flat. The horizontal grid lines represent the boundaries of the vertical bins over which the percentiles are computed. Percentiles are only shown for vertical bins that contained at least 20 data points. All plots are vertically bounded by mean low water (MLW) and mean high water (MHW), apart from (h) that contained also a substantial amount of data points below MLW. Absence of data at the top of the tidal window in (d), (e), and (h) is due to the limited height of these flats, while absence of data at the bottom of the tidal window is solely due to absence of measurements at those elevations.

in the Eastern Scheldt. The bed level dynamics are computed by dividing the elevation change of two successive measurements (corrected for the 5 year moving average) by the time interval. The bed level dynamics are shown versus the average elevation of the two

successive measurements. For each intertidal flat, data from all measurement locations were merged. The average duration between successive measurements was 40 days. For each bin of 0.5 m, the 25^{th}, 50^{th}, 75^{th}, and 95^{th} percentiles were determined.

The vertical trends are relatively consistent along the different percentiles. Consistently for all sites in the Western Scheldt (i.e., excluding Galgeplaat), the bed level dynamics reduce by approximately one order of magnitude from the lower to the higher part of the flat. In contrast, such a pattern in bed level dynamics was not observed for Galgeplaat, where the bed was actually more dynamic above MSL (mean sea level). In the Western Scheldt 3—22% of the variance in the logarithm of the bed level dynamics is explained by elevation, whereas none of this variance is explained by elevation for the Eastern Scheldt samples (see coefficients of determination in Figure 4.3).

4.2.2. INHOMOGENEOUS MORPHOLOGICAL IMPACT OF A STORM EVENT

The long-term data infer a spatiotemporally inhomogeneous character in the evolution of intertidal flats. To reveal the mechanisms that drive this spatiotemporal inhomogeneity, measurements of wind, water levels, flow, waves, suspended sediment concentrations, and bed levels during a single storm event (20 November 2016) were analyzed in detail. Time series of these processes at three stations across the Zuidgors intertidal flat (Figure 4.4a) are shown in Figures 4.4b–4.4n.

The peak of the storm (hourly-averaged wind speeds up to 22 m/s, Figure 4.4b) coincided with low water (Figures 4.4c–4.4e). The storm surge reached 1.3 m. The lowest elevated frame F_L (0.4 m above mean low water; MLW) was submerged during the storm peak (Figure 4.4d), while it would have been emerged in absence of the storm. This station faced a water depth of 0.8—1.3 m for four successive hours around low water. Instead, the highest elevated frame F_H (1.0 m above MSL) was emerged during the peak of the storm.

Under mild wind conditions (e.g., the first and last tide in Figure 4.4), the velocities were flood-dominant, with maximum velocities occurring just before high water. The velocities were predominantly alongshore directed (not shown here), with spring-tidal velocities near the MLW line up to 1.5 m/s. The velocity magnitudes gradually decreased toward higher bed elevations of the flat.

While the flow in the channel reversed precisely at low water (Figure 4.4h), the flow at F_L reversed two hours before (Figure 4.4g), despite the two locations were only 200 m apart. At F_L, the velocity exceeded 0.7 m/s for two hours around low water. The flow at F_H was also modified: it was almost solely ebb-directed in the tide preceding the storm peak (second tide in Figure 4.4f). The largest amplification of the flow occurred at F_L, as F_H was emerged during the peak of the storm. But even with the 0.7 m/s amplification at F_L during low water, larger velocities occurred during calmer wind conditions (e.g., first tide in Figure 4.4f). However, these larger velocities occurred for larger water depths and for shorter durations.

Significant wave heights exceeded 0.60 m at both frames. However, waves were absent (by emergence of the bed) or depth-limited (roughly half the water depth) at F_H for a large portion of time. While F_L was submerged during the peak of the storm, waves were there depth-limited for more than three successive hours around low water.

Suspended sediment concentrations were measured at 0.1 m and 0.6 m from the bed

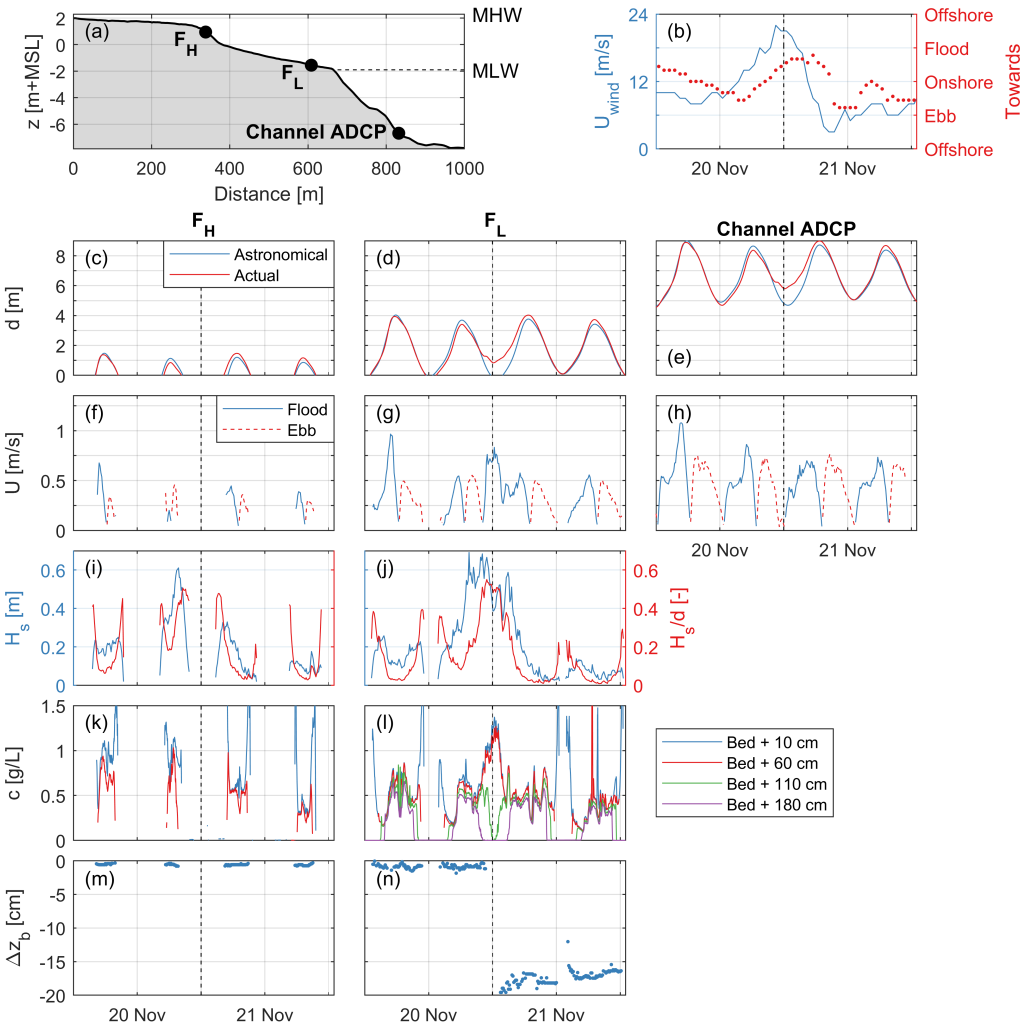

Figure 4.4: Process measurements for four tides along a storm event in 2016 on the Zuidgors intertidal flat. (a) Measurement stations (see Figure 4.1a for location of the transect). (b) Hourly-averaged wind speeds and directions at Vlissingen meteorological station (location in Figure 4.1). (c)–(e) Water depths, including the derived astronomical water depths (difference is storm surge). (f)–(h) Flow velocity magnitudes (flood and ebb directions indicated in Figure 4.1). (i)–(j) Significant wave heights (the wave logger of F_H was positioned 50 m downslope), including the significant wave height over depth ratio. (k)–(l) Suspended sediment concentrations at various distances from the bed. (m)–(n) Bed level changes relative to the initial elevations. The vertical black dashed lines indicate the peak of the storm. All time series are in CET (UTC+1).

at both frames, and also at 1.1 m and 1.8 m from the bed at F_L (Figures 4.4k–4.4l). The concentrations were relatively uniform over the water column (differences smaller than 30%). Concentration peaks are observed during flow peaks and during conditions for which the wave heights were depth-limited. These two conditions did not occur simul-

taneously for the tides with mild wind conditions. However, during the low water at the storm peak, the amplified flow and breaking waves coincided for hours at F_L. As a result, concentrations exceeded 1 g/L for 2.5 hours. This concentration peak had a one order of magnitude longer duration compared to the other observed concentration peaks.

The changes in bed level at F_H were less than half a centimeter during these four tides. The storm did not cause a distinctive impact here (Figure 4.4m). Conversely, the bed level at F_L lowered 20 cm during the storm (Figure 4.4n). This drop in elevation occurred within a 3 hour window around low water at the peak of the storm. This 3 hour window at F_L coincided precisely with the windows during which the water depth was limited to 0.8-1.3 m, the velocity was amplified to ~0.7 m/s, the waves experienced depth-induced breaking, and the concentrations were above 1 g/L. A comparable simultaneous peaking of the forcing processes for hours did not occur at F_H. Already after the first tide after the storm peak (last tide in Figure 4.4n), 20% of the impact (0.04 m) at F_L was recovered.

4.2.3. INHOMOGENEITY OVER LONGER TIME SCALES

The spatiotemporal variability in the forcing processes drove the inhomogeneity of the storm impact. Substantial variations in the forcing processes were also present over longer time scales. Figure 4.5 shows the measurements over the full one-month measurement campaign at Zuidgors.

Figure 4.5a indicates that the bed level at F_H was not only relatively stable during the storm, but also over the full month (less than 2 cm erosion over 30 days). Before the 20 cm erosion, the bed level at F_L was relatively stable (comparable evolution as at F_H). Half of the erosion (0.1 m) recovered within three days after the storm. After two weeks, the bed returned to a relatively stable and similar evolution as at F_H. However, 25% of the erosion (5 cm) persisted.

The largest waves occurred during the highlighted storm event (Figure 4.5b). The other smaller wave events, with significant wave heights up to ~0.4 m, did not coincide with sudden changes in evolution.

Over the month, the tides varied substantially (Figure 4.5c). The tidal range fluctuated between 3.0 and 4.9 m. Spring-neap fluctuations were present (spring tide at the beginning, halfway, and end of the record) while the storm surges also affected the water levels (e.g., Figure 4.4e). While the storm event occurred in-between spring tide and neap tide, the storm surge reduced the tidal range during the storm event to almost the smallest of all measured tides. Variations between spring-neap cycles were also present. The spring tides in the middle of the record reached a tidal range up to 4.3 m, more than 0.5 m smaller than the preceding and proceeding spring periods.

Spring-neap fluctuations were reflected in the peak flood velocities, with variations between 0.35 and 1.46 m/s (a ratio of maximum variation of 4.2) at F_L (Figure 4.5d). Figures 4.5f–4.5h show a proportionality between the tidal range and the peak velocity for all measurement locations (77—83% of the variance in the peak velocities was explained by the tidal range). The storm event of Figure 4.4 is an outlier at F_L in Figure 4.5g, although this was the only velocity peak that occurred during low water (Figure 4.4g). The spring-neap fluctuations in the ebb peaks were much less, these varied only between 0.43 and 0.58 m/s (a ratio of maximum variation of 1.3). Therefore, there were not only variations

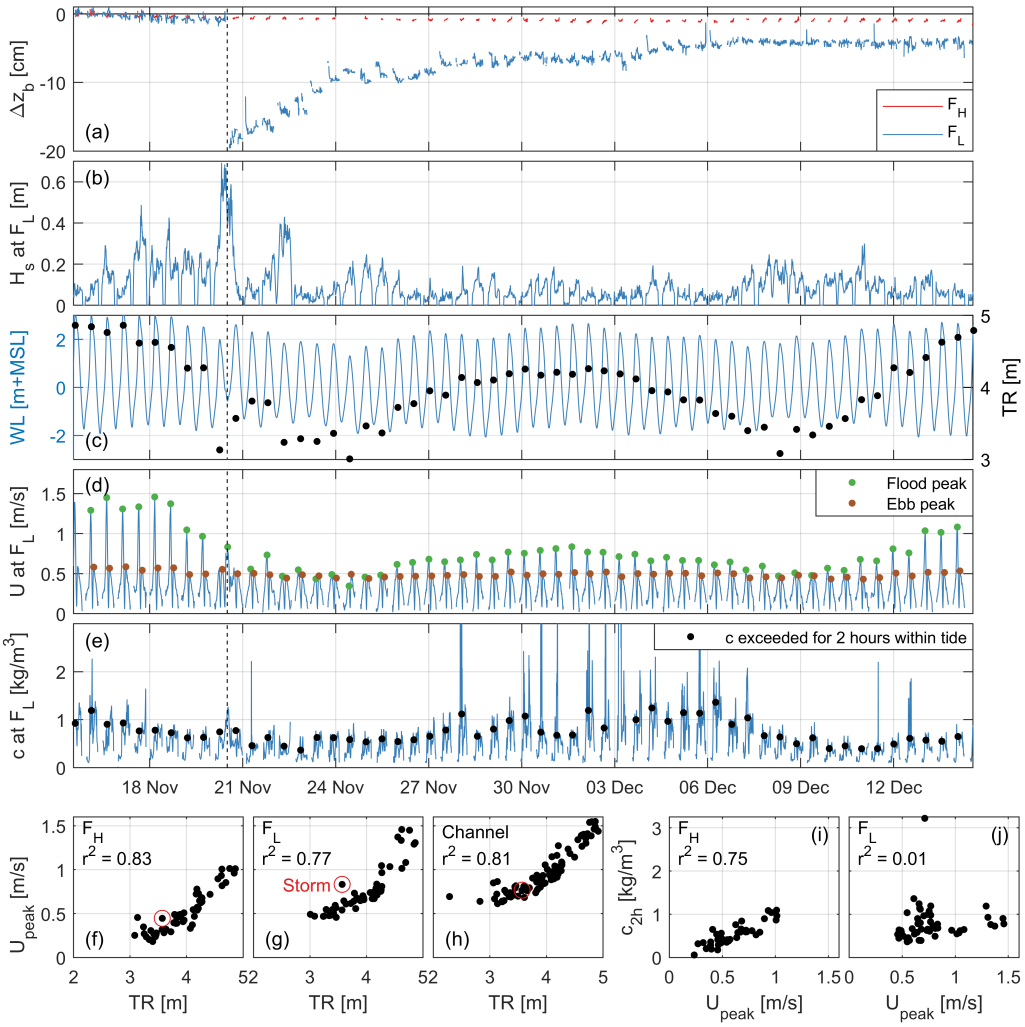

Figure 4.5: Process measurements for the full one month campaign on the Zuidgors intertidal flat (see Figures 4.1a and 4.4a for the locations). (a) Bed level changes for both frames relative to the initial elevations. (b) Significant wave heights at F_L (near mean low water). (c) Water levels as measured in the channel (indicative for the full flat), the markers indicate the tidal range. (d) Flow velocity magnitudes at F_L, the markers indicate the flood and ebb peaks. (e) Suspended sediment concentrations 60 cm above the bed at F_L, the markers indicate the concentration that was exceeded for two hours. (f)—(h) the maximum velocity of each tide versus the tidal range. The storm of Figure 4.4 is indicated with the open circle. (i)—(j) the suspended sediment concentrations that were exceeded for two hours versus the maximum velocity of each tide. The vertical black dashed lines indicate the peak of the storm of Figure 4.4. All time series are in CET (UTC+1).

in peak velocities across the spring-neap cycles, but also in velocity asymmetries.

Figure 4.5d shows for F_L the variations in suspended sediment concentrations 0.6 m above the bed, with the values that were exceeded for two hours each tide indicated separately (less sensitive to outliers than the maxima). The suspended sediment concen-

trations show variations along the spring-neap cycles. However, even though the spring tides in the middle of the record did not feature the largest tidal range and peak velocities in the record, the concentrations were higher than during the preceding and following spring periods. This is expressed in Figure 4.5j as well, which shows no clear relation (r^2 of 0.01) between the concentrations that were exceeded for two hours and the peak velocities at F_L. However, these concentrations did correlate well to the peak velocities at F_H (r^2 of 0.75).

Figures 4.5f–4.5h indicate that peak flow velocities decrease for increasing distances from the channel (i.e., for increasing bed elevations). Figure 4.6 presents modeled average peak velocities in relation to the bed level for the full Western Scheldt and Eastern Scheldt. For both estuaries the peak velocities are generally smaller at higher bed elevations. In the Western Scheldt, 51% of the variance in the average peak velocities on the intertidal flats is explained by only the elevation, in the Eastern Scheldt (which has closed branches) this is 9%. Almost all data points in the Eastern Scheldt are below the linear fit of the Western Scheldt. There is thus an inhomogeneity in flow velocities over different elevations, within an estuary (spread across the linear fits), and between different estuaries.

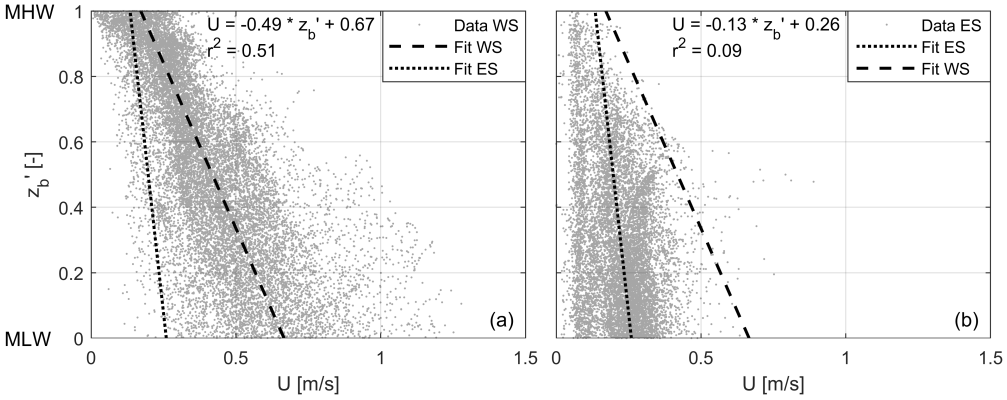

Figure 4.6: Bed level, scaled along mean low water (MLW; 0) and mean high water (MHW; 1), versus the average peak flow velocity from a one month simulation. All points on the intertidal areas of the full (a) Western Scheldt (WS) and (b) Eastern Scheldt (ES) are shown. Linear fits are provided with coefficients of determination (r^2). The fits of both estuaries are shown in both graphs to allow comparisons.

Over long time scales, the distributions of both the occurrence and strength of the forcing processes vary across intertidal flats. Figure 4.7 shows the relative timing of the various hydrodynamic processes across the elevations of Zuidgors. Because of temporal variations in the changes in water level (Figure 4.7a), the water level occurrence is not homogeneously distributed (Figure 4.7b). Even with surge and spring-neap fluctuations, the probability of occurrence of a water level near MLW and MHW (mean high water) is largest (Figure 4.7c). This distribution prescribes the probability of occurrence of a certain water depth (water level - bed level) over a variation in bed level (Figure 4.7h).

The strength of the processes varies with water depth and bed elevation. Tidal flow velocities decrease with a decrease in water depth (Figure 4.7d). Outliers are part of the

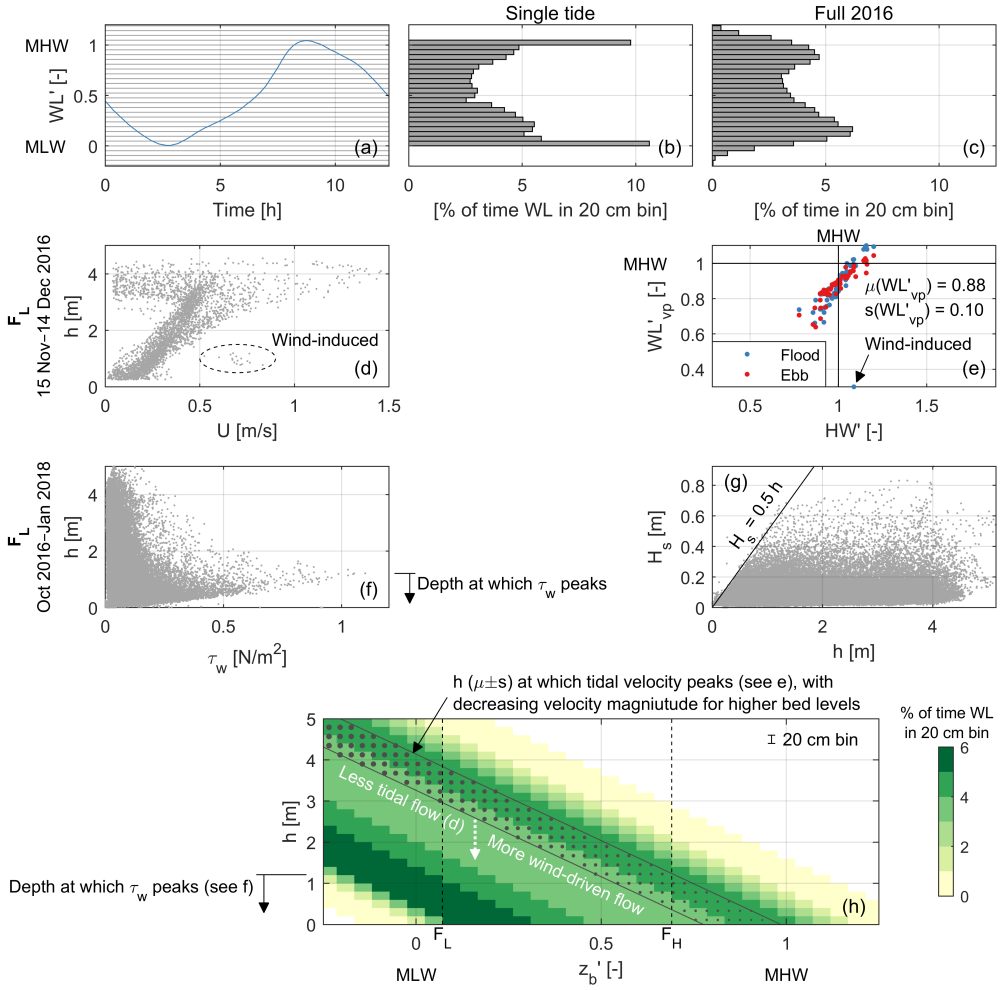

Figure 4.7: Distributions in hydrodynamic forcing for variations in water depth and bed level. (a) Example of the water level over a single tidal cycle at the Zuidgors intertidal flat (29 November 2016). The horizontal lines indicate 20 cm bins. (b) The corresponding probability distribution of the water level across the 20 cm bins. (c) The probability distribution of the water level over a full year (2016). (d) Water depth versus the flow velocities at F_L (10 minute interval). The wind-induced flow during the storm event of Figure 4.4 is marked with the ellipse. (e) Water levels at which the velocities peak at F_L, versus the high water of each tide. The storm of Figure 4.4 is indicated. Both axes are scaled along mean low water (MLW; 0) and mean high water (MHW; 1). (f) Water depth versus the wave induced shear stresses at F_L (10 minute interval). (g) Significant wave height versus water depth measured at F_L (10 minute interval). (h) For a range in bed levels (scaled along MLW and MHW) the probability that the water depth is within a certain 20 cm bin is indicated with the colors, using the distribution of (c). The diagonal dotted area indicates the water depths at which the tidal velocities peak, using the average and standard deviation of (e). The decay in dot size represents a decay in peak velocities. The range of depths at which the wave induced shear stress peaks, based on (f), are indicated on the left. The vertical dashed lines show the position of the frames. The increase in wind-driven flow is discussed in the discussion.

wind event of Figure 4.4. The reversal of the flow at high water causes also smaller velocities at large water depths. The higher the high water level of a tide, the higher the water level at which tidal flow velocities peak (r^2 = 0.85 at F_L; Figure 4.7e). The average water level at which the tidal flow velocities peak equals 0.88±0.10 (scaled between MLW and MHW) at F_L and almost identically 0.93±0.10 at F_H. Therefore, tidal velocities peak for smaller water depths at higher bed levels (Figure 4.7h), which goes together with a decrease in peak velocity magnitude (Figures 4.5f–4.5h and Figure 4.6). Significant wave heights do not exceed half the water depth at this location (Figure 4.7g). Within the 16 months of wave measurements, the maximum wave-induced shear stress occurred for water depths smaller than 1.2 m (Figure 4.7f). For any of these processes yields, the longer the duration they are effective (probability of occurrence of a certain water depth), the larger their impact.

4.2.4. INHOMOGENEOUS IMPACT ON BENTHIC MACROFAUNA

In this section, we show that the spatiotemporal inhomogeneity of storm impacts on intertidal flats may also be reflected by the ecology. Figure 4.8 presents the logarithm of the abundance (mean and standard deviation) of benthic macrofauna before and after two storms in 2017 (in October and November, respectively; i.e., different storms than the one of Figure 4.4) over six stations along a transect of 210 m with various emersion times on the Zuidgors intertidal flat (1 km west of the frames of Figure 4.4). During both storm events, the hourly-averaged wind speed exceeded 15 m/s for several hours.

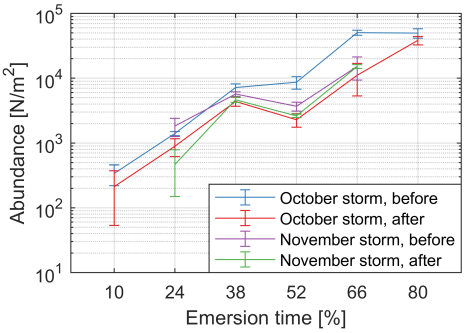

Figure 4.8: The abundance of benthic macrofauna (number of individuals per m^2) across six stations equally spaced in emersion time on the Zuidgors intertidal flat. Benthic macrofauna were sampled around the 5 October 2017 and the 23 November 2017 storm events, with at most 10 days between the before storm and the after storm measurements. The error bars (one standard deviation above and below) are based on three replicates.

The abundance was already spatially inhomogeneous before the storms. In general the abundance increases with increasing emersion time (i.e., increasing bed level). However, the highest two stations (66% and 80% emersion time) had an almost equal quantity of benthic macrofauna before the first storm. Despite this similarity, the responses to the October storm were different: the 66% emersion time station reduced 80% in abundance, while the 80% emersion time station reduced only 20% in abundance. The data before the November storm showed only a limited recovery. A reduction in abundance followed the November storm, although smaller compared to the October storm. The

highest measured location (66% emersion time) remained even equally abundant. The main species affected by these storms were the mudshrimp *Corophium sp.* (< 1 year life span) and the red thread worm *Heteromastus filiformis* (1—2 year life span).

4.3. Discussion

Substantial spatiotemporal inhomogeneities in the impact of storm events on bed level dynamics of intertidal flats have been identified. There is a variation in the spatial extent of storm impacts on intertidal flats, in which variations in storm intensity and duration play a role (similar to *Talke and Stacey*, 2008). We can distinguish the short-term bed level variations around a storm event and the long-term evolution of an intertidal flat. But also sudden bed level changes during storm events can persist in the long-term evolution, even if they partially recover. Sudden bed level changes during storm events are relevant to consider in the long-term evolution of intertidal flats, as they may compare to years of continuous evolution. Systems that face shortages in sediment supply (such as the Eastern Scheldt) have typically less recovery capacity (*Yang et al.*, 2003). Differences in recovery will also relate to differences in tidal forcing (the sole forcing present during calm conditions), which varies over elevations and across estuaries (e.g., Figure 4.6). Whether or not the impact is in line with the long-term evolution direction (i.e., towards a possible equilibrium) may also affect the recovery. But long term consequences will persist even in case the morphology completely recovers, e.g., benthic macrofauna eroded or washed out during events are not instantly replaced (Figure 4.8) and changes in erodibility of the bed may follow (*Zhu et al.*, 2019).

Consistently across the intertidal flats in the Western Scheldt, the bed was more dynamic at lower bed elevations (Figures 4.3a–4.3g). A similar trend was observed in other studies in this estuary (*Belliard et al.*, 2019; *Hu et al.*, 2017; *Willemsen et al.*, 2018). In contrast to our decades of measurements with an average measurement interval of 40 days, these studies measured the dynamics with an interval of about one day over approximately one year. The relation between bed level dynamics and the bed elevation persists hence over various measurement intervals (tides—weeks) and is present over various time frames (years—decades). For the Galgeplaat intertidal flat (Eastern Scheldt), such a trend was not observed (Figure 4.3h).

To explain differences in bed level dynamics across intertidal flats, we consider the sediment conservation equation for an alongshore uniform intertidal flat (i.e., no gradients in sediment transport in alongshore direction):

$$\frac{\partial z}{\partial t} = -\frac{1}{1-p}\frac{\partial S}{\partial x}, \tag{4.1}$$

where z is the bed level, t time, p the porosity, S the sediment transport rate, and x the distance in cross-shore direction. This equation shows that bed level changes/dynamics are a consequence of gradients in the sediment transport rates. We showed that the forcing processes, and hence also the resulting sediment transport rates, are partly a function of the bed elevation (Figures 4.6 and 4.7h). Therefore, it is meaningful to consider the gradients in sediment transport over the bed elevations. Substituting the bed slope

($\beta = \partial z/\partial x$) in Equation 4.1, it results in:

$$\frac{\partial z}{\partial t} = -\frac{\beta}{1-p}\frac{\partial S}{\partial z}. \tag{4.2}$$

This shows that the bed level dynamics are proportional to (1) the local steepness of an intertidal flat and (2) the gradient in sediment transport (i.e., forcing processes) over the bed level.

Component (1) of Equation 4.2 reveals that the bed level dynamics of intertidal flats are linearly proportional to their local bed slope. In the Western Scheldt, the bed slope typically decreases by one order of magnitude for elevations from MLW to MHW (Chapter 2; *De Vet et al.*, 2017). This implies that the bed level dynamics decrease by one order of magnitude across these elevations due to variations in bed slope alone, which is precisely the trend observed in Figure 4.3. The bed slope gradients are less across the intertidal flats in the Eastern Scheldt (Chapter 2; *De Vet et al.*, 2017), which is (part of) the explanation for the smaller variation in bed level dynamics over the vertical in the Eastern Scheldt (Figure 4.3). As bed slopes of intertidal flats can evolve significantly over decades (Chapter 2; *De Vet et al.*, 2017), this equation implies hence also changes in bed level dynamics.

Following component (2) of Equation 4.2, the bed level dynamics are also proportional to the variations in the sediment transport (i.e., forcing processes) over bed elevations. The frame measurements revealed spatiotemporal variations over an individual storm event. The erosion at the lowest elevated frame was two orders of magnitudes larger than at the highest elevated frame. The large bed level changes at the lowest elevated frame related to a concurrence of: an almost maximum water depth for which the acting waves still broke, flow velocities (mainly wind-driven) that were relatively large for these water depths, higher suspended sediment concentrations than during calm conditions for these water depths, and this all for a large duration (hours). This concurrence of processes, in contrast with the emerged higher elevated frame, was conducive to the large bed level change. As the peak of the storm coincided with low water, the flow in the channel (only 200 m from the MLW line) was almost stagnant (Figure 4.4h). Firstly, this implies that the 0.7 m/s flow on the intertidal flat was not tide-driven but largely wind-driven instead. This is in line with the estimate of wind-driven velocities of order 1/40 of the wind speed (Chapter 3; *De Vet et al.*, 2018), with smaller contributions for larger tidal forcing (limited these hours) and larger water depths (where inertia is significant). Secondly, the limited flow and wave effects in the channel imply large variations in sediment transport between the channel and the intertidal flat.

Figure 4.7h reveals that it was not a coincidence that the largest bed level dynamics, resulting from the variations in forcing processes, occurred at the lowest elevation of the intertidal flat. Wave impacts relate strongly to water depth (*Fagherazzi et al.*, 2006; *Green and Coco*, 2014; *Le Hir et al.*, 2000; *Mariotti and Fagherazzi*, 2013), with maximum wave induced shear stresses for the largest water depth at which the waves are depth-limited (*Green and Coco*, 2014). At the low elevations of the intertidal flat the tidal flow velocities are small for these water depths (Figure 4.7h), but can be amplified by the wind especially for small tidal velocities (Chapter 3; *De Vet et al.*, 2018). At higher elevations the tidal velocities peak for these small water depths (Figure 4.7h), but there the peak veloc-

ities are less (Figures 4.5f–4.5h and Figure 4.6). Figure 4.7h indicates that the duration of the effective small water depths is the longest just above the MLW line. This means that the long-term likelihood of having a storm event occurring with favorable conditions for large bed level dynamics is the largest for the lowest part of the intertidal flat. This is an extension to studies that stressed the crucial role of timing and duration of events (*Fan et al.*, 2006; *Talke and Stacey*, 2008; *Yang et al.*, 2003), and that observed the largest bed level changes during short fractions of the tidal period (*Shi et al.*, 2017).

A secondary effect of the bed slope on the bed level dynamics through component (2) has to be discussed. Even though the forcing processes are largely a function of the bed elevation, the bed slope may still affect the waves and the flow. The gradient in wave height over bed elevations is inversely proportional to the wave-breaking index $\gamma = H/h$ (with H the wave height and h the water depth) within the wave-breaking zone:

$$\frac{\partial \mathrm{H}}{\partial z} = \gamma \frac{\partial h}{\partial z} = -\gamma. \tag{4.3}$$

As γ decreases with decreasing bed slopes (*Le Hir et al.*, 2000; *Salmon and Holthuijsen*, 2015), both the wave height and the gradient in wave height over z are smaller for smaller bed slopes. Therefore, a decrease in bed slope implies a decrease in bed level dynamics, just as component (1). For systems in which the flow has large alongshore components (like in the Eastern Scheldt and Western Scheldt), no general relation exists between a change in bed slope and a change in flow velocity, as they depend on the geometry of the channel-flat system. The transport gradients may hence also increase for milder bed slopes. However, due to the wind, the effect of the bed slope on the tidal velocities is irrelevant for at least the lowest part of intertidal flats, as the tidal flow is there limited at water depths for which waves are important. There, the decrease in bed level dynamics for a decrease in bed slope remains a general concept.

The pattern of decreasing tidal velocities for higher bed elevations (Figure 4.6) is present in many other estuaries (*Friedrichs*, 2011; *Yang et al.*, 2008). Furthermore, the relatively long duration of water levels around low water is a general consequence of the shape of a tidal wave. Therefore, in other estuaries similarities in the likelihood distribution of the bed level dynamics across intertidal flats are expectable. Apart from gradients in sediment transport and the bed slope, bed level dynamics may also be affected by aspects such as grain size variability (*Daidu et al.*, 2013; *Yang et al.*, 2008), benthos (*Austen et al.*, 1999; *Herman et al.*, 2001; *Widdows et al.*, 2004), and bed erodibility (*Zhu et al.*, 2019). Furthermore, differences around an individual intertidal flat may result from differences in wave climate, for example, following variations in fetch (*Mariotti and Fagherazzi*, 2013).

Compared to previous studies that solely compared the wave and tidal forcing to explain bed level dynamics patterns (*Belliard et al.*, 2019; *Hu et al.*, 2017, 2018; *Willemsen et al.*, 2018), the key role of wind-driven flow is under-explored. We showed that, for the lowest elevations of an intertidal flat, the wind essentially replaces the tidal forcing which is small for water depths at which waves are most efficient. Furthermore, the role of the bed slope on the bed level dynamics of intertidal flats was not revealed before, although it explains differences in bed level dynamics proportional to the differences in bed slope. The identified spatiotemporal inhomogeneities in forcing processes and bed

level dynamics have direct implications for inhomogeneities in benthos (e.g., Figure 4.8). When the bed level or bed slope of an intertidal flat evolves over time, structural changes in bed level dynamics will follow and related changes in benthic macrofauna can occur.

STUDY AREAS

This study focused on various intertidal areas within the Eastern Scheldt and Western Scheldt (both located in the Netherlands; see Figure 4.1). Both estuaries are connected to the North Sea. The Eastern Scheldt has no river inflow, and has since 1986 a storm surge barrier at its mouth which closes under severe storm conditions. The mean tidal range in the Eastern Scheldt ranges from 2.5 m in its mouth up to 3.5 m in one of its branches. The Western Scheldt has an average river discharge of about 100 m^3/s, which is at the mouth only approximately 0.1% of the tidal discharge. The mean tidal range in the Western Scheldt ranges from 3.5 m in its mouth up to 5 m near the Belgian border (upstream). For the deepening and maintenance of the navigation channel of the Western Scheldt, sediment relocations take place. The human interventions in both systems affect the long-term evolutions of the intertidal flats. Past decades, the intertidal flats in the Western Scheldt mainly raised and steepened, while in the Eastern Scheldt the intertidal flats lowered and flattened out (Chapter 2; *Louters et al.*, 1998; *De Vet et al.*, 2017; *Wang et al.*, 2015).

METHODS

Rijkswaterstaat (the Dutch Ministry of Infrastructure and the Environment) has been extensively measuring the long-term morphological changes of intertidal flats over various temporal and spatial scales for decades. Annual dGPS-RTK elevation transects have been measured on intertidal flats in both the Eastern Scheldt and Western Scheldt since 1987. Additionally, point-elevation measurements have been measured at fixed locations on the intertidal flats of both estuaries since 1984. Time series of Zuidgors and Galgeplaat are used in this study to analyze the effect of storm events on the long-term evolution of these areas. Furthermore, the data of also other intertidal flats in the Western Scheldt are systematically analyzed to study a possible relation between bed elevation and the bed level dynamics. The average measurement interval was 40 days. These data have been gathered with Sediment Erosion Bars until 2008, and with RTK-dGPS afterward. For every measurement, 15 samples were averaged within a 2 m radius, such that local irregularities were excluded. The bathymetric maps in this study are based on single beam and LiDAR measurements (*Marijs and Paree*, 2004; *Wiegmann et al.*, 2005).

Complementary to these long-term morphological datasets, we have deployed instruments to measure the hydro-morphodynamics over one month (15 November – 15 December 2016). These data are used to study the hydro-morphodynamic processes during an individual storm event, and the calm period surrounding this event. The instruments were placed along a cross-shore transect on the Zuidgors intertidal flat in the Western Scheldt (Figures 4.1a and 4.4a). Two measurement frames were deployed on the intertidal flat (F_H 1.0 m above MSL; F_L 1.6 m below MSL). In the adjacent channel, an Acoustic Doppler Current Profiler (ADCP) was deployed (6.8 m below MSL), which measured velocities on a 10 minute interval with a 0.5 m bin size.

Each frame contained an Acoustic Doppler Velocimeter that sampled bed elevations at 10 minute intervals. Each frame also contained a vertical array of two (F_H) or four (F_L) Optical Backscatter Sensors (OBSes) that were at least 50 cm spaced. After a post-campaign calibration against water samples with suspended sediment from the site, the OBSes provided time series of suspended sediment concentrations. Near each frame, an upward-looking ADCP was deployed which measured the velocities in the water column on a 10 minute interval with a 0.1 m bin size. Also a 10 Hz pressure sensor was deployed in the bed near each frame to measure water levels and waves (these were deployed for a longer period, October 2016 – February 2018). The pressure signals were corrected for measured atmospheric pressure fluctuations. Wave-induced shear stresses were computed following *Soulsby* (1997). Water levels measured at the nearby tidal gauge station Borssele (7 km downstream of Zuidgors) were used for the analyses that required continuous long-term water level data (the instruments on the intertidal flat emerged). Wind data was retrieved from the KNMI Vlissingen wind station (17 km west of Zuidgors).

For the derivation of system-wide peak velocities on the intertidal flats of both estuaries (Figure 4.6), depth-averaged numerical simulations with the Delft3D model (*Lesser et al.*, 2004) are used. While these simulations are the same as presented in Chapter 2 and *De Vet et al.* (2017), we consider in this study the peak velocities in relation to the bed level, instead of visually on a map. For both estuaries, the simulations had been calibrated and validated with measured hydrodynamics (*Pezij*, 2015; *Van der Werf et al.*, 2015a).

Before and after two storms in 2017 (October and November), benthic macrofauna (i.e., macroinvertebrates > 1 mm) were sampled (3 sediment core replicates, Ø10 cm, 30 cm depth) on the Zuidgors intertidal flat. These were sampled over a cross-shore transect 1 km west and parallel of the 2016 measurement frames. The benthic macrofauna samples were determined to species level and the abundance (N/m^2) of the community was calculated. The six sampling stations were equally distributed in emersion time (between 10% and 80% emersion time).

Chapter 5

Sediment Disposals in Estuarine Channels Alter the Eco-Morphology of Intertidal Flats

This chapter has been published as:
Journal of Geophysical Research: Earth Surface (*De Vet et al.*, 2020),
co-authors: Van Prooijen, Colosimo, Ysebaert, Herman, and Wang.

Cover photo: aerial photograph of the Zuidgors intertidal flat.

The results of Chapter 2 revealed that human interventions can significantly influence the evolution of intertidal flats. However, anthropogenic forces may be spatiotemporally inhomogeneous, which applies especially to sediment relocations. This challenges the decomposition of underlying mechanisms on a system scale. Therefore, this chapter focusses on the mechanisms that drive the response of an individual intertidal flat to sediment disposals in its adjacent channel. Decades of bathymetric data are analyzed to reveal the eco-morphological chain of consequences that was initiated after the disposals started.

ABSTRACT

Dredging of navigation channels in estuaries affects estuarine morphology and ecosystems. In the Western Scheldt, a two-channel estuary in the Netherlands, the navigation channel is deepened and the sediment is relocated to other parts of the estuary. We analyzed the response of an intertidal flat to sediment disposals in its adjacent channel. Decades of high-frequency monitoring data from the intertidal flat show a shift from erosion toward accretion and reveal a sequence of cascading eco-morphological consequences. We document significant morphological changes not only at the disposal sites, but also at the nearby intertidal flats. Disposals influence channel bank migration, driving changes in the evolution of the intertidal flat hydrodynamics, morphology, and grain sizes. The analyzed disposals related to an expansion of the channel bank, an increase in bed level of the intertidal flat, a decrease in flow velocities on this higher elevated flat, and locally a decrease in grain sizes. These changes in turn affect intertidal flat benthic communities (increased in quantity in this case) and the evolution of the adjacent salt marsh (retreated less or even expanded in this case). The shifts in evolution may occur years after dredged disposal begins, especially in zones of the flats farther away from the disposal locations. The consequences of sediment disposals that we identify stress the urgency of managing such interventions with integrated strategies on a system scale.

5.1. INTRODUCTION

Sediments are relocated in estuaries for the deepening and maintenance of navigation channels (e.g., *Kerner*, 2007; *De Vriend et al.*, 2011; *Monge-Ganuzas et al.*, 2013; *Zhu et al.*, 2015). The economic gains come with possible side-effects, such as increased suspended sediment concentrations (*Van Maren et al.*, 2015; *Dijkstra et al.*, 2019), increased estuarine circulation (*Zhu et al.*, 2015), water quality deficiencies (*Kerner*, 2007), destabilization of ebb-flood channel systems (*Monge-Ganuzas et al.*, 2013; *Jeuken and Wang*, 2010; *Wang and Winterwerp*, 2001), and morphological changes of intertidal flats (e.g., Chapter 2; *Wang et al.*, 2015; *De Vet et al.*, 2017). Sediment is preferably retained within these systems, as extraction would weaken their resilience to sea level rise. Together with salt marshes, intertidal flats provide an important buffering function for flood protection (*Temmerman et al.*, 2013; *Reed et al.*, 2018) and are ecologically valuable (*Smaal and Nienhuis*, 1992; *Barbier et al.*, 2011). Apart from minimizing costs, system managers are increasingly challenged to limit the consequences of sediment disposals such that the values of these areas are preserved for future generations.

To achieve such sustainable sediment management strategies, it is crucial to examine interactions between sediment disposals and the eco-morphological evolution of intertidal flats. However, these relationships have lacked strong field evidence. Identifying these links is complicated in part because morphological impacts may arise long after disposals occur. Furthermore, other anthropogenic and natural pressures affect these estuarine systems simultaneously (*Elliott and Whitfield*, 2011).

For these reasons, we studied an intertidal flat (in the Western Scheldt estuary, the Netherlands) that experienced significant and abrupt changes in its morphological and ecological evolution after the introduction of dredge disposals in the adjacent channel. These changes were captured by decades of approximately monthly/annual measurements of channel, intertidal flat, and salt marsh morphology, along with measurements of grain sizes and benthic macrofauna on the intertidal flat. We extended these data with numerical hydrodynamic model simulations to characterize the associated changes in flow velocities. Our analyses revealed a sequence of consequences of channel disposals changing the evolution of the channel and intertidal flat hydrodynamics, morphology, and grain sizes, along with, benthic communities and the adjacent salt marsh morphology.

5.2. DATA AND METHODS

The Western Scheldt (Figure 5.1a), the Netherlands, is a two-channel estuary. Its navigation channel toward the Port of Antwerp is deepened and maintained (*De Vriend et al.*, 2011; *Wang et al.*, 2015). This results in approximately 10 million m^3 (Mm^3) of sediments deliberately relocated within the system each year. Net extractions from the system are no longer practiced. Disposal location D1 in the Everingen channel has been in use since 1997 (Figure 5.1b). This disposal location was slightly extended in 2000 (Figure 5.1c). On average, 1.6 Mm^3 has been disposed annually at this location. We consider the effects of these disposals on the nearby intertidal flat Zuidgors (Figure 5.1a). The mean tidal range in this area equals 4.2 m. The effects of other disposal locations in the Western Scheldt are not part of this study (e.g., as D2 in Figure 5.1b expired in 2001).

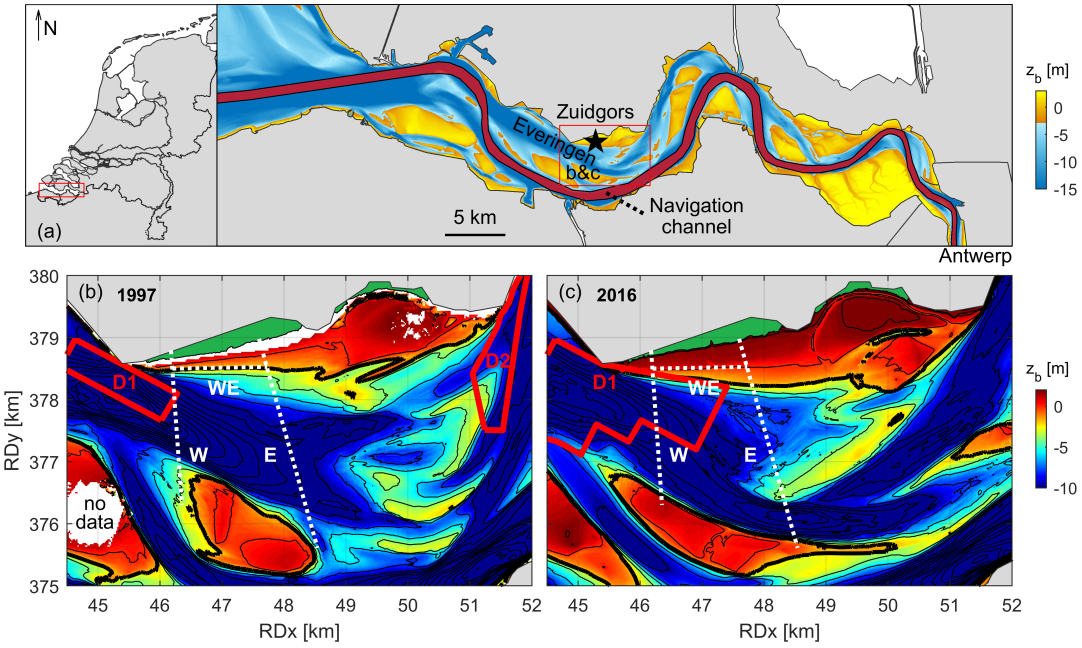

Figure 5.1: An overview of the Western Scheldt is provided in (a), with its position within the Netherlands. The Everingen channel is indicated, the navigation channel is marked with the red polygon, and the Zuidgors intertidal flat is marked with the star. The area of interest is shown in more detail in (b) with the 1997 bathymetry (single-beam) and in (c) with the 2016 bathymetry (single-beam and LiDAR). In both maps, the 2 m contour lines are indicated in black, with the mean low water contours marked as thick lines and the salt marshes as green polygons. The disposal locations within this area (D1 and D2) are marked with red lines. Transect W, Transect E, and Transect WE (along the 1997 mean low water line) are shown with the dotted white lines. The elevations in the color bars are truncated.

Extensive data on morphology, bed composition, and ecology have been measured in the Zuidgors area by Rijkswaterstaat (Dutch Ministry of Infrastructure and the Environment), and the first measurements predate the start of the disposals. The observations analyzed in this study extend from 1992 to 2017. Bathymetric maps were constructed approximately annually, from single-beam sonar and, in recent years, LiDAR measurements (*Marijs and Paree*, 2004; *Wiegmann et al.*, 2005). Since 1992, the intertidal sections of Transects W and E (Figure 5.1) have been measured annually with dGPS-RTK equipment and include the edges of the adjacent salt marshes. Additionally, frequent point-elevation measurements have been gathered approximately seven times per year at three locations on Transect E, by averaging fifteen samples each time (based on Sediment Erosion Bars, and since 2008 RTK-dGPS). Disaggregated grain sizes (D_{50}) have been measured annually at four locations on Zuidgors from 1992 to 2011 (locations are indicated in Figure 5.3b), as part of the MOVE dataset (*Rijkswaterstaat*, 2006). Benthic macrofauna has been sampled on the Zuidgors intertidal flat at 34 randomly distributed locations (Figure 5.5a), also as part of the MOVE dataset. Every location was sampled once between 1994 and 2008. The bed level corresponding to these samples was derived

from the annual bathymetric maps. Three random cores of 8 cm diameter were taken at the location and then pooled and sieved over a 1 mm mesh in the field. Animals were sorted out in the lab. Undetermined species were removed from the species list (only a few individuals). Finally, annual dredging and disposal quantities have been registered by the Flemish government.

A depth-averaged implementation of the Delft3D hydrodynamic model (*Lesser et al.*, 2004) was used to assess the impact from changes in bathymetry on the flow velocities in the estuary. The model schematization, with a resolution of 40–60 m in the area of interest, covers the full Western Scheldt. The model has been validated to measured hydrodynamics (*Van der Werf et al.*, 2015a). For every simulation, all tidal constituents of one representative month (August 2014) were imposed at the boundaries. This approach allows for a focus on differences in flow velocities solely caused by differences in bathymetry.

5.3. RESULTS

5.3.1. OBSERVATIONS ON MORPHOLOGY, GRAIN SIZES, AND ECOLOGY

To determine the morphological response of the Zuidgors intertidal flat to the disposal in the Everingen channel, the bed levels at Transects W and E (~1.5 km apart) are shown in Figures 5.2a and 5.2b for 1992–2017. At both Transects W and E, the intertidal area accreted several meters. As shown in more detail in Figures 5.2c and 5.2d, the intertidal flat rapidly expanded near the mean low water line with migration of the channel bank within a few years (Figures 5.2a and 5.2b); at higher elevations, the response is slower by an order of magnitude (annotations in Figure 5.2c). The shape of the intertidal flat at Transect E changed, such that the profile below MSL is now almost linear, while above MSL a sharp transition to a convex-up profile has formed. The transition between the different shapes coincides with a sharp transition in grain size observed in the field: D_{50} of 150–200 μm for the linear section and approximately 50 μm for the convex-up section.

To analyze the detailed morphological evolution over time and to identify the consequence of the disposals (Figure 5.3a), time series of the bed elevation of three points on each transect are shown in Figures 5.3c and 5.3d. The elevation of Zuidgors was generally stable or even erosive between 1992 and 1999. After 1999, two years after the start of the disposals but still before the expansion of the disposal location, both transects switched toward accretion. This abrupt trend shift is especially apparent in the frequent point-elevation measurements (Figure 5.3d). For months the accretion rates exceeded locally 0.05 m per month, and in recent years these still equal to about 0.1 m per year. The peak in accretion rates occurred at Transect W more than three years earlier than at Transect E (~1.5 km eastward of Transect W), indicating a significant delay. This is evidence for an eastward propagating accretion front (< 0.5 km/y), originating from the disposal location.

This alongshore propagating expansion is captured in more detail by the transect along the original 1997 mean low water line (Figure 5.2e). The more eastward from the disposal location, the longer the delay until effects arise. Figure 5.4 shows the boundaries of the area that increased at least 0.5 m in bed level since 1997. Also from this figure, the eastward propagating character of the accretion front is evident, with a smaller

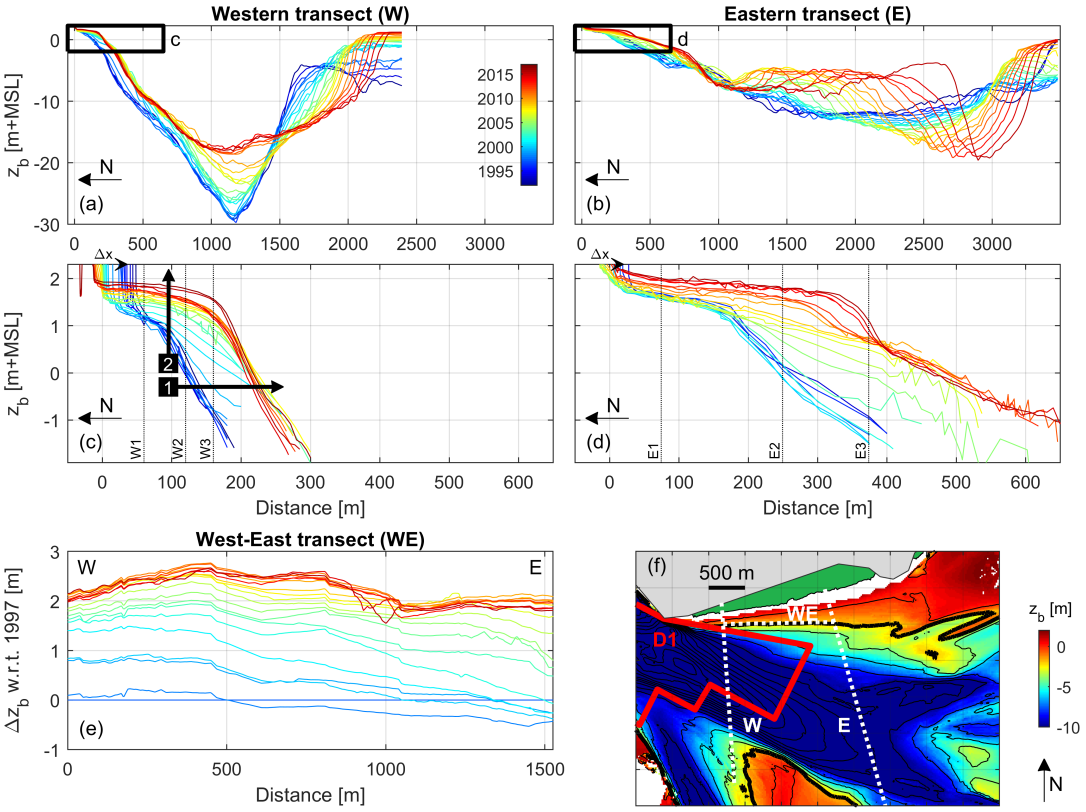

Figure 5.2: The evolution of Transects W, E, and WE (along the 1997 mean low water line) are shown in (a), (b), and (e), respectively, based on single-beam and LiDAR data. The location of these transects are indicated in (f), with the 1997 bathymetry data and the largest extent of the D1 disposal polygon. In (c) and (d) the focus is on the intertidal part of Transects W and E (between mean low water and mean high water), only considering available RTK-dGPS measurements. The location of Points W1–W3 and E1–E3 are included, for which in Figures 5.3c and 5.3d the time series are shown. Also the positive direction of the marsh edge propagation Δx is indicated, see Figure 5.3e for the time series. The arrows in (c) illustrate the expansion (1) and the successive increase in height (2) of the intertidal flat.

celerity for larger distances from the channel (i.e., for higher elevations on the intertidal flat). Bathymetry data were absent for the highest part of the intertidal flat in Figure 5.4 in 1997, but Figure 5.3c indicates that W1 (near the salt marsh) reached a 0.5 m bed level increase thirteen years after the start of the disposals, while W3 (near the channel) reached this already after three years.

The salt marsh edge evolution also changed after the start of the disposals. *Van der Wal et al.* (2008) traced the position of the salt marsh cliff on transect data (representative for Transect W) for the period 1993–2004. In Figure 5.3e, we extended the analysis with data after 2004 and applied it on both transects. In line with *Van der Wal et al.* (2008), both salt marsh edges became less erosive around 2000. Salt marsh W retreated with an almost constant rate of 4.0 m/y before 1999, while this rate was only 1.3 m/y between

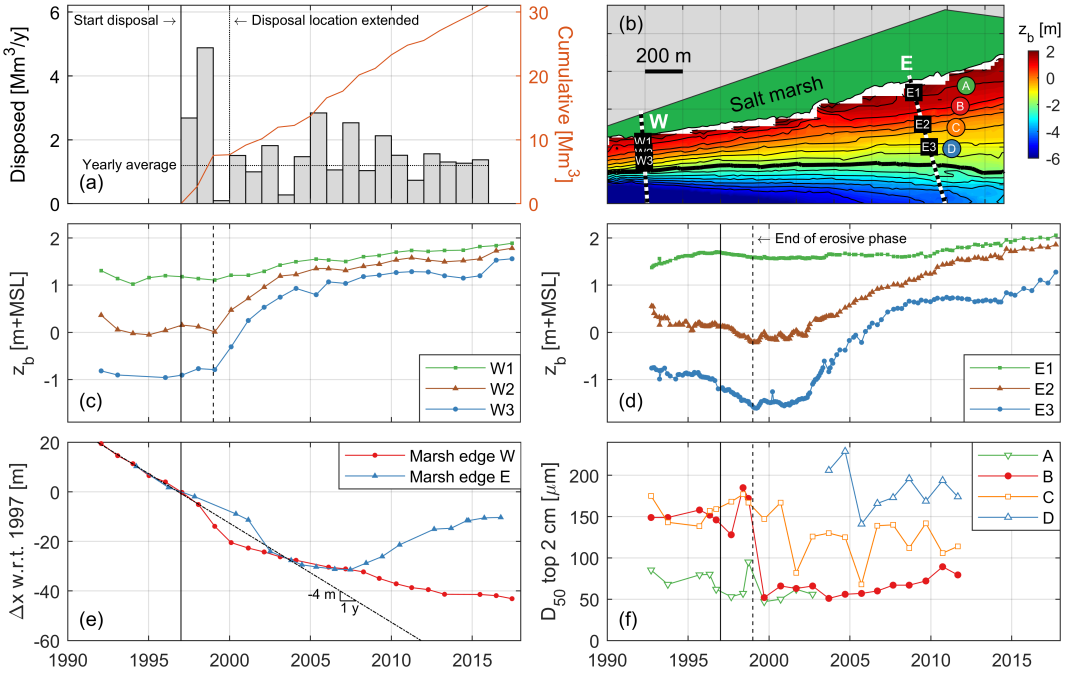

Figure 5.3: (a) Time series of the annual and cumulative sediment disposal quantities in the D1 disposal location. (b) The locations of Transects W and E, elevation measurement points W1–W3 and E1–E3, and grain size sampling points A–D. The 0.5 m contour lines are indicated in black, with the mean low water contour marked as a thick line, based on the 1996/1997 bathymetric data. (c) Elevation time series for Points W1–W3, based on a spatial interpolation of the transect data of Figure 5.2c. (d) Elevation time series for Points E1–E3, which are the frequent point-elevation measurements (see Section 5.2). (e) The horizontal propagation of the salt marsh for both transects, based on a spatial interpolation of the transect data of Figures 5.2c and 5.2d at mean high water level. (f) The evolution of the median grain size (D_{50}) of the surface sediment (2 cm top layer) of sampling points A–D. The vertical solid and dashed black lines (explained with the annotations) are consistent for the different subfigures.

1999 and 2017. Salt marsh E even expanded after 2008.

Temporal changes of the median grain sizes on the intertidal flat are revealed in Figure 5.3f, for four locations (~100 m apart) on a cross-shore transect near Transect E. Especially at Point B, an abrupt but persistent change was observed: a decrease in median grain size from ~150 μm before 1999 (two years after the start of the disposals), to ~50 μm directly afterwards. Closer to the channel, at Point C, the grain size reduced less. Closer to the marsh, at Point A, the grain size was already similar to the fine material that settled in the accretion phase at Point B.

As benthic macrofauna was not repeatedly sampled at the same locations, we consider the relation between bed elevation and abundance of benthic communities. Changes in elevation of the intertidal flat have important consequences for the benthic communities. Figure 5.5c indicates, based on randomly distributed samples (Figure 5.5a), that the abundance correlates with bed elevation (44% of the variance was explained by the bed level) but was not related to the year of sampling ($p > 0.1$). The abundance was on

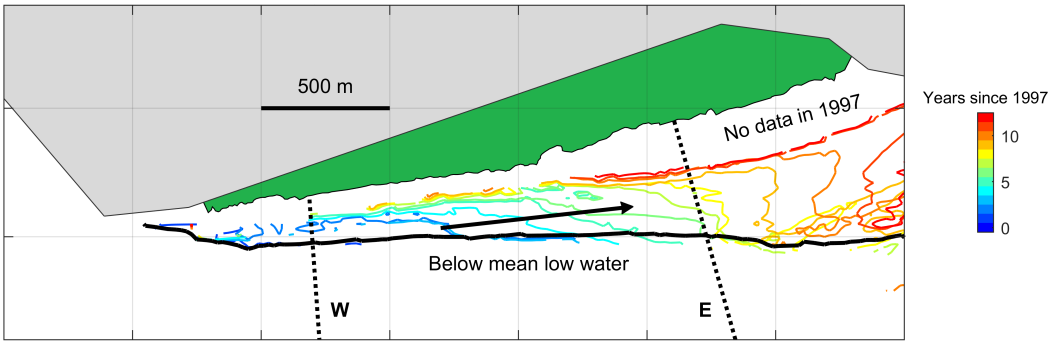

Figure 5.4: Contour lines of the accretion front, defined as the boundaries of the area where the bed level increased at least 0.5 m compared to 1997, based on the single-beam and LiDAR data. As a reference, Transect W and Transect E are shown with the dotted lines, and the 1997 mean low water line is shown with the thick black line. Only the data on the Zuidgors intertidal flat are visualized to improve clarity. The arrow indicates the propagation direction of the front.

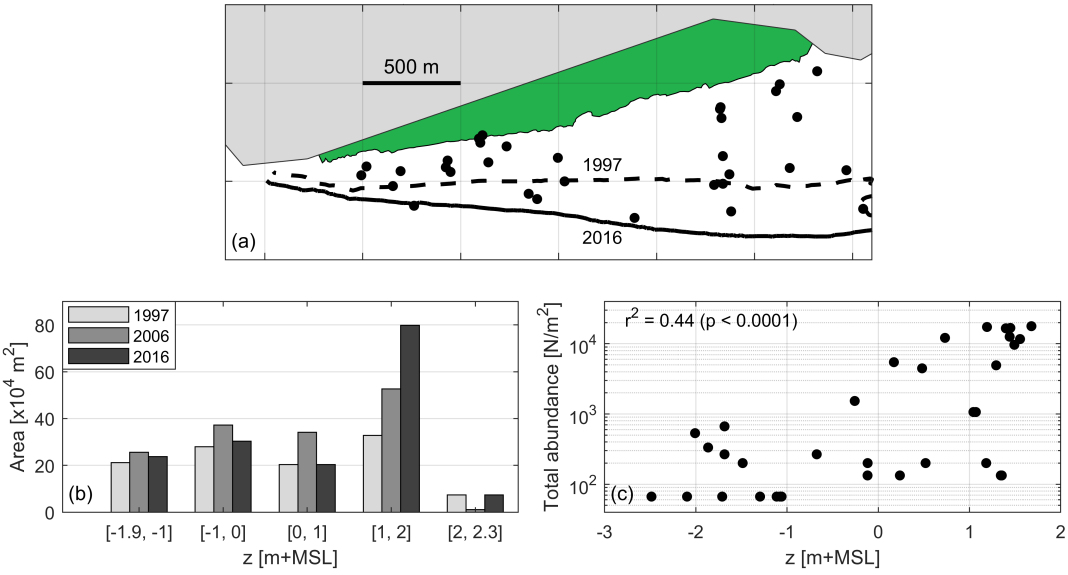

Figure 5.5: (a) Locations of benthic macrofauna measurements, with the 1997 and 2016 mean low water lines. Every location was sampled once between 1994 and 2008. (b) The area of the intertidal flat in 1997, 2006, and 2016 for 1 m bed level classes (bounded by mean low water and mean high water), based on the single-beam and LiDAR data. Gaps in the 1997 data (Figure 5.1) were complemented with more recent data. (c) The total abundance of benthic macrofauna versus the bed elevation.

average 7 times larger above MSL+1 m than below MSL+1 m. Therefore, for points that substantially heightened (e.g., more than 2.5 m at W3 and E3; Figures 5.3c and 5.3d) the abundance of benthic macrofauna increased (approximately by one order of magnitude at W3 and E3). Even though the steepness of the intertidal flat initially changed (e.g.,

Figures 5.2c and 5.5b), the area (and hence the abundance of benthic macrofauna) corresponding to bed elevations below MSL+1 m was in 2016 similar to 1997 (Figure 5.5b). In contrast, the area of the intertidal flat with bed levels above MSL+1 m (on average 7 times richer in benthic macrofauna) more than doubled from 1997 to 2016.

5.3.2. MODELED HYDRODYNAMICS

The accretion on the intertidal flat might be caused by a reduction in tidal energy, resulting from the changed bathymetry (Figures 5.2 and 5.6b). To test whether the tidal energy on the intertidal flat reduced, simulated flow velocities using the 1996 and 2014 bathymetry, respectively, are compared. Local peak flow velocities on the intertidal flat decreased comparing identical locations (Figure 5.6a), but increased (especially in flood direction) comparing identical bed levels (Figure 5.6c). Therefore, the expansion of the intertidal flat coincided actually with an increase in tidal energy on the flat.

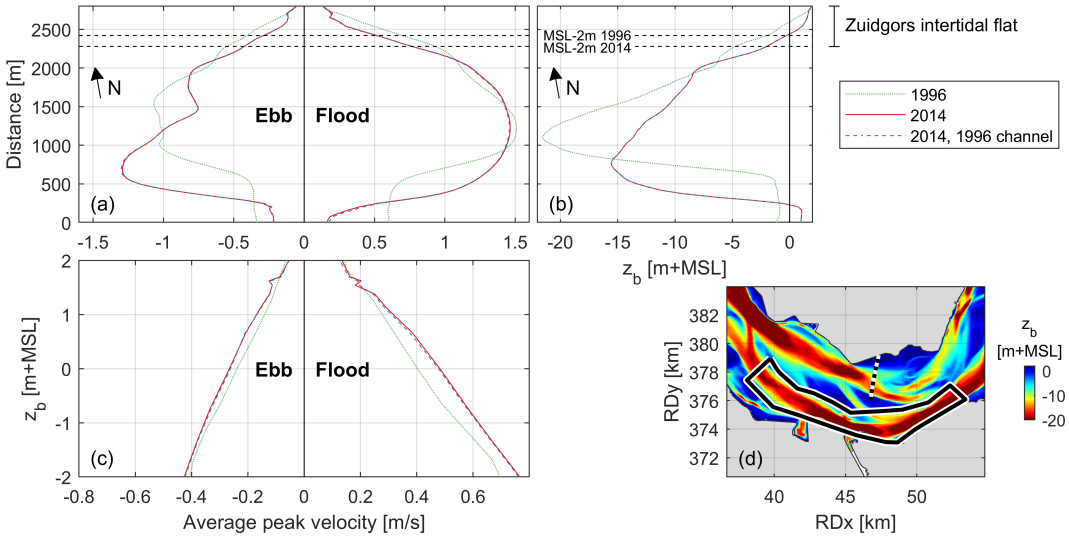

Figure 5.6: In (a), the average flood and ebb peak velocities are shown along the cross-section as indicated in (d). The distance along the cross-section increases toward the Zuidgors intertidal flat (which is shown on the top of this graph). These velocities are computed from a one month simulation with the 1996 bathymetry, the 2014 bathymetry, and a combination of the 2014 bathymetry with the 1996 navigation channel. The bathymetry data along the cross-section are visualized in (b). In (c), the velocities are shown versus the elevation, for the northern part of the cross-section (Zuidgors). Finally, in (d) the 2014 bathymetry is visualized with the navigation channel transplanted from 1996 (polygon), with the dotted line indicating the cross-section.

To reveal the influence of the deepening of the navigation channel on the intertidal flat hydrodynamics, velocities were simulated also for the 2014 bathymetry with the original 1996 navigation channel (prior to the deepening), see Figure 5.6d. The implementation of the original navigation channel in the 2014 bathymetry resulted in almost identical flow velocities in the Everingen channel and on the Zuidgors flat as seen with the actual 2014 bathymetry (Figure 5.6). The navigation channel deepening therefore did not significantly affect the tidal flow velocities on the intertidal flat.

5.4. DISCUSSION

5.4.1. MORPHODYNAMIC IMPLICATIONS

We showed that sediment disposals in estuarine channels have a direct influence on the channel cross-section (shown conceptually in Figure 5.7; Consequence 1), with consequential changes in evolution of the intertidal areas (channel-flat interaction). The accretion of the intertidal flat was not caused by a reduction in hydrodynamic energy. The velocities on the intertidal flat actually increased considering similar elevations (Figure 5.6c). The altered velocities result directly from changes in bathymetry caused by the disposals and associated bank and flat expansion, and not from deepening of the navigation channel (Figure 5.6). Even though dredging activities may eventually induce an estuarine regime shift toward fine sediment import and tidal amplification (*Winterwerp and Wang*, 2013), the impact on the intertidal flat started within several years and had a more local character. The shift of the channel bank, induced by the adjusted channel geometry, led to intertidal flat expansion (Figure 5.7; Consequence 2). Our findings suggest that sediment disposals in channel systems can significantly affect proximal intertidal flats if the increased sediment availability impacts channel bank migration.

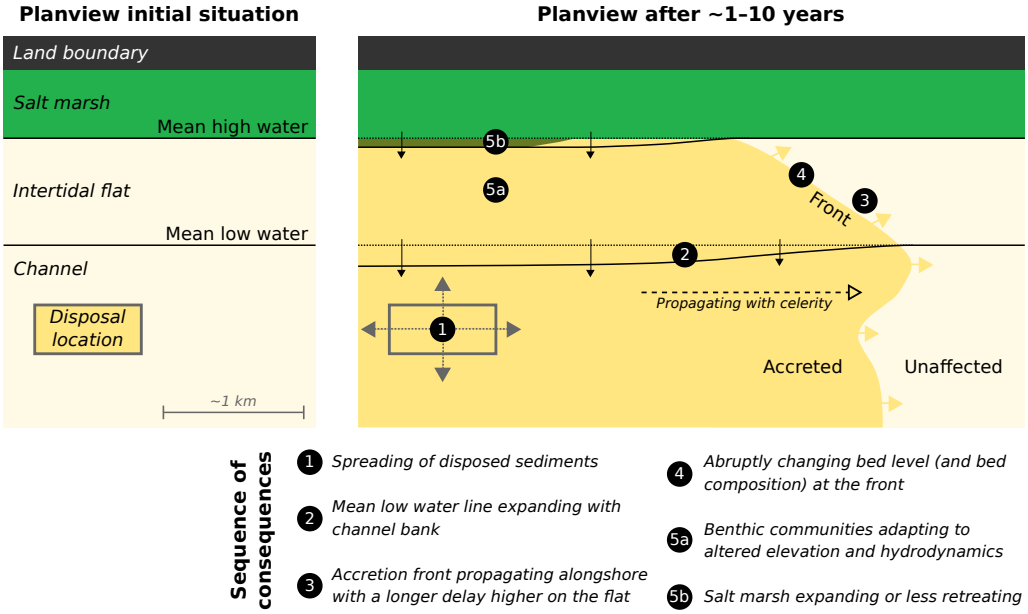

Figure 5.7: Conceptual diagram on the sequence of consequences of sediment disposals in channels for the eco-morphology of intertidal flats.

Intertidal flats do not necessarily respond uniformly in space and with a constant rate to disposals in channels. The adaptations around the mean low water line were an order of magnitude faster (~years) than at higher elevations (~decades). Also, Transect E became more erosive for several years before the accretion started (Figure 5.3d). This lag can be explained by the time required for an accretion front (Figure 5.4) to propagate along an intertidal flat (Figure 5.7; Consequence 3) — years, in this case (celerity smaller

than 0.5 km/y). Such channel-flat systems may thus have an intrinsic adaptation and/or response time of considerable duration. Extreme accretion rates — up to 0.05 m per month in our observations (two orders of magnitude larger than sea level rise rates) — may then likewise persist for years.

We suggest two mechanisms that might explain changing grain sizes for a changing intertidal flat morphology. On intertidal areas in tide-dominated estuaries, grain sizes typically decrease with reduced current velocities toward higher elevations (Figure 5.3f; see also *Yang et al.*, 2008; *Friedrichs*, 2011). Therefore, with reduced tidal velocities on a heightened intertidal flat (Figure 5.6a), those areas gradually become more amenable to the accumulation of fines. Through this mechanism, accretion of coarser sediments at the lower elevations of a flat could facilitate the accommodation space for fines higher on the flat (see the two stages in Figure 5.2c). A second mechanism might explain the abrupt changes in grain sizes that we observed. When an erosive intertidal flat becomes accretive, the newly accreted sediments determine the surface bed composition (Figure 5.7; Consequence 4). In the data, we examined a significant transition in median grain size (from 150 μm to 50 μm), which occurred abruptly in time (Point B in Figure 5.3f) and coincided precisely with the end of the erosive phase (Figure 5.3d). The accreted sediment was finer than the sediment originally present in the bed. Abrupt transitions in grain size can occur by changes in morphological evolution during storms (*Yang et al.*, 2008) and seasonal variations (*Yang et al.*, 2008; *Van der Wal et al.*, 2010), but we find the changes induced by disposal persisted. Sediment disposals in channels can be a direct cause of both gradual and abrupt changes in grain size on intertidal areas.

5.4.2. ECOLOGICAL IMPLICATIONS

Channel disposals may also affect benthic communities on intertidal flats. Changes in benthic communities have direct ecological consequences, including effects on the foraging habitat for birds, but can also have implications for bed erodibility (*Austen et al.*, 1999; *Herman et al.*, 2001). We showed a significant increase in abundance of benthic macrofauna with bed elevation. Locally, the bed rose vertically as much as 2.5 m, which is associated with increases in quantity of benthic macrofauna (by approximately one order of magnitude). Even though the intertidal flat decreased initially in steepness after the start of the disposals, the steepness (i.e., also the area) of the bed level classes below MSL+1 m was twenty years later again similar as before. Instead, the area of the intertidal flat above MSL+1 m, the richest in benthic macrofauna, more than doubled. There was hence a net increase in total quantity of benthic macrofauna on the intertidal flat. With ongoing heightening, large parts of the intertidal flat may eventually rise above mean high water which implies that intertidal benthic communities may decay again in the future (e.g., by settlement of salt marsh vegetation). Apart from bed level height (i.e., exposure time), *Ysebaert and Herman* (2002) showed that also grain sizes and current velocity (both relate to bed elevation; Figures 5.3f and 5.6c) explain part of the variation in these benthic communities. The sudden decrease in grain sizes from 150 μm to 50 μm may have induced more sudden changes in benthic communities. Therefore, by altering the morphology, hydrodynamics, and grain size of an intertidal flat, sediment disposals also can affect the flat's benthic communities (Figure 5.7; Consequence 5a).

The immediate and diffuse effects of sediment disposals on the evolution of inter-

tidal flats also have direct consequences for the evolution of adjacent salt marshes. In line with *Van der Wal et al.* (2008) and *Mariotti and Fagherazzi* (2010), the local geomorphic regime shift of the intertidal foreshore from erosion toward accretion also induced a shift in evolution of the salt marsh edge (Figure 5.7; Consequence 5b). Cross-shore arrays of wooden poles (~100 m arrays) deployed in 1992 near Transect E might have influenced this marsh evolution locally. However, the consistent reduction in salt marsh erosion at both transects, promptly after the start of the disposals, is only explained by these disposals. After the heightening of the foreshore, salt marsh edge erosion was reduced. This can be ascribed to reduced wave forcing (*Houser and Hill*, 2010; *Pethick*, 2001; *Callaghan et al.*, 2010), reduced current velocities in front of the marsh (Figure 5.6a; see also *Bouma et al.*, 2005), reduced inundation times (*Balke et al.*, 2014), related faster recovery from episodic erosion (*Van Belzen et al.*, 2017), and less extreme bed dynamics on higher intertidal forelands (*Hu et al.*, 2017; *Bouma et al.*, 2016). With ongoing accretion of the intertidal flat, it is expected that the full salt marsh will eventually expand. This has been the case for Transect E since 2008 (Figure 5.3e; see also *Balke et al.*, 2014). Even though the salt marsh cliff has still been eroding at Transect W, there are signs of a future expansion also there: pioneer vegetation (*Salicornia*) has settled in front of the eroding cliff (observed 26 June 2019; Figure 5.8).

Figure 5.8: Photo of the salt marsh edge of the Zuidgors intertidal flat, taken in western direction. The erosive salt marsh cliff is visible with recently settled pioneer vegetation (*Salicornia*) on the intertidal flat in front. Photo taken between both transects, 0.5 km east of Transect W and 1.0 km west of Transect E, on 26 June 2019.

5.4.3. IMPLICATIONS FOR ESTUARINE MANAGEMENT STRATEGIES

We suggest that strategies for estuarine sediment management need to consider and address, with an integrated approach, the non-local sequence of morphodynamic and ecological consequences of channel disposals (Figure 5.7). This includes disposal strategies that influence the morphology of channel banks or intertidal flats, such as when sediments are disposed directly on the channel edges (e.g., *Van der Wal et al.*, 2011; *Plancke et al.*, 2014). The impact on the full system should be considered, as other locations may experience contrasting consequences: for example, if a reach of channel bank near the disposals retreats (e.g., the channel bank opposing the Zuidgors area in Figures 5.1b, 5.1c, and 5.6b). Our results indicate that changes in morphological evolution, grain size, and ecology can occur simultaneously. Still, these eco-morphological responses can take

years to decades to arise, especially farther away from the disposal location. This lag challenges monitoring and management of estuary responses to interventions.

In this section of the Western Scheldt, the state of the estuarine system has changed (e.g., Figures 5.1b and 5.1c), largely as a result of the disposals. By extension, stopping the disposals would not guarantee a return to the "natural" historical state. System managers must address the possibility of irreversible consequences of sediment management strategies. There are potentially ways to minimize negative impacts and benefit from effects of dredged disposals (e.g., *Plancke et al.*, 2014; *Baptist et al.*, 2019), but this requires a strategy that can account for eco-morphological consequences and is adaptable under intensive eco-morphological monitoring (*Depreiter et al.*, 2012). In the era in which both human interventions and accelerated sea level rise increasingly pressure the resilience of estuaries and their intertidal habitats (*Meire et al.*, 2005), such a sustainable sediment management strategy is crucial.

5.5. CONCLUSIONS

We identified a sequence of eco-morphological consequences for intertidal flats that results from sediment disposals in an estuarine channel. Following such sediment disposals, increased availability of sediment affects the channel geometry and the channel bank migration. The changes in channel bank migration drive changes in the intertidal flat hydrodynamics, morphology, and grain sizes. The formerly erosive intertidal flat has been increasing in bed elevation, the flow velocities reduced with these higher bed elevations, and the grain sizes decreased locally. Intertidal flat benthic communities and the location of the edge of adjacent salt marshes are affected by these changes. The total quantity of benthic macrofauna increased and the salt marsh edge became less erosive and expanded locally. An accretion front was formed that propagated over the intertidal flat, causing alterations in hydrodynamics, morphology, and grain sizes after years of delay, especially farther away from the disposal location. The identified non-local sequence of eco-morphological consequences of sediment disposals calls for integrated sediment management strategies on a system scale, sustained by long-term monitoring.

Chapter 6

A Discussion on the Implications for System Management Strategies

Cover photo: sediment nourishment activities with the Eastern Scheldt storm surge barrier in the background. Courtesy of Rijkswaterstaat, beeldbank.rws.nl, Jan van den Broeke.

Intertidal flats in engineered estuaries face consequences of human interventions (Chapters 2 and 5). System managers aim at minimizing negative and maximizing positive effects on system/ecological functioning. To prevent loss of the ecological value of intertidal flats, mitigation measures may be introduced (e.g., sediment nourishments). Apart from understanding the consequences of human interventions, knowledge of the natural processes driving intertidal flats (Chapters 3 and 4) is essential to incorporate into the development of effective management strategies. Implications of this dissertation's results regarding management strategies for estuaries are discussed in this chapter.

System management strategies for estuaries deal with a broad spectrum of human interventions and physical processes. To serve both the ecological and economic needs, balanced management strategies are needed, taking into account the short-term and long-term developments as well as the local and system-wide consequences.

In this chapter, implications for the management of intertidal flats resulting from insights from this dissertation are discussed. In Section 6.1, the focus is placed on the effects of human interventions on intertidal flats which are generally initiated for economic purposes. First, systems with sediment relocation works for the construction and maintenance of navigation channels are considered (such as in the Western Scheldt). Second, consequences of a storm surge barrier and its operation are discussed (such as in the Eastern Scheldt). Third, insights on the Eastern Scheldt and Western Scheldt are integrated with a focus on the underlying local and system-wide mechanisms driving intertidal flats. Section 6.2 considers sediment nourishments on intertidal flats to mitigate negative consequences of human interventions on ecology.

As the insights resulted specifically from analyses on the Eastern Scheldt and Western Scheldt, they may not explain the detailed response of other systems to such interventions. Differences arise as the response of such systems is not only dependent on the highlighted human interventions, but also on the other forcings and geometry of these systems. Instead, especially the underlying principles and mechanisms are transferable to other systems around the world. These contribute to the understanding and improvement of sediment management strategies for intertidal flats, and are discussed hereafter.

6.1. EFFECTS OF HUMAN INTERVENTIONS ON INTERTIDAL FLATS

6.1.1. SEDIMENT RELOCATION WORKS

Estuarine navigation channels provide access to major ports around the world, e.g., in the Western Scheldt (the Netherlands) to the port of Antwerp (Belgium) or in the Yangtze to the port of Shanghai (China). Navigation channels require sediment relocation works for deepening and maintenance. With possible delays, sediment relocations can affect the eco-morphology of intertidal flats, even if the sediments are disposed in channels.

Steepening and heightening of intertidal flats In the Western Scheldt, the intertidal flats increased in height and steepened over time while sediments were relocated for the deepening and maintenance of the navigation channel (Chapter 2). We revealed that a steepening also implies a possible increase in bed level dynamics (Chapter 4). Yet, the responses in the Western Scheldt were so large, e.g., the average increase in height of the studied intertidal flats exceeded sea level rise by one order of magnitude, that it is unequivocal that relocation works can substantially affect intertidal flats, let alone when sea level rise rates would increase. However, changes to intertidal flats are not monotonic over time nor homogeneous over space due to inconsistent nature of the sediment relocation activities. These continuously-changing relocation works obscure the system-wide consequences of individual interventions. Changes to the morphological evolution of the intertidal flat analyzed in Chapter 5 were entirely attributed to the increase in sediment availability following sediment disposals in the adjacent channel. Therefore, this case illustrated that system-wide tipping points (e.g., *Wang et al.*, 2015)

are not necessarily required to alter intertidal flats. Still, these local effects of sediment disposals do not exclude the presence of system-wide effects. For example, tidal amplification (and related increments in velocities) resulting from deepening works may also affect the morphological evolution of intertidal flats on the long-term (*Taal et al.*, 2013).

Sequence of migrating eco-morphological consequences Even if sediment relocations do not induce system-wide changes in forcing processes, intertidal flats may be affected by sediment disposals on kilometers distance (Chapter 5). Intertidal flat morphology undergoes adjustments and, consequentially, also the intertidal flat hydrodynamics, grain sizes, benthic macrofauna, and salt marshes alter. As these responses are not limited to the direct surrounding of the disposals, it was concluded that such interventions must be managed on larger scales (maybe even on a system-level scale). However, since the intertidal flats respond to spatiotemporally inhomogeneous disposals, extensive measurements are required to keep track of all (human-induced) morphological changes. Yet, even with perfect datasets, the complexity of the non-local responses to the many interventions may make it impossible to evaluate and steer strategies on individual disposals. Therefore, judging and managing the consequences of navigation channel dredging works may only be meaningful on system-aggregated indicators regarding the intertidal flat morphology and ecology. Still, local mechanisms (e.g., Chapter 5) are essential input for meaningful large-scale indicators (e.g., height, steepness, volume, and area of intertidal flats, but also the change in grain sizes or the change in evolution of salt marshes).

Delay in response of intertidal flats As intertidal flats can respond to distant sediment disposals, their response may involve delays. The net propagation of the accretion front, along the intertidal flat studied in Chapter 5, was approximately 0.5 km/year. This is orders-of-magnitude slower than the movement of individual suspended sediment particles (~10 km each tide considering a typical peak flow velocity of 1 m/s). Furthermore, the most elevated regions of the intertidal flat responded an order of magnitude slower than the lowest elevations of the intertidal flat. Therefore, the response of intertidal flats to such interventions may take years or decades. Regardless of the delay, relatively large accretion rates may still follow. This challenges system managers even further, as it takes years to decades to see the consequences of their actions.

The complex migrating and delayed responses of intertidal flats to sediment relocation works emphasize the necessity of adaptive management strategies for such interventions in estuaries. The management of the Western Scheldt could be seen as a role model: a flexible disposal strategy (*Depreiter et al.*, 2012) is followed in which disposal locations are continuously reconsidered based on monitoring and research insights. The unraveled chain of eco-morphological consequences on intertidal flats following sediment disposals in channels provides potential to actively steer the evolution of intertidal flats. However, as responses of intertidal flats may arise after long time frames, and opposite responses can occur elsewhere (also observed in Chapter 5), system managers should be reserved in disposing sediments with the aim of steering intertidal flats. Also, sediment disposals will affect intertidal flats substantially less if the sediment transport toward the intertidal flats lacks capacity (such as in the Eastern Scheldt).

6.1.2. STORM SURGE BARRIERS

Storm surge barriers, such as in the Eastern Scheldt (the Netherlands), Venice Lagoon (Italy), and those considered in response to recent hurricane events for Galveston Bay and New York Harbor (United States), are typically billion dollar engineering works that protect the hinterland against flooding and therefore only close during severe storm surge events. Storm surge barriers aim, in contrast to permanent barriers, at the preservation of estuarine conditions. These barriers close if the water level exceeds a threshold value. For example, the storm surge barrier of the Eastern Scheldt is closed if the water level outside the estuary is projected to exceed NAP+3 m (NAP is the Dutch Ordnance Level, close to the present mean sea level). To diversify the water levels during long storm events, the target water level within the estuary alternates between NAP+1 m and NAP+2 m for successive tides, as illustrated in Figure 6.1. As the thresholds for closure do not rise with the sea levels (fixed dimensions of the barriers and levees), the closure frequencies of such systems is expected to increase with rising sea levels. To illustrate, the Eastern Scheldt may need to close on average 45 times a year after 1 m of sea level rise (rough first order estimate by *Haasnoot et al.*, 2018), while it has closed on average less than once a year thus far.

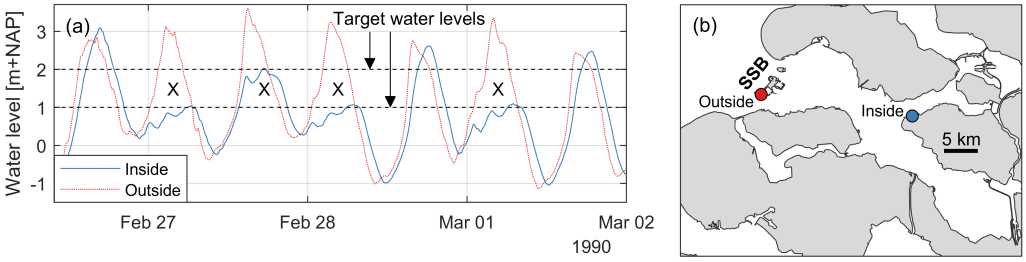

Figure 6.1: (a) Water level during the 26 February – 2 March 1990 storm event, measured inside and outside the Eastern Scheldt. The crosses (×) indicate tides for which the storm surge barrier (SSB) closed. The NAP+1.0 m and NAP+2.0 m target levels are indicated with the horizontal dashed black lines. NAP is the Dutch Ordnance Level, which is nearly equivalent to mean sea level. (b) Location of the water level stations and the SSB.

Despite their open character, storm surge barriers do affect the morphological evolution of intertidal flats (Chapter 2). Even though the impact on these intertidal flats depends on the characteristics of the estuaries and barriers, various mechanisms should be considered for the design and management of such barriers in any estuary.

Increased role of wind-driven flow Even when a storm surge barrier is open, the tidal flow velocities within the estuary are reduced. The reduction of the tidal velocities implies an increase in relative importance of wind-driven flow on intertidal flats. The magnitude of the wind-driven flow is up to ~1/40th of the wind speed (Chapter 3). Wind-driven flow is even more relevant when a barrier closes, as tidal flows are then absent and closures (i.e., large surge levels) may coincide with large wind speeds. Due to the large importance (or even dominance) of the wind, the net sediment transport on intertidal flats is, in such systems, largely controlled by the wind. This also applies to years without closures (e.g., Chapter 3).

Focused erosion zones During closures, there is a limited temporal variation in water level within these estuaries, even if target water levels are alternated (e.g., in the Eastern Scheldt). Long durations (hours–tens of hours) of a near-constant water level, together with depth-limited waves and large (wind-driven) flow velocities (following the large wind speeds during storms), induce morphological changes especially at parts of intertidal flats where waves are exactly depth-limited (Chapter 4). Target water levels hence influence the evolution of intertidal flats. However, there is only a limited set of target water levels feasible as target water levels lower than the water levels outside these estuaries are not reachable unless water is discharged with pumps. The level of control on distributing the erosion zones is limited, especially as storm surges heighten the low water levels outside estuaries.

Effects sea level rise Sea level rise, with the higher low water levels, limits the range of feasible target water levels even further. Furthermore, the increasing closing frequencies make wind-driven flow during (milder) events even more important and increase the frequency of hours-long nearly constant water levels. This makes the erosion zones even more focused. Due to the fixed dimensions of the barriers and levees, the target water levels within estuaries during closures cannot (or only at large costs) raise with sea level rise. With intertidal flats in open estuaries already experiencing difficulties in keeping pace with sea level rise (*Elmilady et al.*, 2018; *Van der Wegen et al.*, 2017), these effects of storm surge barriers threaten the existence of intertidal flats even further.

Adaptation time scale The introduction of the storm surge barrier in the Eastern Scheldt caused a lowering of the intertidal flats. We revealed that the lowering rates reduced within decades (Chapter 2). New measurements are required to reveal whether this trend will persist. The morphology of the intertidal flats changes because the estuarine channels are out of equilibrium (they are too large given the reduced tidal prism *Eysink*, 1990); they face a sand demand ("zandhonger" in Dutch). By the limited sediment import through the barrier due to large scour holes at both sides of the barrier, the intertidal flats are the only source of sediment for the channels (*Huisman and Luijendijk*, 2009; *Van Zanten and Adriaanse*, 2008). Apart from this volume change of the intertidal flats, their shape also adapts due to reduced importance of tidal flow velocities (*Friedrichs*, 2011) following introduction of a storm surge barrier. As the intertidal flats in such systems adapt, both in volume and in shape, multiple time scales are involved. Therefore, in such systems is reduced erosion not necessarily evidence of an approach to an equilibrium.

In the Eastern Scheldt, not just the storm surge barrier, but also the compartment dams that limited the tidal range reduction (Figure 1.4), decreased the tidal flow velocities in the estuary. Also without such compartment dams the tidal velocities on intertidal flats would have generally decreased and the discussed mechanisms would have applied. In any system, both the design and the operation during events of storm surge barriers influence the extent to which intertidal flats adapt. Ideally, both the tidal flow and tidal range are minimally affected when the barrier is open. Storm surge barriers should not block sediment transport such that the channels can still exchange sediment with

the outer delta, and not solely with the intertidal flats. Furthermore, the closing policy of such barriers should be optimized such that the erosion of the intertidal flats during storm events is well-distributed over the different bed levels. These closing policies should be revisited during the lifetime of these barriers, as changing sea levels change the relative impact of closures on intertidal flats. Because multiple time scales are involved in the evolution of intertidal flats, system managers should evaluate the impact of storm surge barriers over long time scales (decades to centuries).

6.1.3. INTEGRAL DISCUSSION ON LOCAL AND SYSTEM-WIDE EFFECTS OF HUMAN INTERVENTIONS

Although intertidal flats respond differently to different human interventions, the mechanisms underlying these responses are similar. In this section, the responses of the intertidal flats in the Eastern Scheldt and Western Scheldt are integrally discussed, with a special focus on the system-wide and local effects on intertidal flats.

In the Western Scheldt, the tidal range and flow velocities increased on a system scale due to the deepening of the navigation channel by dredging (*Kuijper and Lescinski*, 2013). In the Eastern Scheldt, the tidal range and flow velocities reduced on a system scale due to the storm surge barrier and compartment dams (*Louters et al.*, 1998; *Eelkema et al.*, 2009). Following *Friedrichs* (2011), who unraveled that the cross-sectional shape of an intertidal flat is a function of the local tidal forcing (among other processes), these opposing changes in tidal forcing should result in opposing changes in the shapes of intertidal flats. This matches with observations; general increments in steepness of the intertidal flats in the Western Scheldt and general reductions in steepness of the intertidal flats in the Eastern Scheldt. As velocities changed in both estuaries system-wide, intertidal flats adapted over the full systems.

When the local cross-sectional shape of an intertidal flat is completely adapted to system-wide changes in hydrodynamics, it may continue to erode or accrete. *Maan* (2019) showed that a deficiency/abundance of sediment is a driver for retreat/expansion of the equilibrium cross-sectional profile. In the Western Scheldt, sediment disposals affect the sediment availability locally. In the Eastern Scheldt, the reduced transport capacity on its intertidal flats implies that sediment exported to the channels during storm events may not return and cause an ongoing retreat/lowering of the intertidal flats.

We revealed that system-wide changes in hydrodynamics are not required for substantial morphological changes of intertidal flats. The evolution of the intertidal flat studied in Chapter 5 in response to sediment disposals in its adjacent channel was initially even opposite to the system-wide changes: its steepness decreased as the intertidal flat expanded with the channel bank. Ten years later (disposals were still ongoing), the steepness of the intertidal flat largely returned to the initial steepness; only the width of the highest part of the intertidal flat substantially increased. As the tidal velocities did not substantially change (comparing equal bed levels), even in this extreme case (the area of the intertidal flat increased by almost 50%), substantial system-wide changes in hydrodynamics would have had also here consequences on the long-term steepness of the intertidal flat. This means that it is unlikely that such channel disposals, and similarly also disposals on (the edges of) intertidal flats, will induce long-term changes in steepness of intertidal flats. Therefore, it is expected that the disposed sediment will

eventually end up in the channel and/or spread over all bed elevations of these flats.

Intertidal flats respond to a combination of local and system-wide changes in processes. As long as local interventions do not structurally change the local hydrodynamics (comparing equal bed levels), it is likely that the long-term steepness of intertidal flats predominantly adapts to system-wide changes in the hydrodynamics. In these cases, local interventions change the steepness of intertidal flats only temporary. Contrarily, if human interventions do locally induce persisting changes in hydrodynamics (e.g., groins), the long-term cross-sectional shape of intertidal flats will also adapt to these local interventions.

6.2. NOURISHMENTS ON INTERTIDAL FLATS TO MITIGATE NEGATIVE CONSEQUENCES OF HUMAN INTERVENTIONS[1]

Sediment nourishments are interventions that may be utilized to compensate for intertidal flat erosion. In systems with sufficient transport capacity toward the intertidal flats, i.e., sufficient velocities from channels to intertidal flats, the evolution of intertidal flats could be steered with sediment disposals in (or on the edges of) channels (Chapter 5). However, in systems that lack sufficient transport capacity on the intertidal flats and lack sediment import through the barrier, the lowering of intertidal flats can only be mitigated through sediment nourishments on top of these areas (as concluded for the Eastern Scheldt; *Van Zanten and Adriaanse*, 2008; *De Ronde et al.*, 2013). This section specifically focuses on such sediment nourishments on top of intertidal flats. These insights are still relevant for disposals on the edges of intertidal flats, although tidal flow will be relatively more important for sediment disposals at larger water depths.

Sediment nourishments can be used to mitigate the (future) loss in ecological value. Benthic communities at bed elevations with sufficient exposure times are valuable food for wading birds, thus a decrease in elevation of these intertidal areas (Chapter 2) is an ecological threat (*Cozzoli et al.*, 2017). These nourishments may also benefit flood safety as intertidal flats dampen waves (especially at shallow water depths). Such nourishments only temporarily compensate for the sediment volume losses of the intertidal flats as they do not terminate the lowering (or other changes) of these areas. Still, the Dutch government concluded that it is the best solution and has been placing sediment nourishments on four intertidal flats in the Eastern Scheldt since 2008 (see Figure 6.2a).

The nourishments on the Roggenplaat (also studied in Chapter 3) are the most recent (2019; 1,300,000 m^3). The design consisted of six nourishments (Figure 6.2b). The nourishments were designed such that, after 25 years of net lowering, the total area of the intertidal flat with elevations between 50–80% exposure times (the most ecologically valuable) will be at least the same as in 2010. The change in hypsometry directly after the construction is shown in Figure 6.2c. Various findings in this dissertation are relevant for such sediment nourishments and were included specifically in the design of the Roggenplaat nourishments (more details on the design are provided in *Van der Werf et al.*, 2019).

[1] Parts of this section contributed to *Van der Werf et al.* (2019).

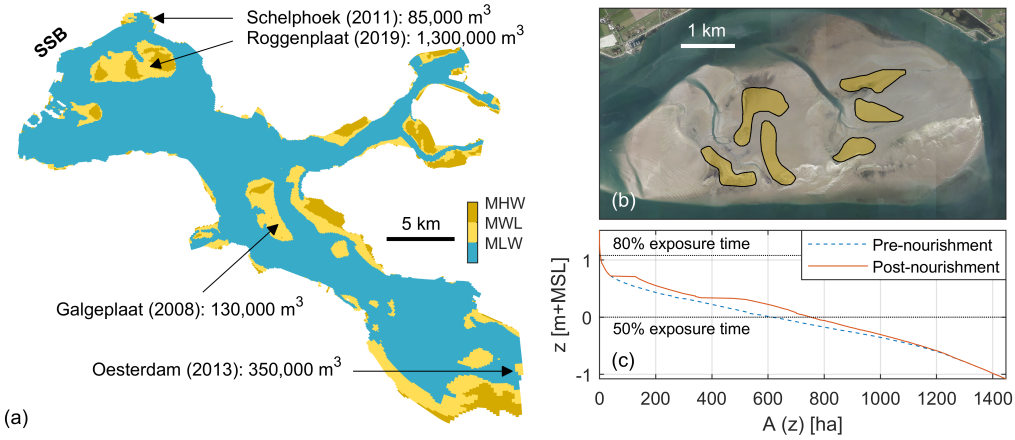

Figure 6.2: (a) Overview of the sand nourishments on the intertidal flats of the Eastern Scheldt, including the in-situ volumes and years of construction. SSB indicates the storm surge barrier. (b) The design of the Roggenplaat nourishments projected on an aerial picture of 2014 (courtesy of Cyclomedia). (c) The hypsometric curve of the Roggenplaat before the nourishment (based on 2013 Vaklodingen and LiDAR data) and after the implementation of the design. The elevations that correspond to the 50% and 80% exposure times are indicated.

Temporal Evolution Pattern Sediment transport on these areas predominantly occurs during storm events (Chapter 3). In the case of the Roggenplaat, the majority (~90–99%) of the sediment transport occurred during only the half of the tides with the largest wind speeds. This was especially the case for the highest elevations (representative of the nourishments). Therefore, strong temporal variations in evolution are expected (in line with field observations of *Van der Werf et al.*, 2015b).

Dominant Evolution Direction At the high elevations, where nourishments are placed, tidal flow velocities are small (Chapter 4) and wind-driven flow (up to ~1/40th of the wind speed; Chapter 3) is relevant. At storm events, during which the largest fraction of the sediment transport occurs, the net flow and sediment transport is largely aligned with the wind-direction. This migration direction was confirmed by numerical model simulations (Delft3D) that included the nourishments (*Van der Werf et al.*, 2019).

Design of Bed Slope of Nourishment The density of early recruits of benthic macrofauna is inversely proportional to the bed level dynamics (*Bouma et al.*, 2001). As the bed level dynamics are proportional to the bed slope (Chapter 4), milder bed slopes enable faster colonization of benthic macrofauna on the nourished areas that void any benthic macrofauna. However, milder bed slopes imply a larger footprint (disturbed area) of the nourishments. Therefore, the design of the bed slope of such nourishments remains a trade-off between various ecological (and economical) considerations. However, if the bed slopes are steeper than the intertidal flat itself, it is likely that the bed slopes will flatten over time to reduce spatial gradients in bed slopes.

Distance between nourishments Some parts of an intertidal flat, such as the tidal creeks, are tide-dominated as they substantially contribute to the inundation and dewatering of these areas (Chapter 3). If distances between the nourishments are narrow, large flow velocities (and related erosion) will likely occur between these nourishments during the inundation and dewatering of the intertidal flat.

Long-term outlook As these nourishments do not fundamentally change the system, they do not solve the cause of the lowering of the intertidal flats. Actually, as the nourished sand is extracted from the channels, the channels are only taken further from equilibrium. In addition, there will be regions of intertidal flats where erosion is enhanced by the nourishments (e.g., the drainage channels between the nourishments). Therefore, repetition of such measures will be required in the long-term as long as the barrier is present and (ecological) objectives for the semi-closed system do not change.

Storm surge barriers are rigid engineering works that are difficult to adapt after construction. Therefore, sediment nourishments may be the only viable solution to mitigate negative eco-morphological consequences on intertidal flats. The discussed aspects related to wind-driven flow, bed slopes of nourishments, and distances between nourishments should be considered in their design. In principle, sediment nourishments on top of intertidal flats could also be used to mitigate the negative consequences of other types of human interventions. The advantage of such nourishments is that the sediments are present directly on the desired locations. For any system yields, the costs and benefits of such mitigation measures should be considered integrally in the perspective of the costs and benefit of all human interventions in the system. For example, mitigating negative consequences following storm surge barriers does not exclude the necessity to (re)assess the long-term perspective of preserving such storm surge barriers under changing physical conditions (e.g., climate change or changing responses of intertidal flats).

Chapter 7

Conclusions and Recommendations

Cover photo: sunrise on an intertidal flat in the Western Scheldt during the fieldwork.

This dissertation aims to identify and quantify the natural and anthropogenic processes driving hydrodynamics and morphodynamics of intertidal flats, and at revealing the implications on ecology and system management. The general conclusions of this study and recommendations for further research are presented in this chapter.

7.1. GENERAL CONCLUSIONS

The general conclusions are formulated as answers to the research questions of Chapter 1. These are followed by further overarching conclusions.

i. How do intertidal flats evolve under influence of human interventions such as sediment relocations and a storm surge barrier?

Engineering works change the hydrodynamics and sediment availability in estuaries. The morphology of intertidal flats adapts to natural forcing processes modified by engineering works. We showed with decades of data that sediment relocations, for the deepening and maintenance of the Western Scheldt navigation channel, increased the height and slope of the intertidal flats. In the Eastern Scheldt, flow velocity reductions resulting from the storm surge barrier and compartment dams initiated erosion and flattening of the previously accreting intertidal flats. For the first time, we revealed through data analysis that the erosion rates in the Eastern Scheldt may be decreasing. The response of intertidal flats to engineering works is neither monotonous over time nor homogeneous over space. The cross-sectional shape of intertidal flats also adapts. Morphological characteristics of intertidal flats are not independent, e.g., larger steepness relates to a higher average elevation of these flats. With ongoing sea level rise, the absolute impact of storm surge barriers will increase.

ii. How do tidal and meteorological forces affect the flow and sediment transport on intertidal flats?

There is a strong spatiotemporal variation in the importance of the natural forcing processes. The flow on intertidal flats is, in the absence of wind, predominantly driven by water level gradients that depend on the geometry of the channel-flat system. The flow over these areas is amplified for higher high water levels resulting from spring-neap fluctuations and storm surges. Regions of intertidal flats that contribute largely to the inundation and dewatering of these areas, such as intertidal creeks, are subjected to flow and sediment transport conditions dominated by the tidal characteristics. In other areas, especially the highly elevated regions, are the magnitudes and directions of the flow and sediment transport largely affected by wind events. We revealed that the adjustment of flow due to wind is substantial if the wind speed exceeds approximately 40 times the tidal velocity. Consequentially, the bulk of the sediment transport in the highly elevated regions occurs during storm events. Waves enhance this effect as they are especially large during these events.

iii. What drives the spatiotemporal variations in bed level dynamics across intertidal flats?
The spatiotemporal variations in the natural forcing processes have consequences for the morphodynamics of intertidal flats. We identified with our field measurements that changes in bed level are mostly the result of a long concurrence of a favorable shallow water depth, a high flow velocity magnitude, and large waves. The intensity of a storm event or the timing of the event within a spring-neap cycle are hence not individually definitive on the magnitude of an impact. A favorable concurrence of forcing processes occurs the longest at the lowest regions of an intertidal flat, implying spatial variations in bed level dynamics. We revealed that the slope of an intertidal flat is also an indicator for patterns of bed level dynamics as bed level changes are proportional to the bed slope. Human interventions influence the bed level dynamics of intertidal flats; not only by modifying the hydrodynamics, but also by imposing changes in bed slopes. Even though bed levels can substantially recover from storm events within days to weeks, morphological impacts may partly persist and benthic communities will not recover simultaneously.

iv. How do sediment disposals in channels affect the eco-morphology of adjacent intertidal flats?
Intertidal flats can also respond to local interventions, without system-wide changes to forcing processes. If sediment disposals change the channel geometry and sediment availability sufficiently, the channel bank migration and the adjacent intertidal flat will adapt. Only a fraction of the disposed sediments will reach an intertidal flat, especially in systems that lack sediment transport capacity toward the intertidal flats. The changes in morphology propagate over intertidal flats orders-of-magnitude slower than the flow. Therefore, the morphodynamic response time of an area scales with the distance to the disposals. We revealed that, after the channel bank migration adapts to the sediment disposals, the hydrodynamics and grain sizes on the intertidal flat adapt with the intertidal flat morphology. Consequentially, these changes in hydro-morphodynamics influence the intertidal flat benthic communities and the adjacent salt marshes. The sequence of eco-morphological consequences develops over a large range of spatial and temporal scales.

Further generalizing, it is the aggregated system of natural and anthropogenic processes that locally and integrally drives the evolution of intertidal flats in engineered estuaries. In spite of spatiotemporal variations in forcing processes, patterns in these forcing processes and morphological responses are revealed. Even if human interventions induce major alterations in morphodynamics, natural forces remain relevant. By affecting the natural forces, human interventions incur not only changes in the evolution of these areas, but also changes to bed level dynamics. The ecological value of intertidal flats will inevitably be pressured by ongoing human interventions and climate change. Both natural and anthropogenic mechanisms revealed in this work provide a basis for the design of adaptive strategies for human interventions with ecosystem consequences as beneficial as possible.

7.2. RECOMMENDATIONS FOR FURTHER RESEARCH

Measuring eco-morphological impacts of human interventions Intertidal flats evolve under human interventions over large time scales (decades/centuries). To capture the eco-morphological impacts of these interventions, extensive datasets are required. For the Eastern Scheldt and Western Scheldt, such datasets have been measured covering various spatial and temporal scales. To improve the predictability of consequences following new interventions in any estuary around the world, comparable datasets should be gathered in other estuaries with other types of interventions and different responses of intertidal flats. These come at high costs, but will contribute to the improvement of conceptual and numerical models. It is crucial to also capture the pre-intervention state of these systems in detail, as to identify trend changes. In the Eastern Scheldt, pre-barrier data was limited, partly because the decision for a storm surge barrier was made while works for a complete closure of the estuary were already ongoing. In contrast, in Chapter 5 we demonstrated that large amounts of data before and after an intervention are essential for a precise analysis of trend changes.

Human interventions as scientific experiments Human interventions (including mitigation measures) disturb estuaries. Therefore, monitoring campaigns are frequently initiated to keep track of the changes to these systems. These datasets provide scientific opportunities as well. Changes in the evolution of estuaries are also indicative for the natural mechanisms. For example, the chain of consequences that followed the sediment disposals in Chapter 5, provides insights on the response of intertidal flats to a natural channel bank migration as well. As spatial and temporal scales are linked, sediment disposals orders of magnitude smaller than intertidal flats may be of special interest as their evolutions occur over much shorter time frames. Human interventions can be seen as scientific experiments. Therefore, if researchers and system managers work together on the set-up of monitoring campaigns, the scientific values of these datasets can be maximized. Scientific insights on these data are of interest for the system managers as well, as these insights may be used to improve their management strategies.

Measuring the morphological impact of storm events We revealed large spatiotemporal variations in the response of intertidal flats to storm events. While instruments on static frames can measure the hydro-morphodynamics on high temporal resolutions, the spatial extent of storm impacts remains difficult to assess. Assessing these spatial extents is essential, as the recovery of an intertidal flat is likely a function of the eroded volume. Attempts to capture the spatial extent of storm impacts were already performed. For example, *Fan et al.* (2006) measured the daily elevation of a cross-shore transect. Still, such datasets do not account for alongshore variations in bed level changes. *Xie et al.* (2017) showed that terrestrial laser scanners provide accurate (centimeter accuracy) digital elevation maps. If such scans would be made every time an intertidal flat emerges, important further steps could be made in unraveling the morphological impact storm events and the recovery afterwards. Results can be obtained especially when these are complimented with other measurements, such as continuous hydro-morphodynamic measurements from static frames.

Forecasts of intertidal flat evolutions Numerical models (e.g., process-based models) are powerful tools to forecast the evolution of intertidal flats under (changing) natural and anthropogenic forces. As these models must cover large temporal scales over which these forces act (decades/centuries), resolving storm events (hours) is computationally expensive. Consequentially, storm events are often idealized, or even excluded. The results of this dissertation indicate that storms are relevant for the long-term evolution of intertidal flats (a single storm may cause a persisting morphological impact that equals to years of continuous evolution). Even if the evolution of intertidal flats is relatively gradual, the exclusion or idealization of (frequently occurring) storms in the forcing conditions may imply that other physical processes are incorrectly altered to match model results with observations. Further research is required to develop a scientifically sound modeling approach. For example, exploratory model simulations with and without simplifications in forcing conditions could be compared. As the morphodynamic impact of a storm event depends on the timing relative to the other forcing processes, it may be required to perform probabilistic simulations (i.e., covering probabilistic distributions as described in Chapter 4).

Data-model integration Numerical models and field measurements are not necessarily separate research lines, as demonstrated in this work. However, instead of applying these approaches side-by-side, data and models could be integrated. The inclusion of measurements to estimate probabilistic distributions of the forcing processes in numerical models is an example of this. Hybrid approaches, in which data is integrated in morphodynamic models with Machine Learning techniques, such as Artificial Neural Networks and Bayesian Networks, provide new opportunities for studies on coastal systems (*Goldstein et al.*, 2019). Such developments demonstrate growing potential with increasing computational resources. With these new approaches, further scientific benefits can be obtained from the extensive existing datasets on intertidal flats (e.g., more accurate model predictions).

REFERENCES

Austen, I., T. J. Andersen, and K. Edelvang (1999), The Influence of Benthic Diatoms and Invertebrates on the Erodibility of an Intertidal Mudflat, the Danish Wadden Sea, *Estuarine, Coastal and Shelf Science*, *49*(1), 99–111, doi: 10.1006/ecss.1998.0491.

Balke, T., P. M. J. Herman, and T. J. Bouma (2014), Critical transitions in disturbance-driven ecosystems: identifying Windows of Opportunity for recovery, *Journal of Ecology*, *102*(3), 700–708, doi: 10.1111/1365-2745.12241.

Baptist, M. J., T. Gerkema, B. van Prooijen, D. van Maren, M. van Regteren, K. Schulz, I. Colosimo, J. Vroom, T. van Kessel, B. Grasmeijer, P. Willemsen, K. Elschot, A. de Groot, J. Cleveringa, E. van Eekelen, F. Schuurman, H. de Lange, and M. van Puijenbroek (2019), Beneficial use of dredged sediment to enhance salt marsh development by applying a 'Mud Motor', *Ecological Engineering*, *127*, 312–323, doi: 10.1016/J.ECOLENG.2018.11.019.

Barbier, E. B., S. D. Hacker, C. Kennedy, E. W. Koch, A. C. Stier, and B. R. Silliman (2011), The value of estuarine and coastal ecosystem services, *Ecological Monographs*, *81*(2), 169–193, doi: 10.1890/10-1510.1.

Bassoullet, P., P. Le Hir, D. Gouleau, and S. Robert (2000), Sediment transport over an intertidal mudflat: field investigations and estimation of fluxes within the "Baie de Marenngres-Oleron" (France), *Continental Shelf Research*, *20*(12-13), 1635–1653, doi: 10.1016/S0278-4343(00)00041-8.

Bearman, J. A., C. T. Friedrichs, B. E. Jaffe, and A. C. Foxgrover (2010), Spatial Trends in Tidal Flat Shape and Associated Environmental Parameters in South San Francisco Bay, *Journal of Coastal Research*, *262*(2), 342–349, doi: 10.2112/08-1094.1.

Becherer, J., J. Hofstede, U. Gräwe, K. Purkiani, E. Schulz, and H. Burchard (2018), The Wadden Sea in transition - consequences of sea level rise, *Ocean Dynamics*, *68*(1), 131–151, doi: 10.1007/s10236-017-1117-5.

Belliard, J.-P., A. Silinski, D. Meire, G. Kolokythas, Y. Levy, A. Van Braeckel, T. J. Bouma, and S. Temmerman (2019), High-resolution bed level changes in relation to tidal and wave forcing on a narrow fringing macrotidal flat: Bridging intra-tidal, daily and seasonal sediment dynamics, *Marine Geology*, *412*, 123–138, doi: 10.1016/J.MARGEO.2019.03.001.

Benninghoff, M., and C. Winter (2019), Recent morphologic evolution of the German Wadden Sea, *Scientific Reports*, *9*(1), 9293, doi: 10.1038/s41598-019-45683-1.

Bishop, C. T., and M. A. Donelan (1987), Measuring waves with pressure transducers, *Coastal Engineering*, *11*(4), 309–328, doi: 10.1016/0378-3839(87)90031-7.

Bolle, A., Z. B. Wang, C. Amos, and J. De Ronde (2010), The influence of changes in tidal asymmetry on residual sediment transport in the Western Scheldt, *Continental Shelf Research*, *30*(8), 871–882, doi: 10.1016/j.csr.2010.03.001.

Booij, N., R. C. Ris, and L. H. Holthuijsen (1999), A third-generation wave model for coastal regions: 1. Model description and validation, *Journal of Geophysical Research: Oceans*, *104*(C4), 7649–7666, doi: 10.1029/98JC02622.

Boon, J. D., and R. J. Byrne (1981), On basin hyposmetry and the morphodynamic response of coastal inlet systems, *Marine Geology*, *40*(1-2), 27–48, doi: 10.1016/0025-3227(81)90041-4.

Bouma, H., J. Duiker, P. de Vries, P. Herman, and W. Wolff (2001), Spatial pattern of early recruitment of Macoma balthica (L.) and Cerastoderma edule (L.) in relation to sediment dynamics on a highly dynamic intertidal sandflat, *Journal of Sea Research*, *45*(2), 79–93, doi: 10.1016/S1385-1101(01)00054-5.

Bouma, T. J., M. B. D. Vries, E. Low, L. Kusters, P. M. J. Herman, I. C. Tánczos, S. Temmerman, A. Hesselink, P. Meire, and S. van. Regenmortel (2005), Flow hydrodynamics on a mudflat and in salt marsh vegetation: identifying general relationships for habitat characterisations, *Hydrobiologia*, *540*(1-3), 259–274, doi: 10.1007/s10750-004-7149-0.

Bouma, T. J., J. van Belzen, T. Balke, J. van Dalen, P. Klaassen, A. M. Hartog, D. P. Callaghan, Z. Hu, M. J. F. Stive, S. Temmerman, and P. M. J. Herman (2016), Short-term mudflat dynamics drive long-term cyclic salt marsh dynamics, *Limnology and Oceanography*, *61*(6), 2261–2275, doi: 10.1002/lno.10374.

Callaghan, D., T. Bouma, P. Klaassen, D. van der Wal, M. Stive, and P. Herman (2010), Hydrodynamic forcing on salt-marsh development: Distinguishing the relative importance of waves and tidal flows, *Estuarine, Coastal and Shelf Science*, *89*(1), 73–88, doi: 10.1016/J.ECSS.2010.05.013.

Cancino, L., and R. Neves (1999), Hydrodynamic and sediment suspension modelling in estuarine systems, *Journal of Marine Systems*, *22*(2-3), 117–131, doi: 10.1016/S0924-7963(99)00036-6.

Christiansen, C., G. Vølund, L. C. Lund-Hansen, and J. Bartholdy (2006), Wind influence on tidal flat sediment dynamics: Field investigations in the Ho Bugt, Danish Wadden Sea, *Marine Geology*, *235*(1-4), 75–86, doi: 10.1016/j.margeo.2006.10.006.

Cleveringa, J. (2013), Ontwikkeling mesoschaal Westerschelde: factsheets, *Tech. rep.*, International Marine & Dredging Consultants/Deltares/Svašek Hydraulics BV/ARCADIS Nederland BV, Antwerp (in Dutch).

Cleveringa, J., and M. Taal (2015), A Smooth Scheldt, in *E-proceedings of the 36th IAHR World Congress*, pp. 22–25, The Hague.

Cozzoli, F., S. Smolders, M. Eelkema, T. Ysebaert, V. Escaravage, S. Temmerman, P. Meire, P. M. Herman, and T. J. Bouma (2017), A modeling approach to assess coastal management effects on benthic habitat quality: A case study on coastal defense and navigability, *Estuarine, Coastal and Shelf Science*, *184*, 67–82, doi: 10.1016/J.ECSS.2016.10.043.

Daidu, F., W. Yuan, and L. Min (2013), Classifications, sedimentary features and facies associations of tidal flats, *Journal of Palaeogeography*, *2*(1), 66–80, doi: 10.3724/SP.J.1261.2013.00018.

Dam, G., M. van der Wegen, R. J. Labeur, and D. Roelvink (2016), Modeling centuries of estuarine morphodynamics in the Western Scheldt estuary, *Geophysical Research Letters*, *43*(8), 3839–3847, doi: 10.1002/2015GL066725.

De Jong, D. J., and V. N. De Jonge (1995), Dynamics and distribution of microphytobenthic chlorophyll-a in the Western Scheldt estuary (SW Netherlands), *Hydrobiologia*, *311*(1-3), 21–30, doi: 10.1007/BF00008568.

De Ronde, J. G., J. P. M. Mulder, L. A. Van Duren, and T. Ysebaert (2013), Eindadvies ANT Oosterschelde, *Tech. rep.*, Deltares, Delft (in Dutch).

De Vet, P. L. M., B. C. van Prooijen, and Z. B. Wang (2017), The differences in morphological development between the intertidal flats of the Eastern and Western Scheldt, *Geomorphology*, *281*, 31–42, doi: 10.1016/j.geomorph.2016.12.031.

De Vet, P. L. M., B. C. Van Prooijen, R. A. Schrijvershof, J. J. Van der Werf, T. Ysebaert, M. C. Schrijver, and Z. B. Wang (2018), The Importance of Combined Tidal and Meteorological Forces for the Flow and Sediment Transport on Intertidal Shoals, *Journal of Geophysical Research: Earth Surface*, *123*(10), 2464–2480, doi: 10.1029/2018JF004605.

De Vet, P. L. M., B. C. Van Prooijen, I. Colosimo, T. Ysebaert, P. M. J. Herman, and Z. B. Wang (2020), Sediment Disposals in Estuarine Channels Alter the Eco-Morphology of Intertidal Flats, *Journal of Geophysical Research: Earth Surface*, *125*(2), doi: 10.1029/2019jf005432.

De Vriend, H. J., Z. B. Wang, T. Ysebaert, P. M. J. Herman, and P. Ding (2011), Eco-Morphological Problems in the Yangtze Estuary and the Western Scheldt, *Wetlands*, *31*(6), 1033–1042, doi: 10.1007/s13157-011-0239-7.

Depreiter, D., M. Sas, K. Beirinckx, and G.-J. Liek (2012), Flexible Disposal Strategy: monitoring as a key to understanding and steering environmental responses to dredging and disposal in the Scheldt Estuary, in *Taking Care of the Sea: conference proceedings of Hydro12*, edited by L. L. Dorst, p. 8, Hydrographic Society Benelux, Rotterdam, doi: 10.3990/2.232.

Dieckmann, R., M. Osterthun, and H.-W. Partenscky (1987), Influence of water-level elevation and tidal range on the sedimentation in a German tidal flat area, *Progress in Oceanography*, *18*(1-4), 151–166, doi: 10.1016/0079-6611(87)90031-0.

Dijkstra, Y. M., H. M. Schuttelaars, and G. P. Schramkowski (2019), Can the Scheldt River Estuary become hyperturbid?: A model analysis of suspended sediment concentrations and transport in response to channel deepening, *Ocean Dynamics*, *69*(7), 809–827, doi: 10.1007/s10236-019-01277-z.

Dronkers, J. J. (1964), *Tidal computations in river and coastal waters*, 518 pp., North-Holland Publishing Company, Amsterdam.

Dyer, K. R., M. C. Christie, and E. W. Wright (2000), The classification of intertidal mudflats, *Continental Shelf Research*, *20*(10-11), 1039–1060, doi: 10.1016/S0278-4343(00)00011-X.

Eelkema, M. (2013), Eastern Scheldt Inlet Morphodynamics, Phd thesis, Delft University of Technology.

Eelkema, M., Z. B. Wang, and M. J. F. Stive (2009), Historical Morphological development of the Eastern Scheldt tidal basin (the Netherlands), in *Coastal Dynamics 2009, 6th International conference, Tokyo, Japan, September 7-11 2009, paper no. 85*, World Scientific Publishing, doi: 10.1142/9789814282475_0087.

Eerdt, M. M. (1985), The influence of vegetation on erosion and accretion in salt marshes of the Oosterschelde, The Netherlands, *Vegetatio*, *62*(1-3), 367–373, doi: 10.1007/BF00044763.

Eisma, D. (1998), *Intertidal Deposits: River Mouths, Tidal Flats, and Coastal Lagoons*, 544 pp., CRC Press, Boca Raton.

Elias, E. P. L., A. J. F. van der Spek, Z. B. Wang, and J. de Ronde (2012), Morphodynamic development and sediment budget of the Dutch Wadden Sea over the last century, *Netherlands Journal of Geosciences*, *91*(03), 293–310, doi: 10.1017/S0016774600000457.

Elliott, M., and A. Whitfield (2011), Challenging paradigms in estuarine ecology and management, *Estuarine, Coastal and Shelf Science*, *94*(4), 306–314, doi: 10.1016/J.ECSS.2011.06.016.

Elmilady, H., M. Wegen, D. Roelvink, and B. E. Jaffe (2018), Intertidal Area Disappears Under Sea Level Rise: 250 Years of Morphodynamic Modeling in San Pablo Bay, California, *Journal of Geophysical Research: Earth Surface*, *124*(1), 2018JF004,857, doi: 10.1029/2018JF004857.

Eysink, W. D. (1990), Morphological response of tidal basins to changes, *Coastal Engineering Proceedings*, *1*(22), doi: 10.9753/ICCE.V22.%P.

Fagherazzi, S., L. Carniello, L. D'Alpaos, and A. Defina (2006), Critical bifurcation of shallow microtidal landforms in tidal flats and salt marshes., *Proceedings of the National Academy of Sciences of the United States of America*, *103*(22), 8337–41, doi: 10.1073/pnas.0508379103.

Fan, D., Y. Guo, P. Wang, and J. Z. Shi (2006), Cross-shore variations in morphodynamic processes of an open-coast mudflat in the Changjiang Delta, China: With an emphasis on storm impacts, *Continental Shelf Research*, *26*(4), 517–538, doi: 10.1016/J.CSR.2005.12.011.

Friedrichs, C. T. (2011), Tidal Flat Morphodynamics: A Synthesis, in *Treatise on Estuarine and Coastal Science*, edited by E. Wolanski and McLuskyDonald, chap. 3.06, pp. 137–170, Elsevier, Waltham, doi: 10.1016/B978-0-12-374711-2.00307-7.

Fujii, T., and D. Raffaelli (2008), Sea-level rise, expected environmental changes, and responses of intertidal benthic macrofauna in the Humber estuary, UK, *Marine Ecology Progress Series*, *371*, 23–35, doi: 10.3354/meps07652.

Gao, A., S. L. Yang, G. Li, P. Li, and S. L. Chen (2010), Long-Term Morphological Evolution of a Tidal Island as Affected by Natural Factors and Human Activities, the Yangtze Estuary, *Journal of Coastal Research*, *261*, 123–131, doi: 10.2112/08-1052.1.

Goldstein, E. B., G. Coco, and N. G. Plant (2019), A review of machine learning applications to coastal sediment transport and morphodynamics, *Earth-Science Reviews*, *194*, 97–108, doi: 10.1016/J.EARSCIREV.2019.04.022.

Gong, Z., Z. B. Wang, M. J. F. Stive, C. Zhang, and A. Chu (2012), Process-Based Morphodynamic Modeling of a Schematized Mudflat Dominated by a Long-Shore Tidal Current at the Central Jiangsu Coast, China, *Journal of Coastal Research*, *285*, 1381–1392, doi: 10.2112/JCOASTRES-D-12-00001.1.

Green, M. O., and G. Coco (2014), Review of wave-driven sediment resuspension and transport in estuaries, *Reviews of Geophysics*, *52*(1), 77–117, doi: 10.1002/2013RG000437.

Green, M. O., K. P. Black, and C. L. Amos (1997), Control of estuarine sediment dynamics by interactions between currents and waves at several scales, *Marine Geology*, *144*(1-3), 97–116, doi: 10.1016/S0025-3227(97)00065-0.

Haasnoot, M., L. Bouwer, F. Diermanse, J. Kwadijk, A. van der Spek, G. O. Essink, J. Delsman, O. Weiler, M. Mens, J. ter Maat, Y. Huismans, K. Sloff, and E. Mosselman (2018), Mogelijke gevolgen van versnelde zeespiegelstijging voor het Deltaprogramma. Een verkenning (Deltaprogramma 2019, Bijlage B), *Tech. rep.*, Deltares rapport 11202230-005-0002, Delft (in Dutch).

Haring, J. (1947), Diepteveranderingen in de Ooster-Schelde over de periode 1827-1933-1947, *Tech. rep.*, Ministerie van Verkeer en Waterstaat, Rijkswaterstaat, Directie Benedenrivieren, Den Haag.

Herman, P. M. J., J. J. Middelburg, and C. H. R. Heip (2001), Benthic community structure and sediment processes on an intertidal flat: results from the ECOFLAT project, *Continental Shelf Research*, *21*(18-19), 2055–2071, doi: 10.1016/S0278-4343(01)00042-5.

Houser, C., and P. Hill (2010), Wave Attenuation across an Intertidal Sand Flat: Implications for Mudflat Development, *Journal of Coastal Research*, *263*, 403–411, doi: 10.2112/08-1117.1.

Hu, Z., Z. B. Wang, T. J. Zitman, M. J. F. Stive, and T. J. Bouma (2015), Predicting long-term and short-term tidal flat morphodynamics using a dynamic equilibrium theory, *Journal of Geophysical Research: Earth Surface*, *120*(9), 1803–1823, doi: 10.1002/2015JF003486.

Hu, Z., P. Yao, D. van der Wal, and T. J. Bouma (2017), Patterns and drivers of daily bed-level dynamics on two tidal flats with contrasting wave exposure, *Scientific Reports*, *7*(1), 7088, doi: 10.1038/s41598-017-07515-y.

Hu, Z., D. van der Wal, H. Cai, J. van Belzen, and T. J. Bouma (2018), Dynamic equilibrium behaviour observed on two contrasting tidal flats from daily monitoring of bed-level changes, *Geomorphology*, *311*, 114–126, doi: 10.1016/j.geomorph.2018.03.025.

Huisman, B. J. A., and A. P. Luijendijk (2009), Sand demand of the Eastern Scheldt : morphology around the barrier, *Tech. rep.*, Deltares, Delft.

Janssen-Stelder, B. (2000), The effect of different hydrodynamic conditions on the morphodynamics of a tidal mudflat in the Dutch Wadden Sea, *Continental Shelf Research*, *20*(12-13), 1461–1478, doi: 10.1016/S0278-4343(00)00032-7.

Jeuken, M., and Z. Wang (2010), Impact of dredging and dumping on the stability of ebb-flood channel systems, *Coastal Engineering*, *57*(6), 553–566, doi: 10.1016/J.COASTALENG.2009.12.004.

Kerner, M. (2007), Effects of deepening the Elbe Estuary on sediment regime and water quality, *Estuarine, Coastal and Shelf Science*, *75*(4), 492–500, doi: 10.1016/J.ECSS.2007.05.033.

Kirby, R. (2000), Practical implications of tidal flat shape, *Continental Shelf Research*, *20*(10-11), 1061–1077, doi: 10.1016/S0278-4343(00)00012-1.

Kohsiek, L. H. M., J. P. M. Mulder, T. Louters, and F. Berben (1987), De Oosterschelde naar een nieuw onderwaterlandschap, *Tech. rep.*, Rijkswaterstaat, RIKZ, Goes (in Dutch).

Kuijper, K., and J. Lescinski (2013), Data-analysis water levels, bathymetry Western Scheldt, *Tech. rep.*, International Marine & Dredging Consultants/Deltares/Svašek Hydraulics BV/ARCADIS Nederland BV, Antwerp (in Dutch).

Le Hir, P., W. Roberts, O. Cazaillet, M. Christie, P. Bassoullet, and C. Bacher (2000), Characterization of intertidal flat hydrodynamics, *Continental Shelf Research*, *20*(12-13), 1433–1459, doi: 10.1016/S0278-4343(00)00031-5.

Lesser, G. R., J. A. Roelvink, J. A. T. M. van Kester, and G. S. Stelling (2004), Development and validation of a three-dimensional morphological model, *Coastal Engineering*, *51*(8-9), 883–915, doi: 10.1016/j.coastaleng.2004.07.014.

Lettmann, K. A., J.-O. Wolff, and T. H. Badewien (2009), Modeling the impact of wind and waves on suspended particulate matter fluxes in the East Frisian Wadden Sea (southern North Sea), *Ocean Dynamics*, *59*(2), 239–262, doi: 10.1007/s10236-009-0194-5.

Louters, T., J. H. van den Berg, and J. P. M. Mulder (1998), Geomorphological changes of the Oosterschelde tidal system during and after the implementation of the delta project, *Journal of Coastal Research*, *14*(3), 1134–1151.

Luan, H. L., P. X. Ding, Z. B. Wang, and J. Z. Ge (2017), Process-based morphodynamic modeling of the Yangtze Estuary at a decadal timescale: Controls on estuarine evolution and future trends, *Geomorphology*, *290*, 347–364, doi: 10.1016/j.geomorph.2017.04.016.

Maan, D. C. (2019), Long-term Dynamics and Stabilization of Intertidal flats: A system approach, Phd thesis, Delft University of Technology.

Maan, D. C., B. C. van Prooijen, Z. B. Wang, and H. J. De Vriend (2015), Do intertidal flats ever reach equilibrium?, *Journal of Geophysical Research: Earth Surface*, *120*(11), 2406–2436, doi: 10.1002/2014JF003311.

Madsen, O. S., Y.-K. Poon, and H. C. Graber (1989), Spectral Wave Attenuation by Bottom Friction: Theory, in *Coastal Engineering 1988*, pp. 492–504, American Society of Civil Engineers, New York, NY, doi: 10.1061/9780872626874.035.

Mallin, M. A., and A. J. Lewitus (2004), The importance of tidal creek ecosystems, *Journal of Experimental Marine Biology and Ecology*, *298*(2), 145–149, doi: 10.1016/S0022-0981(03)00356-3.

Marijs, K., and E. Paree (2004), Nauwkeurigheid vaklodingen Westerschelde en -monding "de praktijk", *Tech. rep.*, Meetinformatiedienst Zeeland, Vlissingen (in Dutch).

Mariotti, G., and S. Fagherazzi (2010), A numerical model for the coupled long-term evolution of salt marshes and tidal flats, *Journal of Geophysical Research*, *115*(F1), F01,004, doi: 10.1029/2009JF001326.

Mariotti, G., and S. Fagherazzi (2013), Critical width of tidal flats triggers marsh collapse in the absence of sea-level rise., *Proceedings of the National Academy of Sciences of the United States of America*, *110*(14), 5353–6, doi: 10.1073/pnas.1219600110.

Mawdsley, R. J., I. D. Haigh, and N. C. Wells (2015), Global secular changes in different tidal high water, low water and range levels, *Earth's Future*, *3*(2), 66–81, doi: 10.1002/2014EF000282.

Meire, P., T. Ysebaert, S. V. Damme, E. V. den Bergh, T. Maris, and E. Struyf (2005), The Scheldt estuary: a description of a changing ecosystem, *Hydrobiologia*, *540*(1-3), 1–11, doi: 10.1007/s10750-005-0896-8.

Monge-Ganuzas, M., A. Cearreta, and G. Evans (2013), Morphodynamic consequences of dredging and dumping activities along the lower Oka estuary (Urdaibai Biosphere Reserve, southeastern Bay of Biscay, Spain), *Ocean & Coastal Management*, *77*, 40–49, doi: 10.1016/J.OCECOAMAN.2012.02.006.

Mulder, J. P. M., and T. Louters (1994), Changes in basin geomorphology after implementation of the Oosterschelde Estuary project, *Hydrobiologia*, *282-283*, 29–39, doi: 10.1007/BF00024619.

Murray, N. J., R. S. Clemens, S. R. Phinn, H. P. Possingham, and R. A. Fuller (2014), Tracking the rapid loss of tidal wetlands in the Yellow Sea, *Frontiers in Ecology and the Environment*, *12*(5), 267–272.

Nio, S.-D., J. H. van den Berg, M. Goesten, and F. Smulders (1980), Dynamics and sequential analysis of a mesotidal shoal and intershoal channel complex in the Eastern Scheldt (southwestern Netherlands), *Sedimentary Geology*, *26*(1-3), 263–279, doi: 10.1016/0037-0738(80)90014-7.

Ostermann, O. P. (1998), The need for management of nature conservation sites designated under Natura 2000, *Journal of Applied Ecology*, *35*(6), 968–973, doi: 10.1111/j.1365-2664.1998.tb00016.x.

Pawlowicz, R., B. Beardsley, and S. Lentz (2002), Classical tidal harmonic analysis including error estimates in MATLAB using T TIDE, *Computers & Geosciences*, *28*(8), 929–937, doi: 10.1016/S0098-3004(02)00013-4.

Pethick, J. (2001), Coastal management and sea-level rise, *CATENA*, *42*(2-4), 307–322, doi: 10.1016/S0341-8162(00)00143-0.

Pethick, J. S. (1996), The geomorphology of mudflats, in *Estuarine shores: Evolution, Environments and Human Alterations*, edited by K. F. Nordstrom and C. T. Roman, chap. 8, pp. 185–211, John Wiley & Sons, Chichester.

Pezij, M. (2015), Understanding and modelling of the Oesterdam nourishment, Msc thesis, University of Twente.

Plancke, Y., K. Beirinckx, G.-J. Liek, G. Vos, and M. Schrijver (2014), A new disposal strategy in the Westerschelde, conciliating port accessibility and nature, in *33rd PIANC World Congress - Navigating the new millenium*, p. 13, PIANC, San Francisco.

Postma, H. (1967), Sediment transport and sedimentation in the estuarine environment, in *Estuaries*, edited by G. H. Lauff, pp. 158–179, American Association for the Advancement of Science, Washington D.C.

Reed, D., B. van Wesenbeeck, P. M. Herman, and E. Meselhe (2018), Tidal flat-wetland systems as flood defenses: Understanding biogeomorphic controls, *Estuarine, Coastal and Shelf Science*, *213*, 269–282, doi: 10.1016/J.ECSS.2018.08.017.

Rijkswaterstaat (2006), Monitoring van de effecten van de verruiming 48' / 43': MOVE eindrapport RIKZ/2007.003, *Tech. rep.*, Rijkswaterstaat Rijksinstituut voor Kust en Zee, Middelburg (in Dutch).

Salmon, J. E., and L. H. Holthuijsen (2015), Modeling depth-induced wave breaking over complex coastal bathymetries, *Coastal Engineering*, *105*, 21–35, doi: 10.1016/j.coastaleng.2015.08.002.

Salmon, J. E., L. H. Holthuijsen, M. Zijlema, G. P. van Vledder, and J. D. Pietrzak (2015), Scaling depth-induced wave-breaking in two-dimensional spectral wave models, *Ocean Modelling*, *87*, 30–47, doi: 10.1016/j.ocemod.2014.12.011.

Santinelli, G., and J. de Ronde (2012), Volume Analysis on RTK Profiles of the Eastern Scheldt, *Tech. rep.*, Deltares, Delft.

Sherwood, C. R., D. A. Jay, R. Bradford Harvey, P. Hamilton, and C. A. Simenstad (1990), Historical changes in the Columbia River Estuary, *Progress in Oceanography*, *25*(1-4), 299–352, doi: 10.1016/0079-6611(90)90011-P.

Shi, B., S. Yang, Y. Wang, Q. Yu, and M. Li (2014), Intratidal erosion and deposition rates inferred from field observations of hydrodynamic and sedimentary processes: A case study of a mudflat–saltmarsh transition at the Yangtze delta front, *Continental Shelf Research*, *90*, 109–116, doi: 10.1016/J.CSR.2014.01.019.

Shi, B., J. R. Cooper, P. D. Pratolongo, S. Gao, T. J. Bouma, G. Li, C. Li, S. Yang, and Y. P. Wang (2017), Erosion and Accretion on a Mudflat: The Importance of Very Shallow-Water Effects, *Journal of Geophysical Research: Oceans*, *122*(12), 9476–9499, doi: 10.1002/2016JC012316.

Smaal, A. C., and P. H. Nienhuis (1992), The eastern Scheldt (The Netherlands), from an estuary to a tidal bay: A review of responses at the ecosystem level, *Netherlands Journal of Sea Research*, *30*, 161–173, doi: 10.1016/0077-7579(92)90055-J.

Soulsby, R. (1997), *Dynamics of marine sands: A manual for practical applications*, 249 pp., ThomasTelford, London.

Stanev, E. V., G. Flöser, and J.-O. Wolff (2003), First- and higher-order dynamical controls on water exchanges between tidal basins and the open ocean. A case study for the East Frisian Wadden Sea, *Ocean Dynamics*, *53*(3), 146–165, doi: 10.1007/s10236-003-0029-8.

Strahler, A. N. (1952), Hypsometric (Area-Altitude) Analysis Of Erosional Topography, *Geological Society of America Bulletin*, *63*(11), 1117–1142, doi: 10.1130/0016-7606(1952)63[1117:HAAOET]2.0.CO;2.

Swinkels, C. M., C. J. L. Jeuken, Z. B. Wang, and R. J. Nicholls (2009), Presence of Connecting Channels in the Western Scheldt Estuary, *Journal of Coastal Research*, *253*, 627–640, doi: 10.2112/06-0719.1.

Symonds, G., K. P. Black, and I. R. Young (1995), Wave-driven flow over shallow reefs, *Journal of Geophysical Research*, *100*(C2), 2639, doi: 10.1029/94JC02736.

Taal, M., C. Jelmer, K. Kuijper, Z. Wang, and G. Holland (2013), Tidal evolution in the Scheldt estuary and its interaction with dredging works, in *Proceedings WODCON XX - Congress and Exhibition: The Art of Dredging*.

Talke, S. A., and M. T. Stacey (2008), Suspended sediment fluxes at an intertidal flat: The shifting influence of wave, wind, tidal, and freshwater forcing, *Continental Shelf Research*, *28*(6), 710–725, doi: 10.1016/j.csr.2007.12.003.

Temmerman, S., P. Meire, T. J. Bouma, P. M. J. Herman, T. Ysebaert, and H. J. De Vriend (2013), Ecosystem-based coastal defence in the face of global change, *Nature*, *504*(7478), 79–83, doi: 10.1038/nature12859.

Van Belzen, J., J. Van de Koppel, M. Kirwan, A. L., D. Van der Wal, P. M. J. Herman, V. Dakos, S. Kéfi, M. Scheffer, G. R. Guntenspergen, and T. J. Bouma (2017), Vegetation recovery in tidal marshes reveals critical slowing down under increased inundation, *Nature Communications*, *8*, 15,811, doi: 10.1038/ncomms15811.

Van de Lageweg, W., and H. Feldman (2018), Process-based modelling of morphodynamics and bar architecture in confined basins with fluvial and tidal currents, *Marine Geology*, *398*, 35–47, doi: 10.1016/J.MARGEO.2018.01.002.

Van den Berg, J. H. (1984), Morphological changes of the ebb-tidal delta of the Eastern Scheldt during recent decades, *Geologie en Mijnbouw*, *63*(4), 363–375.

Van den Berg, J. H. (1986), Aspects of sediment- and morphodynamics of subtidal deposits of the Oosterschelde (Netherlands), Phd thesis, Utrecht University.

Van den Berg, J. H., C. J. L. Jeuken, and A. J. F. Van der Spek (1996), Hydraulic processes affecting the morphology and evolution of the Westerschelde estuary, in *Estuarine shores: evolution, environment and human alterations*, edited by K. F. Nordstrom and C. T. Roman, chap. 7, pp. 157–184, John Wiley & Sons, Chichester.

Van der Wal, D., A. Wielemaker-Van den Dool, and P. M. Herman (2008), Spatial patterns, rates and mechanisms of saltmarsh cycles (Westerschelde, The Netherlands), *Estuarine, Coastal and Shelf Science*, *76*(2), 357–368, doi: 10.1016/J.ECSS.2007.07.017.

Van der Wal, D., T. Van Kessel, M. A. Eleveld, and J. Vanlede (2010), Spatial heterogeneity in estuarine mud dynamics, *Ocean Dynamics*, *60*(3), 519–533, doi: 10.1007/s10236-010-0271-9.

Van der Wal, D., R. M. Forster, F. Rossi, H. Hummel, T. Ysebaert, F. Roose, and P. M. Herman (2011), Ecological evaluation of an experimental beneficial use scheme for dredged sediment disposal in shallow tidal waters, *Marine Pollution Bulletin*, *62*(1), 99–108, doi: 10.1016/J.MARPOLBUL.2010.09.005.

Van der Wegen, M., B. Jaffe, A. Foxgrover, and D. Roelvink (2017), Mudflat Morphodynamics and the Impact of Sea Level Rise in South San Francisco Bay, *Estuaries and Coasts*, *40*(1), 37–49, doi: 10.1007/s12237-016-0129-6.

Van der Werf, J., T. Van Oyen, B. De Maerschalck, A. Nnafie, A. Van Rooijen, M. Taal, T. Verwaest, L. De Vet, J. Vroom, and M. Van der Wegen (2015a), Modeling the morphodynamics of the mouth of the Scheldt estuary, in *E-proceedings of the 36th IAHR World Congress*, pp. 80–86, The Hague.

Van der Werf, J., J. Reinders, A. van Rooijen, H. Holzhauer, and T. Ysebaert (2015b), Evaluation of a tidal flat sediment nourishment as estuarine management measure, *Ocean & Coastal Management*, *114*, 77–87, doi: 10.1016/j.ocecoaman.2015.06.006.

Van der Werf, J. J., P. L. M. De Vet, M. P. Boersema, T. J. Bouma, A. J. Nolte, R. A. Schrijvershof, L. M. Soissons, J. Stronkhorst, E. Van Zanten, and T. Ysebaert (2019), An integral approach to design the Roggenplaat intertidal shoal nourishment, *Ocean & Coastal Management*, *172*, 30–40, doi: 10.1016/J.OCECOAMAN.2019.01.023.

Van Eck, B. T. M. (1999), De Scheldeatlas: een beeld van een estuarium, *Tech. rep.*, Rijksinstituut voor Kust en Zee/Schelde, Middelburg (in Dutch).

Van Maren, D., T. Van Kessel, K. Cronin, and L. Sittoni (2015), The impact of channel deepening and dredging on estuarine sediment concentration, *Continental Shelf Research*, *95*, 1–14, doi: 10.1016/J.CSR.2014.12.010.

Van Rijn, L. C. (2007a), Unified View of Sediment Transport by Currents and Waves. I: Initiation of Motion, Bed Roughness, and Bed-Load Transport, *Journal of Hydraulic Engineering*, *133*(6), 649–667, doi: 10.1061/(ASCE)0733-9429(2007)133:6(649).

Van Rijn, L. C. (2007b), Unified View of Sediment Transport by Currents and Waves. II: Suspended Transport, *Journal of Hydraulic Engineering*, *133*(6), 668–689, doi: 10.1061/(ASCE)0733-9429(2007)133:6(668).

Van Zanten, E., and L. A. Adriaanse (2008), Verminderd getij: verkenning naar mogelijke maatregelen om het verlies van platen, slikken en schorren in de Oosterschelde te beperken, *Tech. rep.*, Rijkswaterstaat, Directie Zeeland, Middelburg (in Dutch).

Wang, Z. B., and J. C. Winterwerp (2001), Impact of dredging and dumping on the stability of ebb-flood channel systems, in *Proceedings of the 2nd IAHR symposium on River, Coastal and Estuarine Morphodynamics*, pp. 515–524, Obihiro, Japan.

Wang, Z. B., M. C. J. L. Jeuken, H. Gerritsen, H. J. de Vriend, and B. A. Kornman (2002), Morphology and asymmetry of the vertical tide in the Westerschelde estuary, *Continental Shelf Research*, *22*(17), 2599–2609, doi: 10.1016/S0278-4343(02)00134-6.

Wang, Z. B., D. S. Van Maren, P. X. Ding, S. L. Yang, B. C. Van Prooijen, P. L. M. De Vet, J. C. Winterwerp, H. J. De Vriend, M. J. F. Stive, and Q. He (2015), Human impacts on morphodynamic thresholds in estuarine systems, *Continental Shelf Research*, p. CSR3681, doi: 10.1016/j.csr.2015.08.009.

Wei, W., X. Mei, Z. Dai, and Z. Tang (2016), Recent morphodynamic evolution of the largest uninhibited island in the Yangtze (Changjiang) estuary during 1998-2014: Influence of the anthropogenic interference, *Continental Shelf Research*, *124*, 83–94, doi: 10.1016/j.csr.2016.05.011.

Widdows, J., A. Blauw, C. Heip, P. Herman, C. Lucas, J. Middelburg, S. Schmidt, M. Brinsley, F. Twisk, and H. Verbeek (2004), Role of physical and biological processes in sediment dynamics of a tidal flat in Westerschelde Estuary, SW Netherlands, *Marine Ecology Progress Series*, *274*, 41–56, doi: 10.3354/meps274041.

Wiegmann, N., R. Perluka, S. Oude Elberink, and J. Vogelzang (2005), Vaklodingen: de inwintechnieken en hun combinaties: vergelijking tussen verschillende inwintechnieken en de combinaties ervan, *Tech. rep.*, Adviesdienst Geo-Informatica en ICT (AGI), Delft (in Dutch).

Willemsen, P. W. J. M., B. W. Borsje, S. J. M. H. Hulscher, D. Van der Wal, Z. Zhu, B. Oteman, B. Evans, I. Möller, and T. J. Bouma (2018), Quantifying Bed Level Change at the Transition of Tidal Flat and Salt Marsh: Can We Understand the Lateral Location of the Marsh Edge?, *Journal of Geophysical Research: Earth Surface*, *123*(10), 2509–2524, doi: 10.1029/2018JF004742.

Wilson, M. A., R. Costanza, R. Boumans, and S. Liu (2005), Integrated assessment and valuation of ecosystem goods and services provided by coastal systems, in *The intertidal ecosystem: the value of Ireland's shores*, edited by J. G. Wilson, chap. 1, pp. 1–24, Royal Irish Academy, Dublin.

Winterwerp, J. C., and Z. B. Wang (2013), Man-induced regime shifts in small estuaries – I: theory, *Ocean Dynamics*, *63*(11-12), 1279–1292, doi: 10.1007/s10236-013-0662-9.

Wolff, W. J. (1973), The estuary as a habitat: an analysis of data on the soft-bottom macrofauna of the estuarine area of the Rivers Rhine, Meuse, and Scheldt, Phd thesis, Leiden University.

Xie, W., Q. He, K. Zhang, L. Guo, X. Wang, J. Shen, and Z. Cui (2017), Application of terrestrial laser scanner on tidal flat morphology at a typhoon event timescale, *Geomorphology*, *292*, 47–58, doi: 10.1016/J.GEOMORPH.2017.04.034.

Yang, S.-L., P.-X. Ding, and S.-L. Chen (2001), Changes in progradation rate of the tidal flats at the mouth of the Changjiang (Yangtze) River, China, *Geomorphology*, *38*(1-2), 167–180, doi: 10.1016/S0169-555X(00)00079-9.

Yang, S. L., C. T. Friedrichs, Z. Shi, P.-X. Ding, J. Zhu, and Q.-Y. Zhao (2003), Morphological response of tidal marshes, flats and channels of the Outer Yangtze River mouth to a major storm, *Estuaries*, *26*(6), 1416–1425, doi: 10.1007/BF02803650.

Yang, S. L., M. Li, S. B. Dai, Z. Liu, J. Zhang, and P. X. Ding (2006), Drastic decrease in sediment supply from the Yangtze River and its challenge to coastal wetland management, *Geophysical Research Letters*, *33*(6), L06,408, doi: 10.1029/2005GL025507.

Yang, S. L., H. Li, T. Ysebaert, T. J. Bouma, W. X. Zhang, Y. Y. Wang, P. Li, M. Li, and P. X. Ding (2008), Spatial and temporal variations in sediment grain size in tidal wetlands, Yangtze Delta: On the role of physical and biotic controls, *Estuarine, Coastal and Shelf Science*, *77*(4), 657–671, doi: 10.1016/J.ECSS.2007.10.024.

Young, I. R., and A. Ribal (2019), Multiplatform evaluation of global trends in wind speed and wave height., *Science (New York, N.Y.)*, *364*(6440), 548–552, doi: 10.1126/science.aav9527.

Ysebaert, T., and P. Herman (2002), Spatial and temporal variation in benthic macrofauna and relationships with environmental variables in an estuarine, intertidal soft-sediment environment, *Marine Ecology Progress Series*, *244*, 105–124, doi: 10.3354/meps244105.

Zhou, Z., G. Coco, I. Townend, M. Olabarrieta, M. van der Wegen, Z. Gong, A. D'Alpaos, S. Gao, B. E. Jaffe, G. Gelfenbaum, Q. He, Y. Wang, S. Lanzoni, Z. Wang, H. Winterwerp, and C. Zhang (2017), Is "Morphodynamic Equilibrium" an oxymoron?, *Earth-Science Reviews*, *165*, 257–267, doi: 10.1016/j.earscirev.2016.12.002.

Zhu, J., R. H. Weisberg, L. Zheng, and S. Han (2015), Influences of Channel Deepening and Widening on the Tidal and Nontidal Circulations of Tampa Bay, *Estuaries and Coasts*, *38*(1), 132–150, doi: 10.1007/s12237-014-9815-4.

Zhu, Q., B. C. van Prooijen, Z. B. Wang, and S. L. Yang (2017), Bed-level changes on intertidal wetland in response to waves and tides: A case study from the Yangtze River Delta, *Marine Geology*, *385*, 160–172, doi: 10.1016/j.margeo.2017.01.003.

Zhu, Q., B. van Prooijen, D. Maan, Z. Wang, P. Yao, T. Daggers, and S. Yang (2019), The heterogeneity of mudflat erodibility, *Geomorphology*, *345*, 106,834, doi: 10.1016/J.GEOMORPH.2019.106834.

Zijl, F., M. Verlaan, and H. Gerritsen (2013), Improved water-level forecasting for the Northwest European Shelf and North Sea through direct modelling of tide, surge and non-linear interaction, *Ocean Dynamics*, *63*(7), 823–847, doi: 10.1007/s10236-013-0624-2.

Zijl, F., J. Sumihar, and M. Verlaan (2015), Application of data assimilation for improved operational water level forecasting on the northwest European shelf and North Sea, *Ocean Dynamics*, *65*(12), 1699–1716, doi: 10.1007/s10236-015-0898-7.

Het is zoals het is, en het is goed

— My grandmother

ACKNOWLEDGEMENTS

Luctor et Emergo — *I struggle and emerge*. The opening sentence of this dissertation, the motto of the Dutch province of Zeeland in which the Eastern and Western Scheldt are located. *I struggled and emerged*. In this beautiful PhD process, I had moments in which I struggled. I went out of my comfort zone, also on purpose. I found sometimes conflicts between my perfectionism and pragmatism. But I also emerged, with a smile, with many valuable steps on self-development made, and with the pride of the final result of this dissertation. My PhD process was everything but a lonely process. The true smile with which I emerged is thanks to the support of many.

Bram and *Wang*, I really value that as supervisors you have trusted me ever since our first talks. This trust, together with the freedom that came with it, gave me the confidence to shape this PhD in a nonlinear project that represents my broad interests. A balance between science and application. A valuable combination of data analyses, modeling, and fieldwork. *Bram*, I took over your passion for the field. We achieved great data also under challenging conditions. My passion for the field is now so great that I am even able to enjoy the toughest field conditions. *Bram*, thanks a lot for always being greatly excited and full of creativity. *Wang*, your good balance between perfectionism and pragmatism was a great example for me and your suggestions always felt effective.

Peter and *Tom*, our talks on the ecology and morphodynamics of intertidal flats made me always excited. You are both great examples for me in this multidisciplinary field. *Peter*, you were able to challenge me at moments I felt my work was "perfect", allowing me to grow even further and to strive for a larger impact of my work. I really valued this. *Tom*, apart from the great interactions within the PhD project, I also highly enjoyed our interactions in the nourishment projects in which I feel we always greatly complemented the ecological and morphological aspects. I look forward to the future joint projects.

Edwin, *Eric*, *Frans*, *Gert-Jan*, *Gijs*, *Lynyrd*, *Marcel*, and *Marco*, I am grateful for your contributions as EMERGO consortium partners. Our meetings were always very fruitful and definitely stimulated me to make this dissertation relevant for system managers and society in general. In special, thank you *Marco* for the efforts of deploying the ADCP instruments at our fieldwork sites, these measurements gave many valuable insights!

Brenda, *Claudia*, *Natalie*, and *Oliver*, it was a pleasure to be working together within the EMERGO project. You taught me a lot on the ecology of intertidal flats, which is also visible in this work. Going in the field one week every six weeks for fourteen months was optimistic and challenging, but it provided us many unique (non-)scientific insights and above all: lots of fun! *Natalie*, it was a pleasure reasoning together on the ecological and morphological outcomes of the fieldwork and I look forward to continuing our work.

With great pleasure I have also been working one day a week at the applied research institute Deltares, which highly benefited the outcomes of my PhD. Having a direct link with applications turned out very fruitful and joyful, with my involvement in the Roggenplaat nourishment design as a beautiful example. It allowed me to turn our academic

system understanding into actual solutions. I am very grateful for the warmth received from all my Deltares colleagues, in special my *AMO colleagues* who made me feel fully part of the group despite my part-time appointment. Specifically, *Jebbe* thanks for your flexibility and positivity through all projects we worked on. *Dirk-Jan*, thank you for your trust throughout the full process and enabling this position. *Bob*, thank you for your motivational attitude. I look very much forward to continuing at Deltares.

These have been five amazing years of my life, to which all colleagues/friends from the TU Delft Waterlab (and other floors) contributed by supporting and enjoying with me. I will highlight some, even though many others are equally important to me. *Andres*, *Cynthia*, *Erik*, *Floris*, *Gonzalo*, *Jakob*, *Marion*, *Matt*, *Matthijs*, *Sotiria*, *Victor*, and *Yorick*, thanks for all joyful (non-)serious coffee breaks and lunches! *Alejandra*, *Irene*, *Liselot*, *Maria*, and *Stuart*, I really enjoyed our dinners! *Merel*, thanks for the refreshing walks. *Claudia* and all former office mates, it was a lot of fun sharing our office. Thanks to all technicians for the support with my fieldwork preparations. *Ana*, *Jill*, and *Nici*, we form a very nice team in the new project! Thanks a lot, also to those not named.

Ana, *Anne*, *Benjamin*, *Ferdi*, *Geert*, *Jiechen*, *Maarten*, *Marco*, *Michiel*, *Mikelina*, *Nefeli*, *Samantha*, *Tim*, *Vera*, and *Yahia*, it was great fun being part of the theses concluding your studies. No matter how much I love solving problems, you made me aware that often one is not looking for direct solutions but for someone reasoning together.

Eva, *Jelle*, *Kris*, and *Senne*, after our BSc we all continued in different fields, but as friends we stayed greatly in touch. Really happy to see how everyone succeeded so well in finding a career that suits his/her personality! Thanks for always being truly interested and the great fun we have. *Dip*, *Jeroen*, *Marjolein*, *Martin*, and *Simone* (x2), also our friendship originates from our studies, actually from the first day. We laughed a lot, also as "normal"-non-academic people, which was a very nice deviation.

Jeroen, *Leo*, *Nick*, and *Willem*. Even though I made the mistake of not mentioning you in the acknowledgments of my MSc thesis (shame on me), know that you mean a lot to me. You made as house mates my life in Delft very joyful. For example, I really enjoyed our discussions (still not settled) on research questions such as "What is the direction of the centrifugal force?" and "How do we convince Nick that the expected value of his beat-the-casino-algorithm equals 0?". Several of my propositions follow our chats. You are all great friends of me. In special, *Jeroen*, thank you for reasoning a lot on life together.

Irene, in so many beautiful roles we supported each other. The friendship that we formed in the past years really colored the joy inside and outside my PhD. Thank you for teaching me not to say thank you every time. Sharing the excitement of the wind, tides, and nature in general. Preparing our field campaigns with military precision. Publishing together. Supporting each other in difficult times. Motivating each other in going forward in our personal developments. Laughing together. A lot. Similar enough to understand each other, different enough to surprise each other. You are important to me.

Lieve familie, dank voor jullie oprechte interesse in mijn onderzoek. *Jan*, *Lucas*, *papa* en *mama*, jullie in het bijzonder. *Papa*, met wederzijdse trots zijn wij sinds kort in het zelfde werkveld actief. Dankzij de management vaardigheden die ik van jou heb overgenomen is het mij gelukt pragmatisch te blijven. *Mama*, dankzij het oog voor detail dat jij mij hebt gegeven, heb ik in alles kwaliteit nagestreefd. Voor jullie ligt een proefschrift waar ik trots op ben; dit gevoel heb ik zeker ook aan jullie te danken.

CURRICULUM VITÆ

Paul Lodewijk Maria DE VET

09-09-1991	Born in Breda, The Netherlands

EDUCATION

2003–2009	Secondary School Meridiaan College Het Nieuwe Eemland, Amersfoort
2009–2012	Bachelor Civil Engineering, *with distinction* Delft University of Technology
2012–2014	Master Hydraulic Engineering and Water Resources Management Double degree programme, *with distinction* Delft University of Technology & National University of Singapore
2014–2019	PhD Researcher, this dissertation, *finished within budgeted time* Delft University of Technology, 0.8 fte

WORK EXPERIENCE

2014–	Researcher & Consultant Marine and Coastal Systems Deltares, 0.2 fte (2014–2020), 0.6 fte (2020–)
2019–	Post-doctoral Researcher, Coping with Deltas in Transition Delft University of Technology, 0.4 fte

List of Publications

Journal Articles

First Author

4. **De Vet, P. L. M.**, B. C. van Prooijen, I. Colosimo, T. Ysebaert, P. M. J. Herman, and Z. B. Wang (2020). Sediment Disposals in Estuarine Channels Alter the Eco-Morphology of Intertidal Flats. *Journal of Geophysical Research: Earth Surface*, *125*(2) doi: 10.1029/2019jf005432. **[Chapter 5]**

3. **De Vet, P. L. M.**, B. C. van Prooijen, I. Colosimo, N. Steiner, T. Ysebaert, P. M. J. Herman, and Z. B. Wang (*submitted*). How Storms Impose Variations in Bed Level Dynamics Across Intertidal Flats. *Scientific Reports*. **[Chapter 4]**

2. **De Vet, P. L. M.**, B. C. Van Prooijen, R. A. Schrijvershof, J. J. Van der Werf, T. Ysebaert, M. C. Schrijver, and Z. B. Wang (2018). The Importance of Combined Tidal and Meteorological Forces for the Flow and Sediment Transport on Intertidal Shoals, *Journal of Geophysical Research: Earth Surface*, *123*(10), 2464–2480, doi: 10.1029/2018JF004605. **[Chapter 3]**

1. **De Vet, P. L. M.**, B. C. Van Prooijen, and Z. B. Wang (2017). The differences in morphological development between the intertidal flats of the Eastern and Western Scheldt, *Geomorphology*, *281*, 31–42, doi: 10.1016/j.geomorph.2016.12.031. **[Chapter 2]**

Co-Author

3. Colosimo, I., **P. L. M. De Vet**, D. S. Van Maren, A. J. H. M. Reniers, J. C. Winterwerp, and B. C. van Prooijen (*submitted*). Tide-Wind Interaction Effects on the Intertidal Flat Sediment Transport. *Journal of Geophysical Research: Earth Surface*.

2. Van der Werf, J. J., **P. L. M. De Vet**, M. P. Boersema, T. J. Bouma, A. J. Nolte, R. A. Schrijvershof, L. M. Soissons, J. Stronkhorst, E. Van Zanten, and T. Ysebaert (2019). An integral approach to design the Roggenplaat intertidal shoal nourishment, *Ocean & Coastal Management*, *172*, 30–40, doi: 10.1016/J.OCECOAMAN.2019.01.023.

1. Wang, Z. B., D. S. Van Maren, P. X. Ding, S. L. Yang, B. C. Van Prooijen, **P. L. M. De Vet**, J. C. Winterwerp, H. J. De Vriend, M. J. F. Stive, and Q. He (2015). Human impacts on morphodynamic thresholds in estuarine systems, *Continental Shelf Research*, p. CSR3681, doi: 10.1016/j.csr.2015.08.009.

Conference Proceedings and Talks

First Author

12. **De Vet, P. L. M.**, B. C. Van Prooijen, I. Colosimo, N. Steiner, T. Ysebaert, P. M. J. Herman, and Z. B. Wang (2019). Long-term morphological evolution of intertidal flats: how do storms affect this? *Symposium on River, Coastal and Estuarine Morphodynamics*, Auckland, New Zealand, 16–21 November.

11. **De Vet, P. L. M.**, B. C. van Prooijen, I. Colosimo, T. Ysebaert, P. M. J. Herman, and Z. B. Wang (2019). Eco-morphological changes of intertidal flats initiated by sediment disposals in estuarine channels. *Ems-Scheldt Workshop*, Delft, The Netherlands, 2–3 May.

10. **De Vet, P. L. M.**, B. C. Van Prooijen, I. Colosimo, N. Steiner, T. Ysebaert, P. M. J. Herman, and Z. B. Wang (2019). The timing of events matters for the eco-morphology of intertidal flats. *NCK days conference*, Enkhuizen, The Netherlands, 20–23 March.

9. **De Vet, P. L. M.**, B. C. Van Prooijen, T. Ysebaert, and Z. B. Wang (2018). Field evidence on major intertidal flat growth initiated by sediment disposals in an estuarine channel. *American Geophysical Union Fall Meeting*, Washington D.C., United States, 10–14 December.

8. **De Vet, P. L. M.**, B. C. Van Prooijen, T. Ysebaert, M. C. Schrijver, and Z. B. Wang (2017). The importance of estuarine geometry on the morphology of intertidal flats. *Coastal & Estuarine Research Federation Conference*, Providence, United States, 5–9 November.

7. **De Vet, P. L. M.**, B. C. Van Prooijen, B. Walles, T. Ysebaert, M. C. Schrijver, and Z. B. Wang (2017). The Inhomogeneous Impact of Low-water Storms on Intertidal Flats. *Symposium on River, Coastal and Estuarine Morphodynamics*, Padova, Italy, 15–22 September.

6. **De Vet, P. L. M.**, B. C. Van Prooijen, R. Schrijvershof, J. J. Van der Werf, T. Ysebaert, M. C. Schrijver, and Z. B. Wang (2017). Hydrodynamics on a large tidal flat surrounded by water: the Roggenplaat. *NCK days conference*, Den Helder, The Netherlands, 15–17 March.

5. **De Vet, P. L. M.**, B. C. Van Prooijen, R. Schrijvershof, J. J. Van der Werf, M. C. Schrijver, and Z. B. Wang (2016). Physical Processes Driving the Morphological Evolution of the Roggenplaat Tidal Flat. *Physics of Estuaries and Coastal Seas Conference*, The Hague, The Netherlands, 9–14 October.

4. **De Vet, P. L. M.**, B. C. Van Prooijen, and Z. B. Wang (2016). Human impact on intertidal flats in the Eastern and Western Scheldt. *NCK days conference*, Ouddorp, The Netherlands, 16–18 March.

3. **De Vet, P. L. M.**, R. T. Mccall, J. P. Den Bieman, J. F. Stive, and M. Van Ormondt (2015). Modelling dune erosion, overwash and breaching at Fire Island (NY) during Hurricane Sandy. *The Proceedings of the Coastal Sediments 2015*, San Diego, United States, 11–15 May. doi: 10.1142/9789814689977_0006.

2. **De Vet, P. L. M.**, B. C. Van Prooijen, and Z. B. Wang (2015). Towards a classification of the morphological development of intertidal flats: a comparison between the Eastern and Western Scheldt. *NCK days conference*, Camperduin, The Netherlands, 18–20 March.

1. **De Vet, L.**, J. Van der Zwaag, and A. Blom (2012). The effect of a varying bedload layer thickness in computations using a sand-gravel morphodynamic model. *American Geophysical Union Fall Meeting*, San Francisco, United States, 3–7 December.

CO-AUTHOR

13. Hanssen, J., B.C. Van Prooijen, **P. L. M. De Vet**, P. M. J. Herman, and Z. B. Wang (2019). Unravelling creek formation on intertidal flats. *Symposium on River, Coastal and Estuarine Morphodynamics*, Auckland, New Zealand, 16–21 November.

12. Steiner, N., C. Morys, **L. De Vet**, B. Van Prooijen, and T. Ysebaert (2019). Hydro- and morphodynamics affecting the spatial distribution of macrozoobenthic communities on estuarine intertidal flats. *NAEM conference*, Lunteren, The Netherlands, 12–13 February.

11. Colosimo, I., D. S. Van Maren, M. Van Regteren, **P. L. M. De Vet**, and B. C. Van Prooijen (2018). 'Winds of Opportunity': the Influence of Wind on Mudflats Accretion. *American Geophysical Union Fall Meeting*, Washington D.C., United States, 10–14 December.

10. Boersema, M. P., J. J. Van der Werf, A. M. Van den Brink, J. N. S. De Paiva, B. Walles, **P. L. M. De Vet**, E. Van Zanten, T. J. Bouma, and T. Ysebaert (2018). Oesterdam sand nourishment for safety and nature conservation. *Littoral conference*, Leeuwarden, The Netherlands, 22–26 October.

9. Colina Alonso, A., Z. B. Wang, B. C. Van Prooijen, D. J. R. Walstra, P. K. Tonnon, and **P. L. M. De Vet** (2018). Unravelling the mechanisms behind the morphodynamic evolution of the Haringvliet ebb-tidal delta. *NCK days conference*, Haarlem, The Netherlands, 21–23 March.

8. Van Prooijen, B., F. Grasso, P. Le Hir, **P. L. M. De Vet**, Z. B. Wang, B. Walles, and T. Ysebaert (2017). Equilibria and Evolution of Estuarine Fringing Intertidal Mudflats. *International Conference on Cohesive Sediment Transport Processes*, Montevideo, Uruguay, 13–17 November.

7. Van der Wegen, M., **L. De Vet**, Z. Zhou, G. Coco, and B. Jaffe (2017). Modeling tidal morphodynamics at the channel-mudflat interface. *Symposium on River, Coastal and Estuarine Morphodynamics*, Padova, Italy, 15–22 September.

6. Broekema, Y. B., M. C. Verbeek, and **P. L. M. De Vet** (2017). Hydro-morphodynamics at the Eastern Scheldt: A wide range of scales. *NCK days conference*, Den Helder, The Netherlands, 15–17 March.

5. Schrijvershof, R. A., J. Van der Werf, **P. L. M. De Vet**, and G. Willemsen (2017). Understanding sediment disposals on the Walsoorden tidal flat in the Western Scheldt. *NCK days conference*, Den Helder, The Netherlands, 15–17 March.

4. Ysebaert, T., B. C. Van Prooijen, B. Walles, **L. De Vet**, M. Boersema, J. Van der Werf, T. Bouma, Z. Wang, and P. M. J. Herman (2017). Tidal flat nourishments: a rare and unexplored eco-engineering practice in estuarine management. *NCK days conference*, Den Helder, The Netherlands, 15–17 March.

3. De Vries, S., M. Gatto, **L. De Vet**, B. Van Prooijen, and Z. B. Wang (2016). Equilibrium Morphology and Tidal conditions in Estuaries. *Physics of Estuaries and Coastal Seas Conference*, The Hague, The Netherlands, 9–14 October.

2. Van der Wegen, M., **L. De Vet**, Z. Zhou, G. Coco, and B. Jaffe (2016). Modeling morphodynamics at the channel-mudflat interface. *Physics of Estuaries and Coastal Seas Conference*, The Hague, The Netherlands, 9–14 October.

1. Van der Werf, J., T. Van Oyen, B. De Maerschalck, A. Nnafie, A. Van Rooijen, M. Taal, T. Verwaest, **L. De Vet**, J. Vroom, and M. Van der Wegen (2015). Modeling the morphodynamics of the mouth of the Scheldt estuary. *IAHR World Congress*, The Hague, The Netherlands, 28 June – 3 July.